2009-06-12

Evaluation of the Benefits of Oxy-combustion on Emissions from a Compression Ignition Engine

Thomas A. Salt
Brigham Young University - Provo

EVALUATION OF THE BENEFITS OF OXY-COMBUSTION ON EMISSIONS FROM A COMPRESSION IGNITION ENGINE

by

Thomas A. Salt

A thesis submitted to the faculty of

Brigham Young University

in partial fulfillment of the requirements for the degree of

Master of Science

Department of Mechanical Engineering

Brigham Young University

August 2009

BRIGHAM YOUNG UNIVERSITY

GRADUATE COMMITTEE APPROVAL

of a thesis submitted by

Thomas A. Salt

This thesis has been read by each member of the following graduate committee and by majority vote has been found to be satisfactory.

Date	Dale R. Tree, Chair
Date	R. Daniel Maynes
Date	Matthew R. Jones

BRIGHAM YOUNG UNIVERSITY

As chair of the candidate's graduate committee, I have read the thesis of Thomas A. Salt in its final form and have found that (1) its format, citations, and bibliographical style are consistent and acceptable and fulfill university and department style requirements; (2) its illustrative materials including figures, tables, and charts are in place; and (3) the final manuscript is satisfactory to the graduate committee and is ready for submission to the university library.

Date

Dale R. Tree
Chair, Graduate Committee

Accepted for the Department

Larry L. Howell
Graduate Coordinator

Accepted for the College

Alan R. Parkinson
Dean, Ira A. Fulton College of Engineering and Technology

ABSTRACT

EVALUATION OF THE BENEFITS OF OXY-COMBUSTION ON EMISSIONS FROM A COMPRESSION IGNITION ENGINE

Thomas A. Salt

Department of Mechanical Engineering

Master of Science

In this research the benefits of applying oxy-combustion in a diesel engine to reduce NO_x and particulate emissions were evaluated. The addition of oxygen to the intake in conjunction with exhaust gas recirculation (EGR) was shown to reduce NO_x without an increase in particulate. Indicated specific NO_x and particulate emissions for oxygen-enhanced EGR (O-EGR) and EGR without oxygen addition (normal or N-EGR) were compared at three engine loads. NO_x emissions correlated with flame temperature for both N-EGR and O-EGR but were slightly lower at a given flame temperature for O-EGR. Flame temperature reduction for N-EGR was primarily through dilution of the available oxygen while for O-EGR both the increase of specific heat and dilution were important in reducing flame temperature. Oxygen addition allowed the use of high levels of EGR without reducing the oxygen concentration, thereby substituting CO_2 and H_2O

for a substantial portion of the N_2 as diluent. Increased dissociation due to higher levels of CO_2 was believed to provide a minor enhancement to flame temperature reduction for O-EGR. An analysis of NO_x formation based on the Zeldovich mechanism suggested that increased NO_x reduction for O-EGR at equivalent flame temperatures is due to lower nitrogen concentrations. Indicated specific particulate increased with increasing EGR for N-EGR and correlated with flame temperature but remained constant for O-EGR and did not correlate with flame temperature. This indicated that O-EGR has a chemical effect on particulate formation and/or oxidation. The literature suggests CO_2 suppresses soot formation by decreasing the radical H concentration which reduces the formation of soot precursors and soot growth.

ACKNOWLEDGMENTS

I would like to thank my wife Margo for all of her support and encouragement, Dr. Dale R. Tree for his mentoring, and Dr. Chiwon Kim for his assistance in the lab.

TABLE OF CONTENTS

LIST OF TABLES

LIST OF FIGURES

1 Introduction

1.1 NO_x and Particulate Tradeoff in Compression Ignition Engines

Compression ignition (CI) engines are used in a wide variety of applications and industries including transportation, shipping, agriculture, construction, and power generation. CI engines have an advantage over spark-ignition (SI) engines in terms of fuel economy, which combined with their durability and reliability have given them an advantage in heavy-use applications (Dollmeyer, 2007). However, CI engines have a distinct disadvantage from SI engines in terms of two major pollutants, NO_x and particulate. NO_x emissions from CI engines are more difficult to control than those from SI engines because catalytic converters cannot function properly at the lean conditions under which CI engines operate (Heywood, 1988). Particulate emissions, which are the total amount of solid particles in the exhaust, are orders of magnitude greater from CI engines than from SI engines. The primary component of particulate in CI engines is soot. In recent years added intensity has been placed on developing methods of controlling NO_x and particulate emissions from CI engines due to increasingly stringent EPA limits on these pollutants.

Conventional CI combustion consists of a fuel rich jet surrounded by a stoichiometric flame. NO_x is formed just outside the boundary of the flame, which is

normally at a very high temperature (2600 - 2700 K) causing atmospheric nitrogen and oxygen to react and form NO_x. Soot is formed in the fuel-rich jet where insufficient oxygen is available for complete combustion. The control strategy for lowering NO_x is to lower the flame temperature, while for soot the strategy is to increase the cylinder temperature or increase the mixing rate of fuel and oxidizer to make the fuel jet less fuel-rich. The competing effects of temperature on NO_x and particulate produce what is know as the NO_x-particulate tradeoff curve. An example of a NO_x-particulate tradeoff curve is shown in Figure 1.1. In this figure, temperature is decreased by adding EGR to the engine. The result is a decrease in NO_x and an increase in particulate along the solid black line. The goal of improved emissions is to produce an improved tradeoff curve as represented by the dashed line.

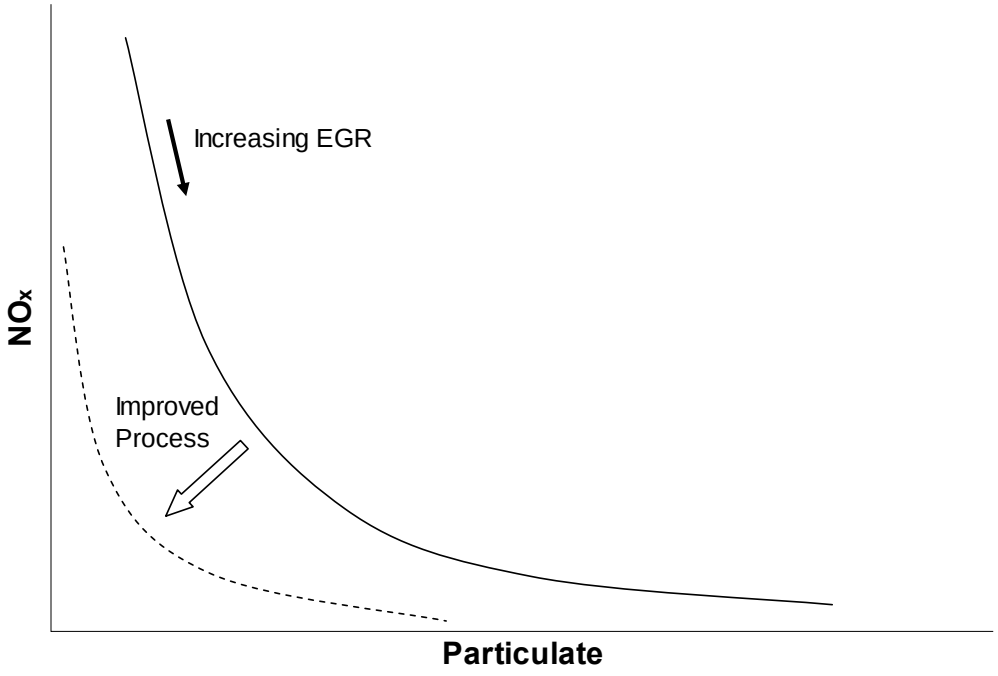

Figure 1.1. NO_x-particulate tradeoff curve. Solid line represents tradeoff by increasing EGR. Dotted line represents improved process shifting tradeoff curve closer to the origin.

Over the past two decades engine manufacturers have been able to move diesel emissions toward the origin by simultaneously decreasing temperature using EGR and increasing fuel oxidizer mixing using higher injection and cylinder pressure. EGR adds CO_2 and H_2O from the exhaust to the intake air and dilutes the amount of available oxygen at the flame. This increases the thermal capacity of the mixture without increasing the chemical energy released by the fuel and thereby lowers the flame temperature. Increased injection pressure allows for smaller hole sizes which increases the relative amount of oxidizer entrained in the fuel jet.

Nitrogen is a natural diluent in air which lowers the flame temperature relative to fuel burning in. However, it can be argued that CO_2 and H_2O are better diluents in diesel combustion for emissions purposes because they have higher molar heat capacities than N_2, which allows them to be more effective at lowering the flame temperature and reducing NO_x formation (Ladommatos *et al*., 1998). Additionally, CO_2 is known to suppress soot formation in laboratory diffusion flames (Guo and Smallwood, 2008). Normal EGR does not replace N_2 with CO_2 but rather adds CO_2 and H_2O to the mixture, which limits the amount of CO_2 that can be added because the O_2 becomes too dilute to sustain stable combustion.

1.2 Oxy-combustion as an Emissions Control Strategy for CI Engines

In this study a source of pure O_2 has supplemented the oxygen supplied by air in order to sustain a constant O_2 concentration when EGR was increased, which allowed O_2 and EGR to replace N_2 rather than adding to it. This allowed the CO_2 and H_2O

concentrations to be higher than any known previous study in order to identify the possible benefits of oxygen enhancement in conjunction with EGR on CI emissions. This process of substituting pure O_2 for part or all of the oxidizer and EGR for N_2 as the diluent is often referred to as oxy-combustion. In CI engines oxy-combustion is essentially a modification to EGR (EGR with oxygen addition) and will be referred to herein as oxygen-enhanced EGR (O-EGR). EGR without oxygen addition will be referred to as normal EGR (N-EGR) in order to allow the use of the term EGR to generically describe either process. Combining oxygen addition with EGR has the potential to reduce both NO_x and particulate emissions from a CI engine.

N-EGR: $\text{Fuel} + \text{Air} + \text{EGR} \rightarrow \text{Products}$

O-EGR: $\text{Fuel} + \text{Air} + \text{EGR} + \text{O}_2 \rightarrow \text{Products}$

1.3 Research Objective

The objective of this research was to investigate the potential benefits of oxygen addition together with EGR in a diesel engine by comparing NO_x and particulate emissions when using oxygen-enhanced EGR (O-EGR) to emissions when using normal EGR (N-EGR). Although previous researchers have investigated the mechanisms by which EGR influences NO_x and particulate emissions, no study is known in which O_2 was added to a CI engine in conjunction with high levels of EGR in an oxy-combustion process.

2 Background

As a result of extensive optical studies of compression ignition combustion, Dec (1997) presented an updated conceptual model of diesel combustion applicable to single injection, compression ignition combustion events as produced by an engine of the type used in this study. A diagram of Dec's conceptual model is given in Figure 2.1. Dec's models will be reviewed below to provide an understanding of the combustion process occurring in the engine used in this study.

Compression ignition engines employ injectors which spray fuel at high pressure (on the order of 100–150 MPa) into the combustion chamber through small holes (on the order of 0.15-0.20 mm). As the fuel jet travels into the cylinder (from left to right in the diagram), it entrains hot gas trapped in the cylinder at the start of compression. Modern injection pressures are high enough and create strong enough atomization that evaporation of the spray is not controlled by the droplet size in the jet but rather by the rate of energy transported into the jet. The penetration of the liquid phase into the cylinder has been shown to be self-similar and scales with the energy entrained into the conical zone which is fixed by the spray angle (Siebers, 1999). The maximum penetration length of the liquid fuel into the cylinder is termed the liquid length.

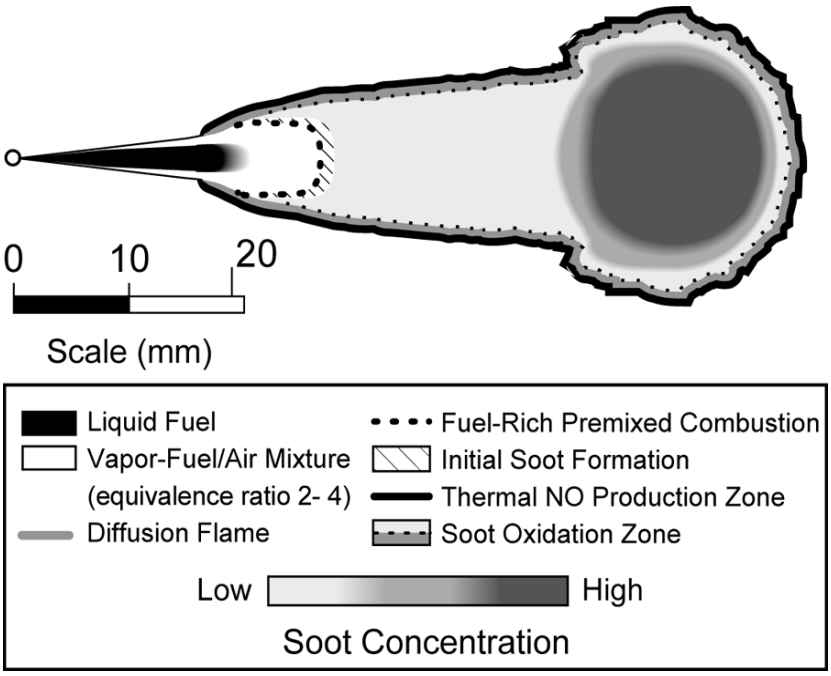

Figure 2.1. Conceptual model of diesel engine combustion proposed by Dec (1997). Figure obtained and used by permission.

At typical injection pressures, nozzle size, and surrounding gas temperature, a diffusion flame surrounds the entire region downstream of the liquid penetration and extends upstream to a fixed distance from the nozzle tip termed the lift-off length. The diffusion flame is positioned where the fuel air mixture is stoichiometric around most of the perimeter, but near the nozzle the velocity of the jet and the time required to react the fuel/air mixture determines how far from the nozzle tip the flame is located. Downstream of the location where the diffusion flame begins, products of combustion and not fresh cylinder gases are entrained into the jet. Thus, the diffusion flame pinches off or restricts the entrainment of O_2 into the jet and sets a limit on the amount of unreacted oxygen available within the envelope of the diffusion flame. This axial location has been defined by Siebers and Higgins (2001) as the lift-off length and is critical to soot formation in

compression ignition engines. In terms of similarity to laboratory flames, this quasi-steady period after the lift-off length is established and before the end of injection is most like a lifted, partially premixed, turbulent, diffusion flame.

For the conditions used to establish Dec's model which are applicable to this study, the equivalence ratio at the end of the liquid length and beginning of the vapor region were measured to be in the range of 2 to 4. Upon additional heating, the rich premixed mixture downstream of the liquid length reacts at a location depicted by the thick dashed black line. This creates fuel rich products at a moderate temperature (1300–1600 K) within the core of the reacting jet. On the boundaries of the jet, where the surrounding oxidizer is sufficient to produce a stoichiometric mixture, a diffusion flame is formed where the remainder of the fuel is burned and the temperature reaches the stoichiometric, adiabatic, flame temperature.

A transient period occurs prior to the quasi-steady period shown in Figure 2.1. During this transient period (ignition delay), the fuel is injected, begins to penetrate into the cylinder, and some portion of the fuel is evaporated and mixed with the surrounding charge air. The reaction of this mixture formed during the ignition delay period is called the "initial premixed burn". This "initial premixed burn" should be clearly distinguished from the premixed burn of the quasi-steady flame described earlier.

At the end of injection, the injector hole is covered by the injector needle and flow is terminated. After injection is completed, the jet has no momentum source and the remaining momentum is dissipated into the surrounding charge gas. The jet structure evolves into a pocket of rich premixed products surrounded by a diffusion flame and is no longer distinguishable as a jet. The pocket of rich products reduces in size and breaks

into smaller pockets as combustion continues. Late in the cycle, numerous pockets of burning fuel have been observed. The temperature is initially high enough that a flame will surround any pocket of unburned gas. What happens after these pockets of burning fuel are produced is only speculative. It is hypothesized that as temperatures drop, reaction rates slow down relative to mixing rates and reaction of the fuel becomes more distributed, burning out the more reactive species first and potentially leaving soot and more stable species unoxidized.

2.1 NO_x Formation

NO_x is a major contributor to urban air pollution. It is a precursor to smog, which causes reduced air visibility and can contribute to respiratory problems (Neeft *et al.*, 1996). The primary source of NO_x in internal combustion engines is the oxidation of atmospheric N_2 at high temperature which is referred to as thermal NO_x (Heywood, 1988). Thermal NO_x formation increases exponentially with temperature and is therefore highest on the lean side of the hot stoichiometric flame (Heywood, 1988). In Fig. 2.1, NO_x is seen to form around the perimeter of the oxidizer side of the flame. Inside the flame the gas species and temperature produce a reducing environment where any NO_x formed would be converted back to N_2, while away from the flame bulk gas temperatures are too low to form NO_x. The global reaction mechanism for thermal NO_x formation is given by Equation (2.1). The global reaction rate can be represented by Equation (2.2), where E_A is the activation energy.

$$N_2 + O_2 \rightarrow 2\,NO \tag{2.1}$$

$$\frac{d[NO]}{dt} \propto [N_2][O_2]\exp\left[-\frac{E_A}{R_u T}\right] \tag{2.2}$$

The above rate equation highlights the exponential effect of temperature and the linear relationship of O_2 and N_2 concentrations on thermal NO_x production. The global reaction may be more accurately described by three primary elementary reaction equations collectively referred to as the extended Zeldovich Mechanism (Turns, 2000). The first reaction, N.1, is rate controlling.

$$O_2 + N_2 \Leftrightarrow NO + N \tag{N.1}$$

$$N + O_2 \Leftrightarrow NO + O \tag{N.2}$$

$$N + OH \Leftrightarrow NO + H \tag{N.3}$$

EGR is effective in reducing NO_x by diluting the intake air with recirculated exhaust gases, which decreases the oxygen concentration and lowers the flame temperature. Ladommatos *et al.* (1998) studied the methods whereby EGR impacts NO_x reduction and concluded EGR reduces NO_x through three primary means:

1. Dilution effect – Diluting the O_2 concentration with EGR, thereby reducing the availability of O_2 for combustion which leads to a larger total thermal mass of gases to be heated per unit of fuel burned.
2. Specific heat effect – Replacing part of the O_2 and N_2 with CO_2 and H_2O which have higher molar specific heats than O_2 and N_2, thereby increasing the heat absorbing capacity of the gases in the flame.
3. Chemical effect – Contributing chemically to the reduction of NO_x, perhaps through the dissociation of CO_2 and H_2O at high temperatures.

The first two of these effects are primarily thermal in nature, achieving reduced NO_x by lowering the flame temperature. Ladommatos *et al.* (1998) also demonstrated that CO_2 has beneficial chemical effects on NO_x reduction. In their experiments the CO_2 concentration was never greater than 5%, and the chemical and specific heat effects were minor in comparison to the dilution effect. O-EGR allows CO_2 levels to be raised significantly beyond what can be obtained with N-EGR, which could increase the significance of both the specific heat and the chemical effects from dissociaton on NO_x reduction. An additional chemical effect not significant in the study by Ladommatos *et al*. is the reduction of N_2 available for participation in the Zeldovich mechanism, which may become significant at the high levels O-EGR.

Unfortunately, N-EGR alone is insufficient to achieve both NO_x and particulate reduction because the reduced flame temperature caused by using N-EGR also tends to increase particulate emissions. Alriksson *et al*. (2005) showed that at very high levels of N-EGR (>60%) it was possible to simultaneously reduce both NO_x and particulate, but combustion under those conditions was incomplete, leading to high levels of CO, unburned hydrocarbons, and high fuel consumption. Using high injection pressures, increased swirl, and increased boost pressures with EGR cooling has produced improvements in the NO_x-particulate tradeoff, though there are still limits on how much EGR is used (Helmantel, 2008; Dollmeyer *et al.*, 2007).

2.2 Particulate Formation and Oxidation

Particulate consists of partially burned hydrocarbons in the form of carbonaceous soot and agglomerated organic compounds resulting from incomplete combustion of fuel

(Heywood, 1988). Particulate is believed to be related to respiratory problems and is thus the focus of much regulation. Particulate formation begins in the fuel rich product region inside the fuel jet. In this region the fuel has been partially burned and the temperature is high enough to produce reactions in the gas phase. The more stable carbon species such as benzene and other aromatics combine and dehydrogenate to nucleate soot particles which grow and agglomerate. Equivalence ratio in this fuel-rich region has a strong impact on particulate formation (Siebers and Higgins, 2001). The equivalence ratio is controlled by the amount of entrained oxidizer upstream of the flame length. Decreasing the O_2 concentration in the gas surrounding the jet (as occurs with increasing EGR) leads to lower O_2 entrainment and increased soot formation. Longer injection processes (increased overall fuel-air equivalence ratio) produce larger jets with larger soot formation regions inside the jets. This leads to increased total soot formation even though the local concentrations of soot within the jet are not increased.

Soot is oxidized as it exits the jet on the fuel-lean side. It is not known exactly where the soot that exits the engine in the exhaust comes from, but two sources are possible: 1. Soot escapes the jet through gaps in the flame when the flame temporarily opens due to turbulence and strain, and 2. The surrounding flame is extinguished or quenches at low temperature leaving the remaining soot inside the flame unburned (Tree and Svensson, 2007).

In oxy-combustion the gas surrounding the flame can have elevated concentrations of O_2 and CO_2 which will be entrained into the fuel jet. These changes in concentration can lead to chemical effects on soot formation. Numerous researchers have shown that CO_2 addition to a diffusion flame suppresses soot formation (e,g. McLintock,

1962; Oh and Shin, Du *et al*. (2000), and Angrill *et al*. (2000)). Changing the surrounding gas composition can also have chemical effects on particulate oxidation. Oxidation of particulate occurs on the lean side of the flame where oxidizing species are encountered at high temperatures. Soot oxidation is a heterogeneous reaction. Oxygen and/or OH are adsorbed onto the surface of the particles and react to form CO. Bartok and Sarofim (1991) report that OH is most likely to dominate soot oxidation under fuel-rich and stoichiometric conditions, while under lean conditions soot is oxidized by both OH and O_2. Haynes and Wagner (1981) state that about 10-20% of all OH collisions with soot are effective at gasifying a carbon atom. Several researchers have verified that particulate emissions from CI engines are strongly correlated with flame temperature (e.g. Plee *et al*., 1981; Iida, 1993; Nikolic and Iida, 2007). This suggests that even though large amounts of soot may be formed in the fuel jet, the amount exiting in the exhaust is related to the ability to oxidize soot late in the expansion process. Increased levels of OH could potentially allow soot to be oxidized at lower temperatures.

2.3 Literature Review

While oxygen-enhanced EGR has to the best of this researcher's knowledge not previously been specifically investigated in diesel engines, several researchers have looked at the individual effects of EGR, CO_2, and O_2 addition on diesel emissions. Because N-EGR has been developed over the past two decades into a commercially accepted practice, the literature is full of its use and implementation. The components of N-EGR that are of greatest interest are CO_2 and H_2O. Therefore studies to investigate these components as well as O_2 addition will be reviewed more specifically.

Ladommatos *et al*. (1998) performed a study in which simulated EGR either replaced oxygen in the charge air or else added to it. When EGR replaced oxygen, emissions followed the traditional NO_x-particulate tradeoff, but when EGR was added to the charge air, it was shown that particulate could be held at a constant level with increasing EGR. This result was achieved when the increasing ignition delay due to increased EGR was compensated for with a commercial fuel additive ignition improver.

Iida (1993) used a rapid compression machine with optical access to visualize diesel flames in varying amounts of oxygen concentration from 17-25%. He saw increased flame temperature and reduced soot formation with increasing oxygen concentration. Plee et al. (1982) added O_2 and N_2 to the intake air of a divided chamber diesel engine to create elevated and reduced intake O_2 concentrations. They showed a strong correlation between NO_x and flame temperature. Several other studies have also been done on the effects of O_2 addition and are reviewed by Rakopoulos *et al*. (2004). In general, studies have shown that oxygen addition significantly reduces particulate emissions yet negatively impacts NO_x emissions.

Particulate formation and oxidation rates are both important factors in determining the final engine-out particulate emissions. Idicheria and Pickett (2005) showed that at high levels of EGR the soot formation rate decreased due to lower combustion temperatures, yet the residence time for soot formation increased, thereby leading to overall higher soot concentrations in the exhaust. The eventual emissions of particulate from an engine are determined by the relative effectiveness of particulate oxidation in relation to particulate formation.

In an effort to determine if soot reductions in diffusion flame were caused by thermal or chemical effects and if those effects were during soot formation or oxidation, Guo and Smallwood (2008) produced a detailed kinetic model simulating the data of Gülder *et al*. (1996). In the model and experiments, CO_2 was added only to the fuel side of a co-flow diffusion flame and not to the oxidizer side. They concluded that CO_2 has a chemical effect in reducing soot formation and attributed this reduction to the decreased concentration of H radicals, which decreased the formation rate of PAH. The decrease in H is caused by the higher concentration of CO_2 in the reaction given below by C.1, which shows how an increase in CO_2 can lead to increased levels of CO and OH, the OH then being able to react with soot.

$$CO_2 + H \rightarrow CO + OH \qquad \text{(C.1)}$$

It is believed that emissions data from a diesel engine using a combination of O_2 and EGR has not been collected on diesel engines to date. Quite likely the addition of O_2 has not generally been seen as a practical approach to solving diesel emissions problems. Nevertheless, this research has value for two reasons: 1. To extend the current knowledge on the thermal and chemical effects of CO_2 and H_2O addition on diesel combustion, and 2. To provide information on the potential of O-EGR for emissions control in anticipation of future advancements in air separation technology that would make the practice more feasible.

3 Experimental Setup and Procedure

3.1 Engine Configuration and Measurements

Experiments were conducted on a 1994 Cummins 5.9 L six-cylinder diesel engine. This engine had previously been modified to operate on a single cylinder by deactivating five of the six. With these modifications, all measurements and calculations were done on a single cylinder, thereby removing the concern of cylinder-to-cylinder variability. A more detailed description of the engine modifications can be found in Cooley (2000). Air was supplied to the engine from a compressed air source, which allowed the charge air pressure to be varied. A pressure regulator on the air inlet provided pressure control from approximately 0-25 psig. Oxygen stored in liquid cylinder tanks was used to supplement the intake air such that the oxygen concentration could be maintained constant while the amount of EGR was increased. A surge tank on the inlet side of the engine helped smooth air pressure fluctuations due to valve operation and a similar surge tank on the exhaust side helped to smooth pressure fluctuations in the exhaust line. Figure 3.1 provides a flow diagram for the engine setup and also depicts the air, EGR, and O_2 flow paths.

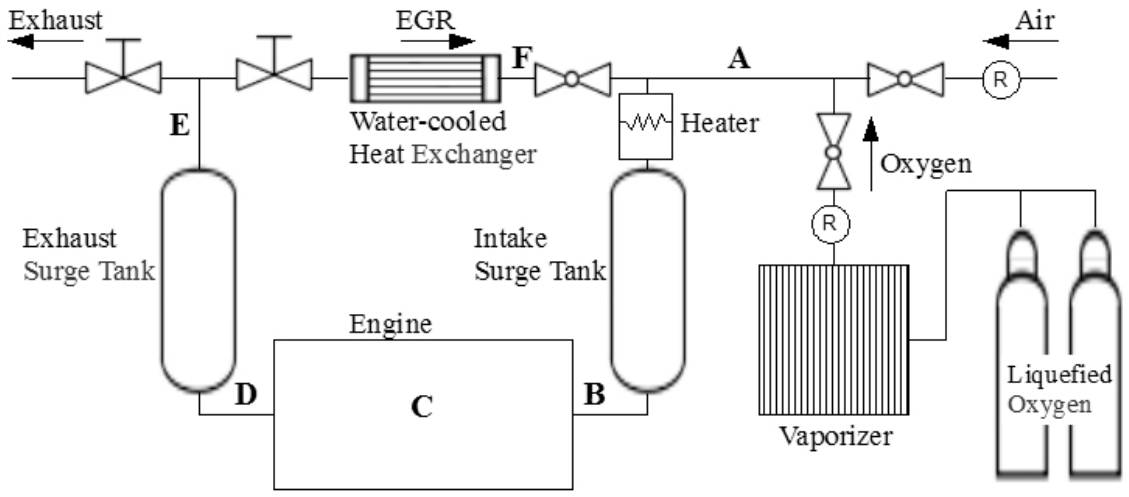

Figure 3.1. Flow diagram of experimental setup

Sweeps of gradually increasing levels of EGR were completed with and without oxygen addition (O-EGR and N-EGR) for three different loads (overall equivalence ratios). The engine speed was maintained at 1500 rpm for all loads. At each operating condition exhaust the following measurements were taken at the lettered locations indicated in Figure 3.1:

A - Volumetric flow rate, pressure, temperature

B - Pressure, temperature, xO_2, xCO_2, xNO_x

C - Engine speed (RPM), engine position (crank angle), in-cylinder pressure

D - Temperature, opacity

E - Pressure, xO_2, xCO_2, xNO_x

F - Temperature

Atmospheric pressure was also recorded, and the gas temperature at the opacity meter was measured in order to determine the density of the exhaust gases flowing through the meter. Due to the potential for transient engine behavior, engine speed, intake pressure,

and emissions data at each set point were recorded five times over the course of several minutes and then averaged.

3.1.1 Measuring In-cylinder Pressure

Dynamic cylinder pressure measurements as a function of engine position (crank-angle) allows one to determine gross engine power, in-cylinder bulk temperature, apparent heat release rate (AHRR), and cumulative heat released (HR) over an engine cycle. Cylinder pressure measurements were taken using an AVL QH32C quartz piezoelectric pressure transducer. This transducer produced a charge that was linear with pressure, which was amplified and sent as a voltage signal to a data acquisition (DAQ) board on a personal computer. The pressure transducer was calibrated using a dead weight tester. LabView software was used to collect and record data from the DAQ, which were triggered every 1/4 crank angle by a BEI Model H25 incremental encoder mounted on the crank shaft, thereby giving 2880 readings per engine cycle. An ensemble average of the pressure data was made over 100 cycles. Noise in the pressure data were smoothed by converting pressure data into the frequency domain using a fast Fourier transformation and then passing them through a power filter, which smoothing prevented noisy numerical derivatives when calculating AHRR and total heat release.

3.1.2 Measuring System Temperatures

Thermocouples were mounted at the engine air intake manifold, on the exhaust manifold, at the air flow meter (to determine air density flowing through the meter), at the EGR heat exchanger outlet, and at the smoke meter inlet. Temperature measurements were recorded and ensemble averaged over the same period as the cylinder pressure data.

3.1.3 Control and Measurement of Fuel Flow

Fuel flow rate was used as an indicator of engine load as well as a means of maintaining a fixed equivalence ratio. Equivalence ratio, ϕ, compares the actual fuel to oxidizer ratio with the stoichiometric fuel to oxidizer ratio. In this research the oxidizer, O_2, was supplied not only from air but also from EGR and liquefied O_2, and hence the equivalence ratio was defined using O_2 rather than air.

$$\phi = \frac{\left(\frac{m_{fuel}}{m_{O_2}}\right)_{actual}}{\left(\frac{m_{fuel}}{m_{O_2}}\right)_{stoich}} \tag{3.1}$$

Three target equivalence ratios were used in this research (ϕ=0.33, 0.50, and 0.65) to represent three load conditions. The fuel flow rate was controlled via a micrometer attached to the rack of the in-line fuel injection pump. Adjusting the rack position changed how much fuel was injected with each stroke of the injector pump plunger. A more detailed description of the fuel injection control is given by Cooley (2000). For the purposes of this research, the injector pump rack position served as a repeatable method of controlling fuel injection rate to achieve a desired equivalence ratio. Fuel flow rate was measured using a Micromotion Coriolis type mass flow meter.

3.1.4 Measuring Air Flow

Volumetric air flow measurements were made at point A indicated in Figure 3.1 using an Omega model FV-510B-D vortex-shedding flow meter. However, during O-EGR sweeps at very high levels of EGR air flow readings could not be made with this flow meter because the air flow rate to the engine dropped below the flow meter's range

of measurement (~6 CFM). In these cases the volumetric efficiency of the engine calculated for no EGR was used to estimate the volumetric flow rate of intake gases. This is shown in Equation (C.16) in Appendix C.

3.1.5 Determining Gas Concentrations

Dry concentrations of O_2, CO_2, and NO_x were measured at the intake and at the exhaust using a Horiba PG-250 gas analyzer. This analyzer was capable of measuring O_2 in concentrations of 0-25%, CO_2 in concentrations of 0-20%, and NO_x in concentrations of 0-5000 ppm. In the O-EGR tests at high levels of EGR the CO_2 concentration of the exhaust exceeded 20% and could no longer be measured with this analyzer. For these cases the concentration was determined using a model of the combustion process which assumed complete combustion of the measured inlet fuel and estimated oxidizer flows. The model and method of calculation are given in Appendix C. H_2O in the intake was insignificant for the N-EGR cases but was significant for the O-EGR cases. The concentration of H_2O in the intake gas was estimated using the model of the combustion process explained in Appendix C.

3.1.6 Evaluating NO_x Emissions

NO_x emissions were normalized on an engine power output basis in order to compare emissions at various engine loads. The NO_x concentration measurement at each set point was converted to a NO_x mass flow rate as shown in Equation (3.2). The exhaust molar flow rate, $\dot{N}_{exh}$, was calculated from the measured fuel and oxidizer flow rates and the calculated molar mass of the product based on the model described in Appendix C. Because of the significance of H_2O in O-EGR tests, separate models were used for N-

EGR and O-EGR. The indicated gross power (P_{ig}) was calculated from the integrated work found from the cylinder pressured data and the measured engine speed as shown in Appendix A.

$$\dot{m}_{NO_x} = xNO_x \cdot \dot{N}_{exh} \cdot MW_{NO_x} \tag{3.2}$$

$$\text{Indicated specific } NO_x = \frac{\dot{m}_{NO_x}}{P_{ig}} \tag{3.3}$$

3.1.7 Evaluating Particulate Emissions

Particulate emission values were calculated from opacity measurements made with an AutoLogic MOT Smoke Meter. Opacity is a measure of the proportion of light that is blocked as it passes through the gas and is given on a scale of 0-100%. It is related to the fraction of transmitted light through the following equation, where τ_λ is the transmissivity of the exhaust.

$$Opacity = \left(1 - \tau_\lambda\right) \cdot 100 \tag{3.4}$$

The smoke meter continuously measured the opacity of the gas flowing through an internal chamber by shining green light through the gas and detecting the portion of the transmitted light. Although opacity is not a direct measure of particulate it may be correlated to the soot volume fraction, $f_v = V_{soot}/V_{gas}$, from which the amount of particulate can be found. If Kirchoff's law for radiation is assumed to apply to soot and particulate are assumed to be non-reflecting, opacity may be related to emissivity by the following expression, where ε_λ is the emisivity of soot and α_λ is the absorbtivity of soot.

$$\varepsilon_\lambda = \alpha_\lambda = 1 - \tau_\lambda = \frac{Opacity}{100} \tag{3.5}$$

Ferguson *et al*. (1987) give an expression for the emissivity of soot based on Beer's law as shown in Equation (3.3), where λ is the wavelength of the light ($5.10E^{-7}$ m was used in

calculations); A_λ is an emittance parameter which has a value of 6.0 for soot (Ferguson *et al*., 1987) ; and L is the effective path length of the light, in this case given by the manufacturer as 0.43 m (Autologic, 2006).

$$\varepsilon_\lambda = 1 - \exp\left(\frac{-A_\lambda f_v L}{\lambda}\right) \tag{3.6}$$

Substituting Equation (3.5) into Equation (3.6) and solving for f_v gives:

$$f_V = \frac{V_{soot}}{V_{gas}} = -\frac{\lambda}{A_\lambda L}\ln(\tau_\lambda) = -\frac{\lambda}{A_\lambda L}\ln\left(1 - \frac{Opacity}{100}\right) \tag{3.7}$$

The bulk density of soot in the gas is the product of the soot volume fraction and the density of a single soot particle as shown in Equation (3.8).

$$\rho'_{soot} = f_v \cdot \rho_{soot} \tag{3.8}$$

The single particle density of soot, ρ_{soot}, is approximately 1800 kg/m^3 (Choi *et al*., 1994). The bulk density of soot in the exhaust can then be used to find the mass flow rate of soot from the engine according to Equation (3.9), where $\overline{\rho}_{exh}$ is the molar density of exhaust gases (kmol/m^3) and $\dot{N}_{exh}$ is the molar flow rate (kmol/s) of exhaust gases.

$$\dot{m}_{soot} = \frac{\rho'_{soot}}{\overline{\rho}_{exh}}\dot{N}_{exh} \tag{3.9}$$

Particulate emissions were normalized on a power output basis similar to NO_x to obtain an "indicated specific particulate (ISPM)" (g/kWh) value as given below.

$$\text{ISPM} = \frac{\dot{m}_{soot}}{P_{ig}} \tag{3.10}$$

3.1.8 Apparent Heat Release Rate (AHRR) and Cumulative Heat Release (HR)

Cylinder pressure measurements were used to calculate the total cycle indicated work and AHRR. AHRR provided an indication of how fuel is being burned. Plots of AHRR provided insights about the start of ignition and the relative size of the premixed combustion versus diffusion controlled combustion, as will be shown in Section 4.1. A relatively simple model for AHRR which assumed constant specific heat was used as given below, where γ is the ratio of specific heats, C_p/C_v (Heywood, 1988).

$$AHRR = \frac{\gamma}{\gamma - 1} P \frac{dV}{d\theta} + \frac{1}{\gamma - 1} V \frac{dP}{d\theta} \tag{3.11}$$

The cumulative heat released at any given crank angle, θ^*, was found by integrating AHHR over θ from the start of injection (SOI) to θ^*. The injection timing was not varied in this research.

3.1.9 EGR Fraction

For the purposes of this research, EGR fraction was defined as the ratio of the molar flow rate of EGR to the molar flow rate of all intake gases as shown below.

$$\text{EGR fraction} = \frac{\dot{N}_{EGR}}{\dot{N}_{Intake}} \tag{3.12}$$

3.2 EGR and Oxygen Addition

EGR was achieved by connecting a line from the exhaust line into the intake line (see Figure 3.1). Adjusting the backpressure on the engine via a valve on the outlet of the exhaust line controlled the amount of EGR added. As the backpressure was increased,

more exhaust gas was forced into the incoming air, and thus the exhaust pressure thus had to be maintained at a slightly higher pressure than the incoming air. In the N-EGR case the EGR was cooled to roughly the same temperature as the air in a water-cooled heat exchanger. Water from the combustion products that condensed due to this cooling was captured in a water trap to prevent liquid water from entering the engine intake. For the O-EGR case the EGR temperature was varied by adjusting the flow rate of cooling water to the heat exchanger. This was required in order to match the ignition delays at different levels of EGR, as will be explained later in this section.

In both N-EGR and O-EGR tests the total molar flow rate of O_2 and fuel were maintained constant in order to maintain a constant equivalence ratio. The required O_2 molar flow rate was determined based on the no EGR case according to Equation (3.13).

$$\dot{N}_{O_2} = xO_2 \cdot \frac{P\dot{V}}{R_u T} \tag{3.13}$$

At constant engine speed $\dot{V}$ was assumed to remain constant, so in order to maintain $\dot{N}_{O_2}$ constant it was necessary to keep the ratio $\frac{xO_2 \cdot P}{T}$ constant. For the N-EGR cases, T was kept relatively constant using a resistance heater. Hence, as EGR was added and xO_2 decreased, P had to be increased to compensate. An iterative process was used to maintain $\dot{N}_{O_2}$ at the original no EGR condition as follows:

1. P and xO_2 were measured at the new increased level of EGR.
2. The required P at current xO_2 was calculated and P was adjusted to this value.
3. The new xO_2 value was measured and iteration were performed on steps 1 to 3 until a new value of P was not required after measuring xO_2.

In the O-EGR case not only was the total O_2 flow rate kept constant, but the dry O_2 intake concentration was also maintained as the EGR level was increased, by adding additional O_2 from liquid O_2 tanks. A passive vaporizer helped to vaporize the liquid O_2 to ensure a high enough flow rate to the engine, and a pressure regulator on the O_2 line provided adjustment to the O_2 flow rate. As the EGR level was increased during O-EGR tests, both the intake air flow rate and the added O_2 flow rate decreased. This was compensated for by increasing the pressure on the air line as well as on the O_2 line to maintain a constant overall O_2 flow rate to the engine. In the O-EGR case maintaining a constant O_2 flow rate was slightly more complicated than the iterative process used for N-EGR for two reasons: 1. H_2O in the intake was no longer insignificant, and 2. The intake temperature had to be varied for different EGR levels. Each of these complications is explained below.

Reducing the amount of EGR cooling meant that the saturation pressure of the EGR was raised and consequently less H_2O condensed out. Hence, H_2O became a significant constituent of the intake gases, and the dry gas O_2 composition measured by the Horiba analyzer no longer represented the total wet O_2 concentration. The H_2O concentration was estimated based on the EGR temperature and an H_2O saturated pressure-temperature table (see Appendix A). The wet O_2 concentration was then determined based on the measured dry gas composition. The wet gas O_2 composition was next used in Equation (3.13) to determine the intake pressure required. In this case, however, no iteration was needed because the O_2 concentration was a fixed variable. However, the intake temperature in the O-EGR tests was varied between set points and had to be accounted for in determining the needed intake pressure.

The intake temperature for O-EGR had to be adjusted because of large changes in gas composition from air. H_2O and CO_2 have lower specific heat ratios, $\gamma=C_p/C_v$, than N_2, which means these gases produce a lower temperature rise during compression as shown in Equation (3.14) for isentropic compression, where r_c is the compression ratio, T_1 is the initial temperature, and T_2 is the temperature following compression.

$$T_2 = T_1 \cdot r_c^{(\gamma-1)} \tag{3.14}$$

Reduced temperatures following compression led to an increased ignition delay. The of varied compression temperatures, T_2, on ignition delay is demonstrated in section 4.1. To be able to compare O-EGR test points at differing amounts of EGR, a similar ignition delay and similar heat release profile was desired for all set points. This was achieved by raising the intake gas temperature, T_1, in order to match the compression temperature (temperature at TDC) for all EGR cases. Although an electric resistance heater was available, the capacity of the heater was not high enough to produce the desired intake heating. Therefore, the increased intake temperature was accomplished by reducing the amount of EGR cooling as well as by adjusting the current to the resistance heater. The ratio of specific heats, γ, was evaluated at an assumed temperature of 800 K using a correlation given by Kee *et al*. (1991) for each intake composition.

3.3 Uncertainty Analysis

Uncertainties were determined for indicated specific particulate and NO_x. To find an expression for the uncertainty in indicated specific particulate, Equation (3.10) was first rewritten as:

$$ISPM = \frac{f_v \left(\frac{\rho_{soot}}{\overline{\rho}_{exh}} \right) \dot{N}_{exh}}{P_{ig}} \tag{3.15}$$

The percent uncertainty in indicated specific particulate (ISPM) was then given by:

$$\frac{U_{ISPM}}{ISPM} = \sqrt{\left(\frac{U_{\overline{\rho}_{exh}}}{\overline{\rho}_{exh}} \right)^2 + \left(\frac{U_{f_v}}{f_v} \right)^2 + \left(\frac{U_{\dot{N}_{exh}}}{\dot{N}_{exh}} \right)^2 + \left(\frac{U_{P_{ig}}}{P_{ig}} \right)^2} \tag{3.16}$$

Conservative uncertainties for parameters in Equation (3.16) were estimated based on the measurement uncertainties and typical random errors for experimental runs. Bias errors were not considered because they did not impact the NO_x-particulate trends and were also thought to be comparatively small. Results for each variable are given in Table 3.1. Evaluation of uncertainty in soot volume fraction, f_v, is explained further on.

For N-EGR, a conservative estimate of the uncertainty in the exhaust molar flow rate, $\dot{N}_{exh}$, was calculated using the equations for N-EGR molar flow rates given in Appendix C. This uncertainty was affected primarily by uncertainties in intake pressure (P_{in}), intake temperature (T_{in}), volumetric flow rate of air ($\dot{V}_{air}$), and the fuel molar flow rate ($\dot{N}_{fuel}$). For O-EGR, the uncertainty in $\dot{N}_{exh}$ was slightly higher than for N-EGR because the values for the molar flow rates for O-EGR were based on more assumptions, as explained in Appendix C. The uncertainty in $\dot{N}_{exh}$ for O-EGR was considered to be the uncertainty for N-EGR plus 4%, which was the largest deviation seen between flow rates calculated using the two different models for the same input data.

Table 3.1. Estimates of uncertainties

	% Uncert.
$\dot{N}_{exh}$ (N-EGR)	3.0%
$\dot{N}_{exh}$ (O-EGR)	7.0%
P_{ig}	2.0%
$\overline{\rho}_{exh}$	1.0%
P_{in}	1.0%
f_v	>8%

The uncertainty in gross indicated power (P_{ig}) was conservatively estimated based on random error in the calculated power output for multiple sets of pressure data taken at same fuel rack position. The uncertainty in the exhaust molar density ($\overline{\rho}_{exh}$) was found based on the uncertainty in the temperature at the smoke meter (T_{smoke}), which was estimated based on its measurement uncertainty.

Uncertainty in f_v was not constant but was highly dependent on the uncertainty in transmissivity, τ_λ, which was directly related to opacity. The relationship between soot volume fraction uncertainty and τ_λ is given by Equation (3.17). The uncertainty in opacity used to calculate the uncertainty in τ_λ was taken as ±2 for all opacities, which was based on observations of random error.

$$\frac{U_{f_v}}{f_v} = \frac{\partial f_v}{\partial \tau_\lambda}\frac{U_{\tau_\lambda}}{f_v} = \frac{U_{\tau_\lambda}}{f_v \cdot \tau_\lambda} \tag{3.17}$$

The percent uncertainty in indicated specific particulate for both N-EGR and O-EGR are presented below in Figure 3.2 on the same plot as the uncertainty in f_v. The percent uncertainty in f_v goes to infinity at an opacity of 0% because at this point f_v =0 and at an opacity of 100% because at this point τ_λ =0. The uncertainty in opacity under all opacities is the largest component of the total uncertainty in ISPM and therefore

dominates. The uncertainty for O-EGR is slightly higher than the uncertainty for N-EGR due to greater uncertainty in $\dot{N}_{exh}$.

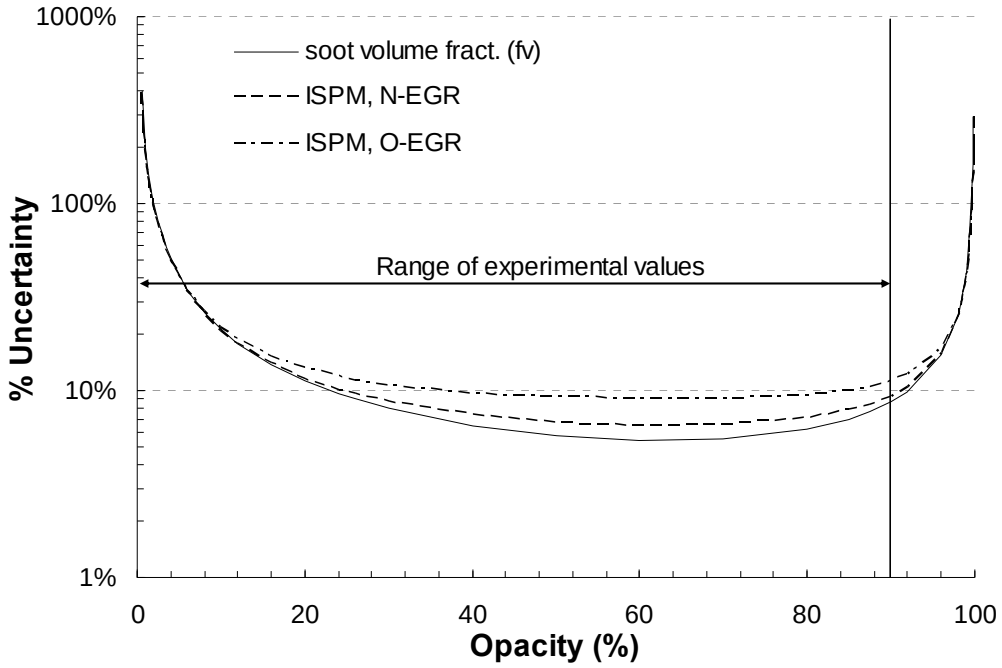

Figure 3.2. Percent uncertainty in indicated specific particulate as a function of opacity. Note that the uncertainty of soot volume fraction dominates.

An expression for the percent uncertainty in indicated specific NO_x ($ISNO_x$) based on Equation (3.3) is given below.

$$\frac{U_{ISNO_x}}{ISNO_x} = \sqrt{\left(\frac{U_{xNO_x}}{xNO_x}\right)^2 + \left(\frac{U_{\dot{N}_{exh}}}{\dot{N}_{exh}}\right)^2 + \left(\frac{U_{P_{ig}}}{P_{ig}}\right)^2} \tag{3.18}$$

An estimate for the uncertainty in xNO_x of 1.0% was used based on typical random errors in experimental data. Using the component uncertainties, the total uncertainty for indicated specific NO_x becomes 3.7% for N-EGR and 7.3% for O-EGR. Error bars will be shown in the results section for estimated uncertainties in the data.

4 Results and Discussion

4.1 NO_x and Particulate for N-EGR and O-EGR

Experimental runs for the N-EGR and O-EGR consisted of sweeps of 4-6 set points of increasing levels of EGR at each of three target equivalence ratios with the engine operating at steady-state. The engine was considered to be at steady-state when temperature and emissions measurements stopped changing. Three runs were conducted at each equivalence ratio in order to ensure repeatability of the data. Each run started with a reference set point for which no EGR was used. For N-EGR, the intake gas temperature was maintained at roughly 50ºC throughout all runs using a resistance heater, while for O-EGR the intake temperature was varied as explained in Section 3.2. Experimental data for all N-EGR and O-EGR runs are presented Appendix G.

Target versus actual equivalence ratios for the N-EGR and O-EGR runs are given in Table 4.1 below. Although the mean equivalence ratios deviated slightly from the targets, the standard deviations were small with respect to the means (within approximately 4% for each case). Thus, although the targets were not achieved precisely, the equivalence ratios were maintained roughly constant, indicating that the O_2 flow rate was maintained constant over all EGR fractions at each of the three engine loads. From Table 4.1 it can be seen that the equivalence ratios varied a little between N-EGR and O-

EGR runs. However, as the equivalence ratios were similar and were chosen simply to represent three varied loads each for EGR and O-EGR, for most purposes they can be treated as equivalent.

Table 4.1. Target versus actual equivalence ratios

Target ϕ		Actual Range	Mean	Std. Dev.	% Dev.
N-EGR	0.33	0.30-0.33	0.32	0.01	3.1%
	0.50	0.50-0.57	0.53	0.02	3.8%
	0.65	0.66-0.67	0.67	0.01	1.5%
O-EGR	0.33	0.35-0.38	0.37	0.01	2.7%
	0.50	0.45-0.52	0.48	0.02	4.2%
	0.65	0.62-0.68	0.64	0.02	3.1%

As the EGR level was increased during each sweep, the composition of the intake gases changed. For the N-EGR cases, the N_2 concentration remained relatively constant with increasing EGR, while the CO_2 concentration increased and the O_2 concentration decreased. The H_2O concentration in the intake remained essentially zero because the EGR was cooled sufficiently to condense out virtually all of the water. For the O-EGR cases, the N_2 concentration decreased significantly with increasing EGR because CO_2 and H_2O replaced N_2 rather than adding to it. Additionally, the CO_2 concentrations for O-EGR were significantly higher than for N-EGR. The O_2 concentration on a dry basis (not accounting for H_2O) for the O-EGR cases was maintained roughly constant due to the addition of pure O_2. However, H_2O was no longer insignificant because the EGR was not cooled as much as in the N-EGR cases. Thus, due to the increasing H_2O concentration, at high levels of EGR the O_2 concentration on a wet basis (accounting for H_2O) decreased slightly. Intake gas compositions for representative sweeps with N-EGR and O-EGR are

given in Table 4.2. H_2O concentrations were estimated based on the saturation pressures and flow rates of the EGR as explained in Appendix C. It can be seen from Table 4.2 that the EGR fractions in the O-EGR case were significantly higher than in the N-EGR case.

Table 4.2. Intake gas compositions, N-EGR (ϕ=0.32, run 2), O-EGR (ϕ=0.37, run 2)

N-EGR	**% EGR**	**0%**	**11%**	**24%**	**35%**	**53%**
	xN_2	0.792	0.794	0.797	0.799	0.804
	xCO_2	0.001	0.006	0.014	0.023	0.041
	xO_2	0.208	0.200	0.189	0.178	0.155
	xH_2O	0.000	0.001	0.002	0.003	0.005
O-EGR	**% EGR**	**0%**	**47%**	**66%**	**74%**	**81%**
	xN_2	0.792	0.738	0.650	0.583	0.511
	xCO_2	0.000	0.049	0.096	0.134	0.174
	xO_2	0.207	0.209	0.197	0.188	0.182
	xH_2O	0.000	0.004	0.060	0.105	0.152

Ignition delay, combustion timing, and combustion duration can all have impacts on cylinder temperature, flame temperature, and fuel air mixing, all which impact the emissions of interest. It would be ideal to produce identical heat release patterns for all set points in order to isolate the impacts of gas compositions, though in these experiments the coarseness of adjustments that could be made to the combustion process (adjustments to intake temperature) only allowed rough matching of the heat release patterns. Heat release plots were used to provide a qualitative indication of how well ignition delays and combustion durations matched in each case. Figure 4.1 shows AHRR profiles for N-EGR at the target equivalence ratio of 0.50. The initial drop in the heat release curves with a minimum near -2 crank angle degrees (CAD) is caused by evaporation of fuel producing an apparent negative heat release. The rapid increase in heat release from -2 to +2 CAD is

caused by the burning of fuel evaporated prior to ignition. The area under this first peak represents the heat released from the initial premixed burn and is an indication of ignition delay. The longer the ignition delay, the larger the area of the premixed burn will be. Following the initial premixed burn the majority of the fuel burns in the main combustion process called the diffusion burn. From this figure it can be seen that increasing EGR in the N-EGR case produced little change in the ignition delay (less than 1 CAD) or the relative size of the premixed versus diffusion burn. Because these changes were small and on the same order of magnitude as the uncertainty (1−2 CAD), there was no need to adjust the intake temperature (~50˚C).

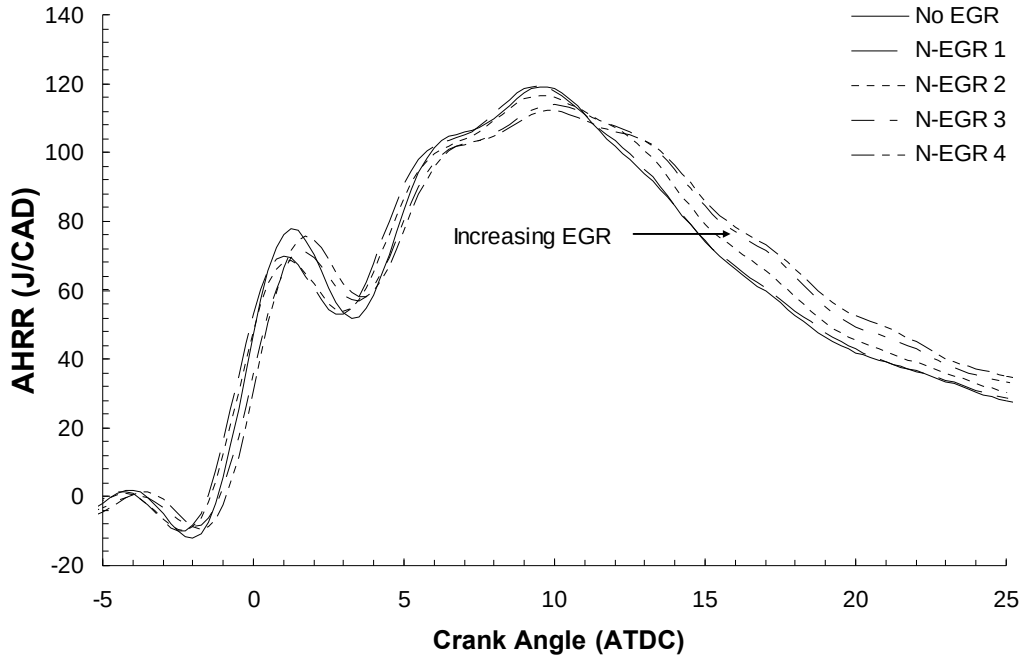

Figure 4.1. AHRR for N-EGR (ϕ=0.53, run 3)

Figure 4.2 shows AHRR for O-EGR at the target equivalence ratio of 0.50 when a constant intake plenum temperature (~35°C) was used for increasing levels of EGR.

This figure shows that the changes in ignition delay (as much 6 CAD) and relative size of the premixed combustion with increasing EGR were more pronounced than in the N-EGR case. This was attributed to a decrease in TDC bulk temperature caused by the lower specific heat ratio from CO_2 and H_2O displacing a large portion of the nitrogen. In this case the difference in TDC bulk temperature for no EGR and high EGR for with 20% CO_2 in the intake mixture was calculated to be around 100°C. (A detailed explanation of how bulk in-cylinder temperature was calculated is given in Appendix C).

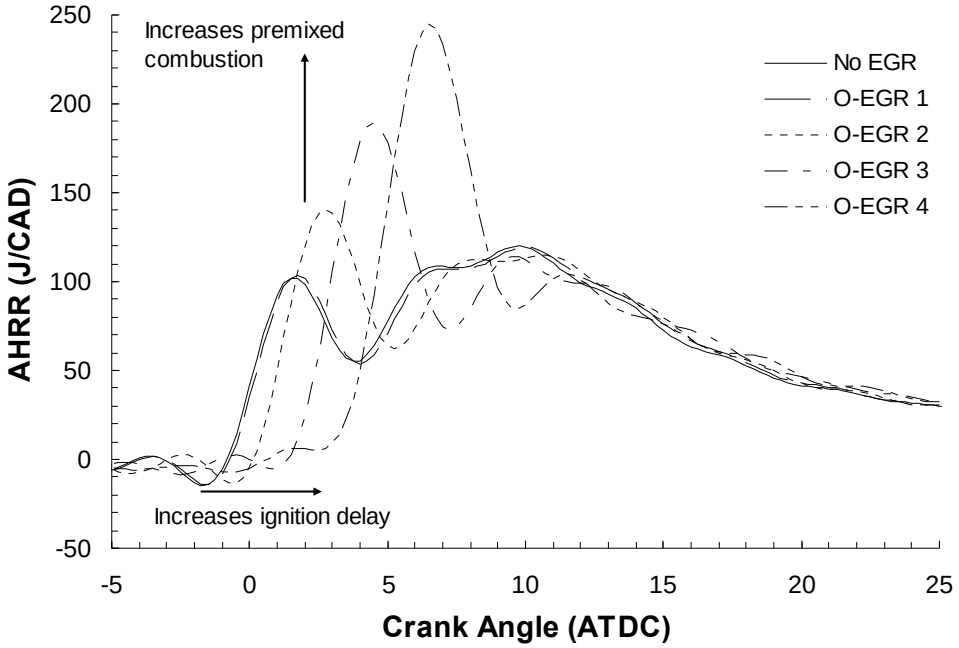

Figure 4.2. AHRR for O-EGR (ϕ~0.5) with constant intake temperature. Effects of lowering TDC temperature on AHRR curve are indicated by arrows.

An attempt was made to match the ignition delays at all EGR levels by increasing the intake temperature as O-EGR was increased using a combination of an electric heater and decreased cooling of the EGR to achieve the desired temperature. Increasing the

intake temperature succeeded in bringing the TDC temperatures for no EGR and high EGR to within approximately 30°C of one another. Better matching of the TDC temperatures than this was difficult to achieve partially due to the assumption of constant specific heat used in calculating the required intake temperature, and partially due to limited heating capacity. With intake heating, substantial improvement in matching ignition delays (within 1 – 2 CAD) was achieved, which can be seen in Figure 4.4. Differences in initial premixed burn fraction and diffusion burn were significantly reduced. Figure 4.4 plots AHRR for the highest EGR and no EGR levels for the N-EGR case and O-EGR case with intake temperature adjustment. The O-EGR profiles have slightly higher initial premixed burn areas but similar diffusion burn periods.

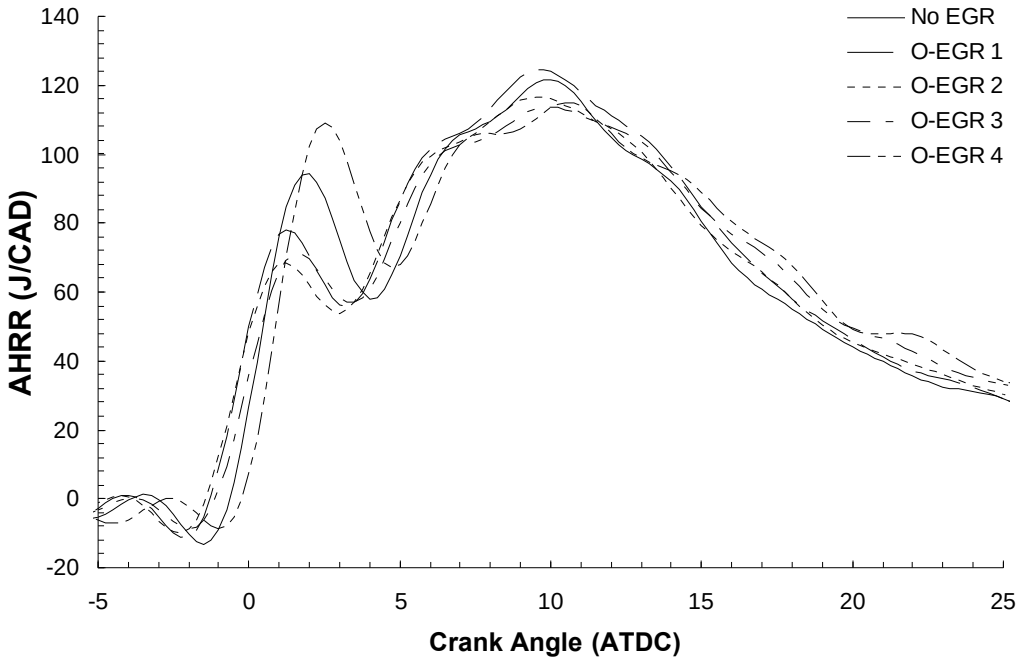

Figure 4.3. AHRR for O-EGR (ϕ=0.48, run 2) with adjusted intake temperature.

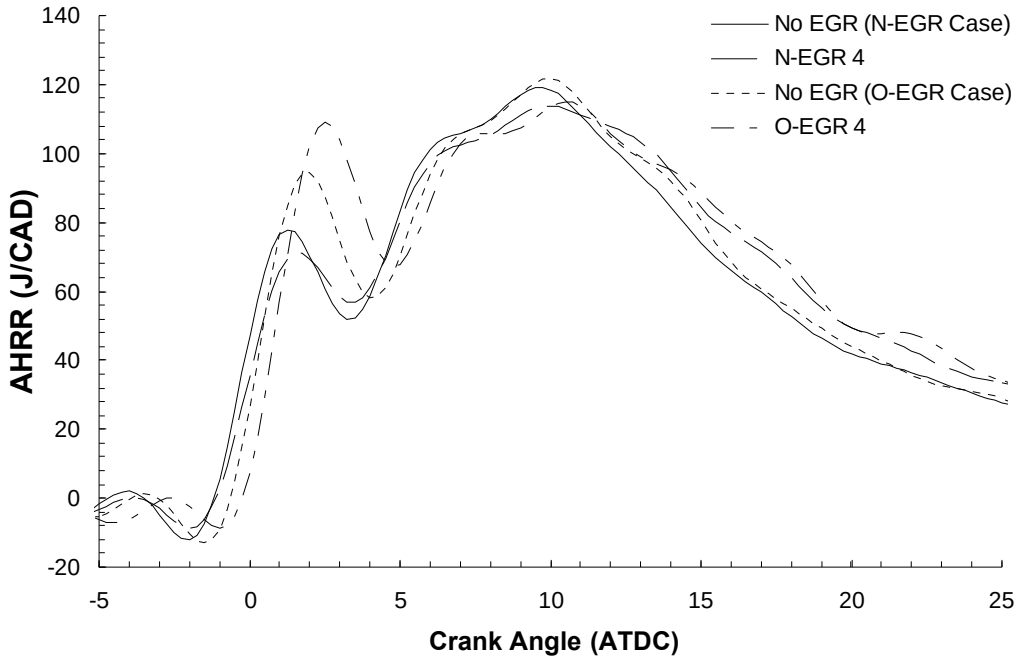

Figure 4.4. AHRR for N-EGR (ϕ~0.53, run 3) and O-EGR (ϕ~0.48, run 2) with adjusted intake temperature. No EGR and highest EGR levels shown for each.

Figure 4.5 to Figure 4.7 present indicated specific NO_x and particulate data for the N-EGR and O-EGR cases. The results for N-EGR at all three equivalence ratios produced the classic NO_x-particulate tradeoff typical of conventional diesel combustion. Increasing EGR reduced NO_x emissions but also increased particulate emissions. At low levels of EGR, NO_x reduction occurred with little increase in particulate, but as the level of EGR continued to increase, particulate emissions began to rise rapidly. For O-EGR, however, particulate emissions remained relatively constant with increasing EGR at all three equivalence ratios. It should be noted that for O-EGR at ϕ~0.33 and ϕ~0.50 the opacity was often below the limit of the meter to detect it. For these points the indicated specific particulate emissions are plotted as zero though in reality particulate emissions were not completely eliminated. Uncertainties are indicated with error bars in the plots.

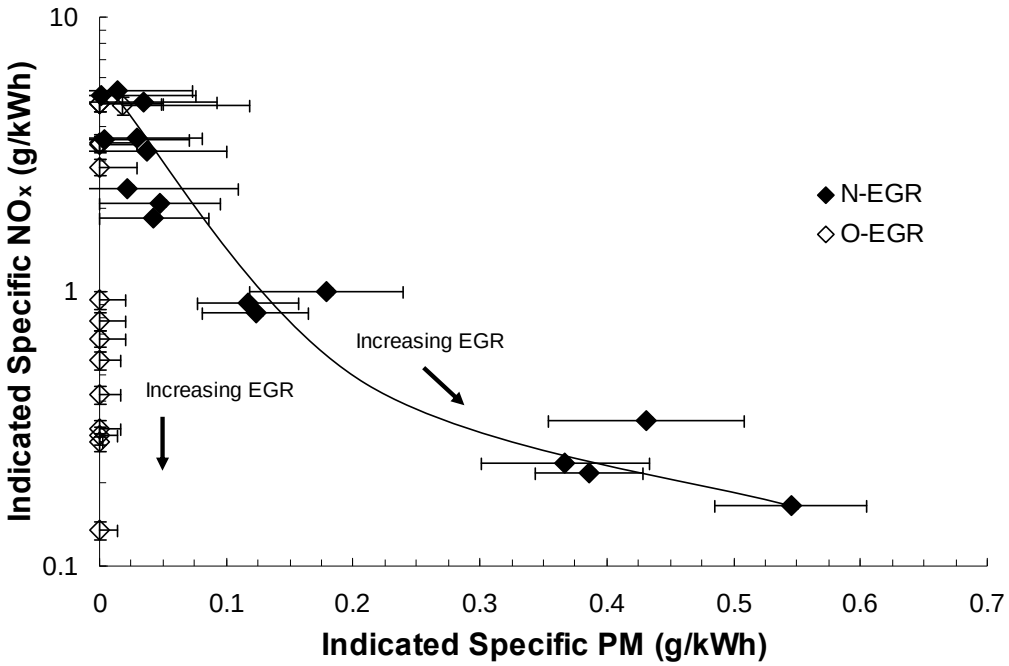

Figure 4.5. NO_x and particulate for N-EGR and O-EGR , ϕ~0.33

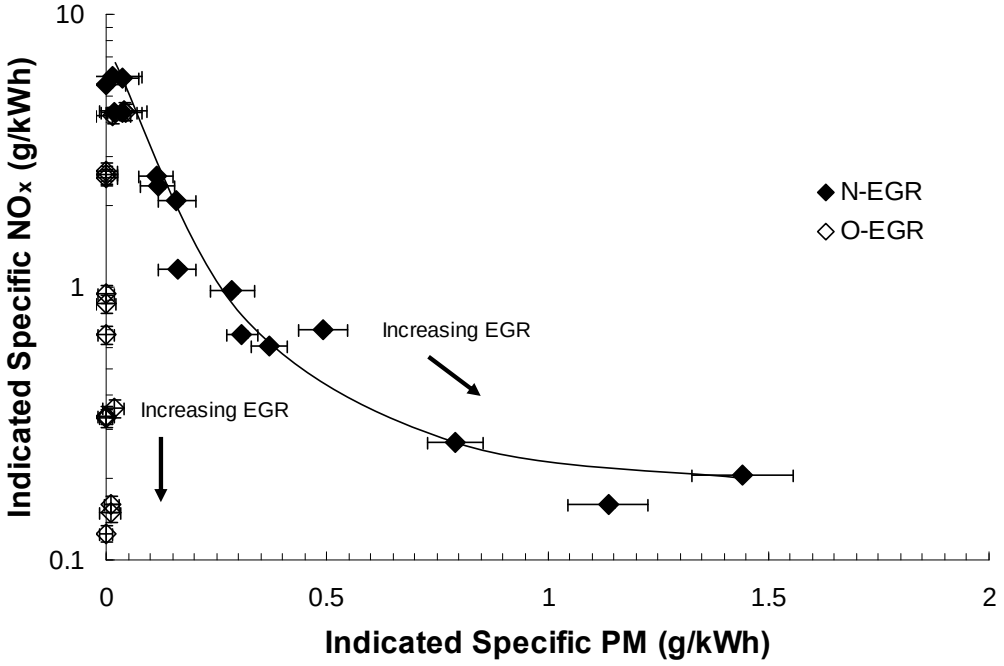

Figure 4.6. NO_x and particulate for N-EGR and O-EGR, ϕ~0.50

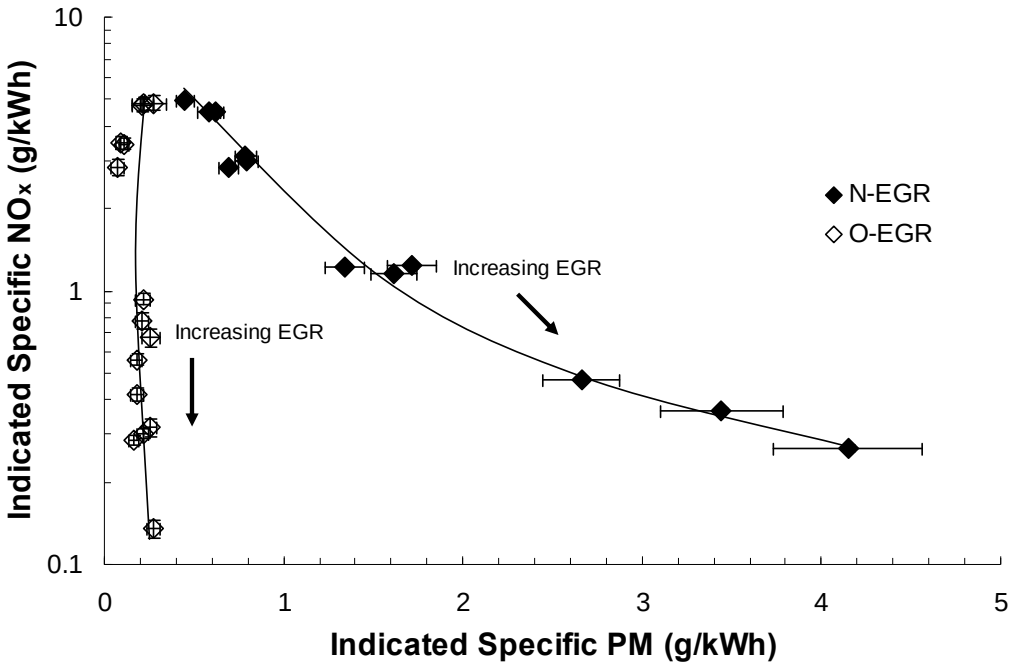

Figure 4.7. NO_x and particulate for N-EGR and O-EGR, ϕ~0.65

4.2 Discussion of O-EGR Effects on NO_x

Chapter 2 discussed three means through which EGR has been shown to reduce NO_x: 1. Diluting the available oxygen, 2. Increasing the specific heat of the charge gas, and 3. Through chemical effects of dissociation. Two other effects that may become important at the high levels of EGR used in O-EGR are the reduction of flame temperature through increased dissociation and the impact of reduced N_2 availability for participation in the Zeldovich mechanism. The amount of NO_x emitted from a CI engine typically correlates with flame temperature, which can be impacted by dilution, increasing the specific heat, and dissociation. According to the global reaction rate equation for NO_x formation, Equation (2.2), a linear relationship is expected between $\log(NO_x)$ and the inverse of peak flame temperature. In this research the peak

stochiometric flame temperature was chosen to approximate the flame temperature for NO_x formation, since this is the point of highest NO_x formation. This temperature was calculated for a stoichiometric flame for each intake gas composition using the NASA-Glenn equilibrium code (McBride and Gordon, 1996). Figure 4.8 to Figure 4.10 plot indicated specific NO_x from experimental data against the inverse of the calculated peak flame temperature on a log scale. For both N-EGR and O-EGR at all three equivalence ratios the log of indicated specific NO_x correlated linearly with $1/T$ with an R^2 fit of at least 0.96. This suggests that in both the N-EGR and O-EGR cases flame temperature reduction was the dominant variable affecting NO_x. In the ϕ~0.50 and ϕ~0.65, the steeper slope of log(NO_x) as a function of peak flame temperature for O-EGR suggests that although temperature may be dominant, other variables such as differences in gas concentrations or chemical effects also played a noticeable role in NO_x reduction.

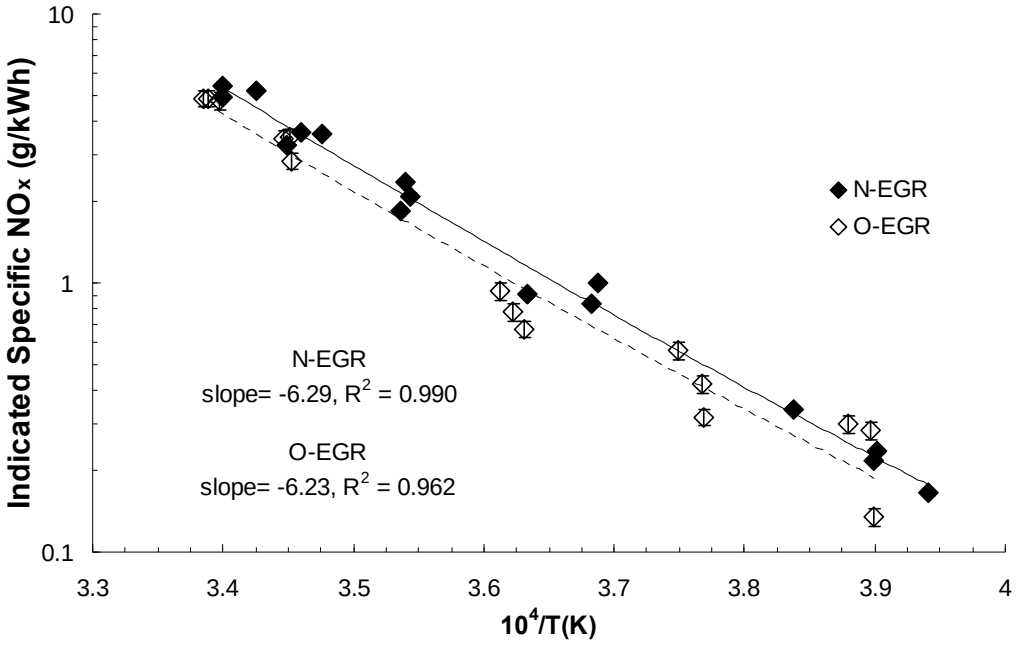

Figure 4.8. Indicated specific NO_x as a function of peak flame temperature, ϕ~0.33

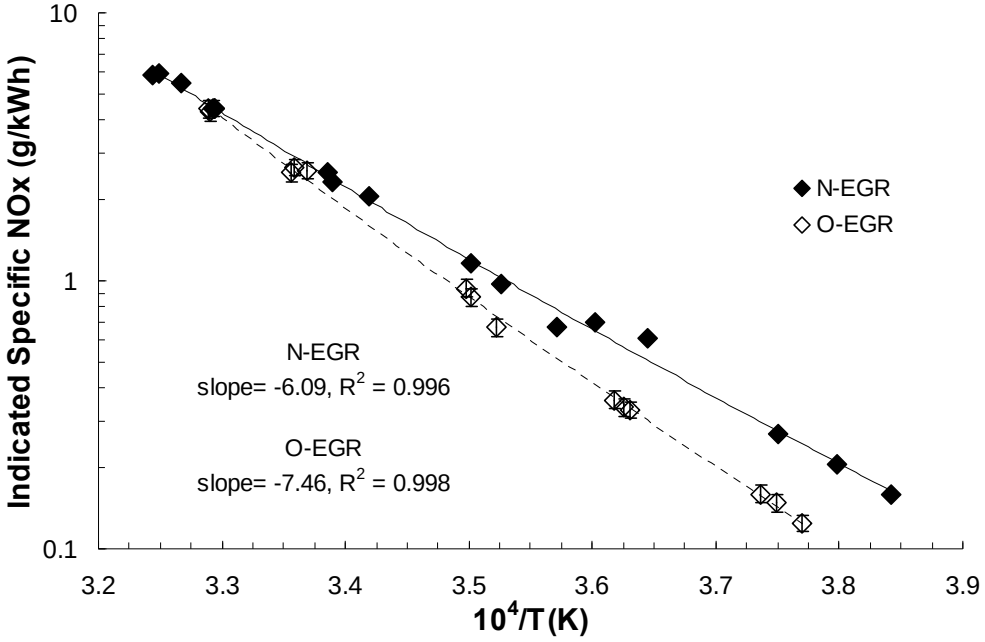

Figure 4.9. Indicated specific NO_x as a function of peak flame temperature, ϕ~0.50

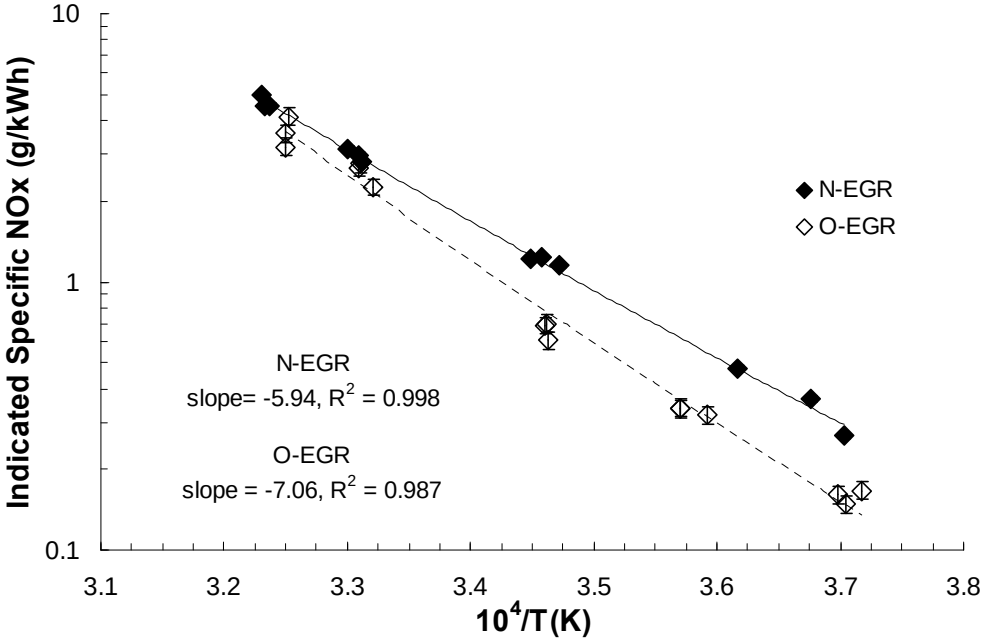

Figure 4.10. Indicated specific NO_x as a function of peak flame temperature, ϕ~0.65

The combined effects of dilution and raising the specific heat lower the flame temperature by changing the total heat absorbing capacity of the flame per mole of fuel, $N \cdot C_p$ (kJ/K/kmol-fuel), where N is the total moles of mixture per mole of fuel in a stoichiometric flame, and C_p is the specific heat of the mixture. Theoretically N-EGR and O-EGR should produce the same temperature rise at the same $N \cdot C_p$, if dissociation is neglected. Ignoring dissociation, the temperature rise of the gases in the flame can be approximated by dividing the heat released during combustion (Q, kJ/kmol) by the heat absorbing capacity of the gases ($N \cdot C_p$, kJ/K/kmol-fuel). This relationship is expressed in Equation (4.1).

$$\Delta T = \frac{Q}{N \cdot C_p} \tag{4.1}$$

The heat released is related to the availability of O_2, and hence we can think of Q being equal to a constant, C_1, multiplied by the moles of available O_2, N_{O_2}, in the stoichiometric flame, where C_1 represents factors other than O_2 which impact the heat release such as the heating value of the fuel. This relationship is expressed in Equation (4.2).

$$Q = C_1 \cdot N_{O_2} \tag{4.2}$$

Substituting (4.2) into (4.1) and dividing by N_{O_2}, the following expression results.

$$\Delta T = \frac{C_1}{\frac{N}{N_{O_2}} \cdot C_p} \tag{4.3}$$

In Equation (4.3) the separate impacts of increasing dilution, N/N_{O2}, and increasing specific heat, C_p, on temperature rise can be clearly distinguished.

Figure 4.11 plots the temperature rise during combustion versus $N/N_{O2} \cdot C_p$ for all N-EGR and O-EGR cases found using the NASA-Glenn code, which does account for dissociation. From this figure it can be seen similar temperature rises were achieved for

N-EGR and O-EGR at similar values of $N/N_{O2} \cdot C_p$. Differences in temperature rise appear to be primarily related to differences in equivalence ratios.

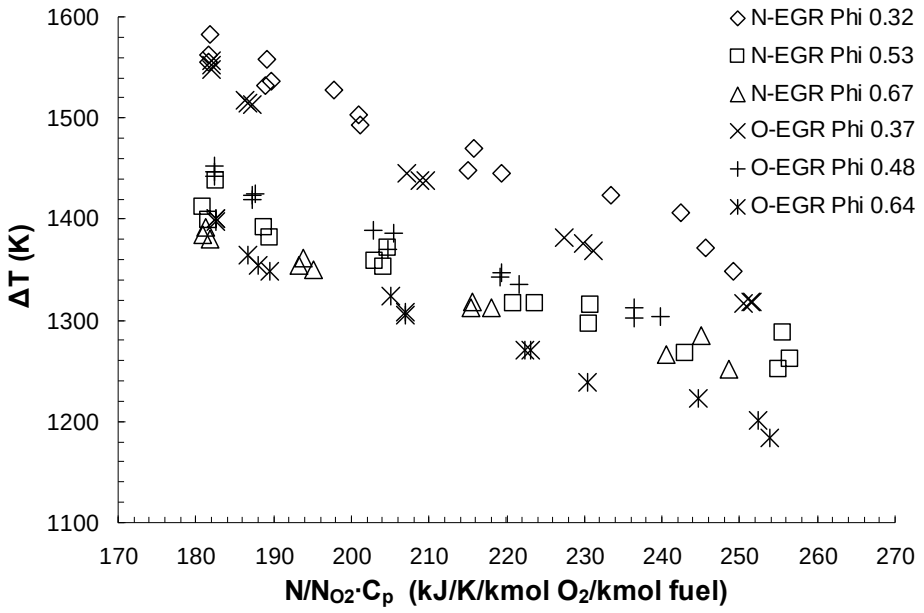

Figure 4.11. Flame temperature rise as a function of $N/N_{O2} \cdot C_p$

Although NO_x reduction correlated with flame temperature for both N-EGR and O-EGR, the relative contributions of dilution versus increasing specific heat on the total heat absorbing capacity of the cylinder gases were different in each case. In the N-EGR case, EGR acted to dilute the O_2 in the intake, whereas in the O-EGR case EGR substituted CO_2 and H_2O for N_2 in the intake without significant dilution of the O_2. Hence, flame temperature reduction is expected to be primarily from dilution (increase in N/N_{O2}) in the N-EGR case and primarily from increased specific heat (increase in C_p) in the O-EGR case. Figure 4.12 and Figure 4.13 plot the percent increase in $N/N_{O2} \cdot C_p$ as a function of EGR fraction for representative runs of N-EGR and O-EGR respectively at

ϕ~0.65. From these figures it can be seen that the increase in $N/N_{O2}\cdot C_p$ for N-EGR was almost entirely due to dilution, while for O-EGR the increase in specific heat and dilution were both important. Dilution was not present for O-EGR at the first level of EGR (5% CO_2) because H_2O was not yet significant and the O_2 intake concentration was still 21% (see discussion in Section 3.2). It can also be seen from these figures that N-EGR achieved a higher increase in $N/NO2\cdot C_p$ for a given EGR fraction. In the N-EGR a 35% increase in $N/N_{O2}\cdot C_p$ was achieved with 32% EGR, while a similar increase required 70% EGR for the O-EGR case. This implies that significantly more EGR was required to achieve the equivalent flame temperature and NO_x reduction with O-EGR, and thus dilution is a more effective way of lowering flame temperature for a given amount of EGR than increasing the specific heat.

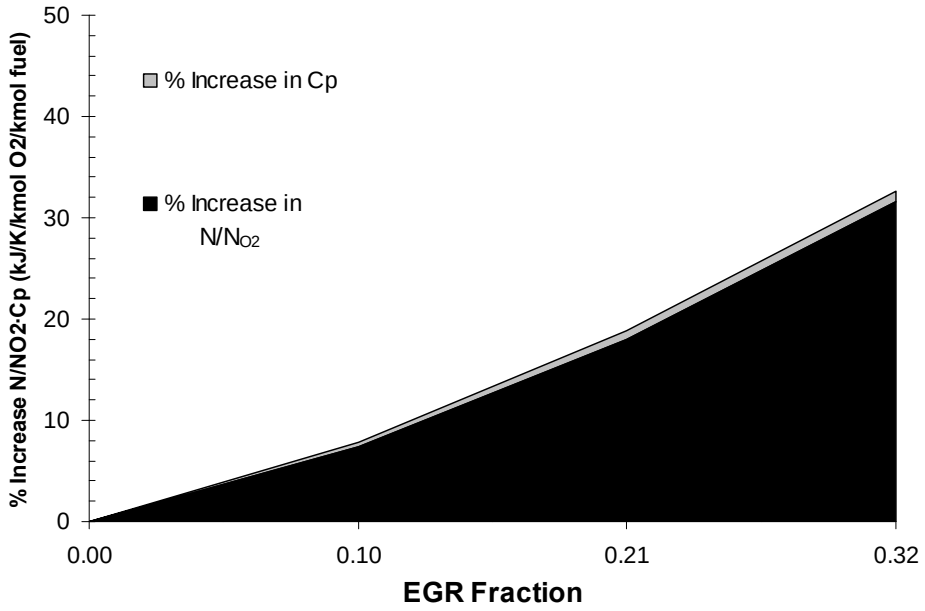

Figure 4.12. Relative contributions to rise in $N/N_{O2}\cdot C_p$ from dilution and specific heat effect, N-EGR (ϕ=0.67, run 1)

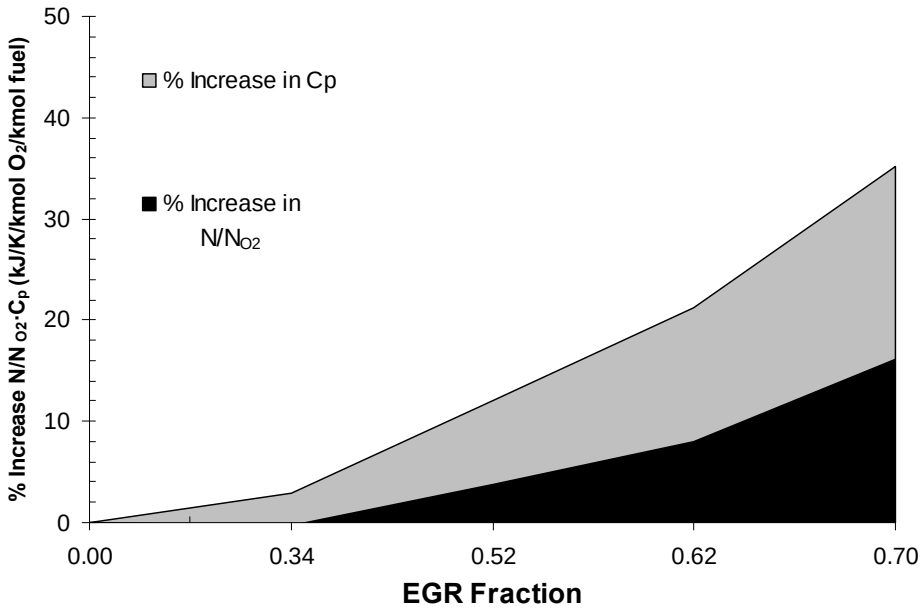

Figure 4.13. Relative contributions to rise in N/N_{O2}·Cp from dilution and specific heat effect, O-EGR (ϕ=0.64, run 1)

In Figure 4.11 it is difficult to distinguish effects of dissociation on temperature rise in the experimental data because of differences in start of combustion bulk temperatures and equivalence ratios. It might be anticipated that dissociation would be stronger and thus contribute more to lowering the flame temperature at a given $N/N_{O2} \cdot C_p$ in the O-EGR case due to the significantly increased concentrations of CO_2 and H_2O. Two test cases were run in the NASA-Glenn code in order to more precisely investigate the effect of dissociation. The two cases were chosen to mimic the gas compositions experienced during experimental N-EGR and O-EGR runs. The gas compositions used for these two cases are given in Appendix E. The same starting temperature (1500 K) and same combustion pressure (8 MPa) were used for each test case. N was determined for each gas mixture assuming a stoichiometric flame, and C_p was calculated at the corresponding peak flame temperature determined for each point.

Equilibrium concentrations of CO and OH were determined using the NASA-Glenn code and are tabulated in Appendix E and plotted in Figure 4.14 versus $N/N_{O2} \cdot C_p$. From this figure it can be seen that the concentrations of the primary dissociation species, CO and OH were predicted to be higher for the O-EGR case as expected. O-EGR may therefore produce lower flame temperatures than N-EGR at the same $N/N_{O2} \cdot C_p$ due to the dissociation of CO_2 to CO. Figure 4.15 plots the calculated temperature rise as a function of $N/N_{O2} \cdot C_p$ for each test case, from which it can be seen that the temperature rise at the same $N/N_{O2} \cdot C_p$ was indeed predicted to be somewhat lower with increasing EGR for the O-EGR case. It can be concluded that dissociation should enhance the flame temperature reduction for O-EGR, though in the experimental data this effect was secondary to the $N/N_{O2} \cdot C_p$ effect and could not be clearly separated.

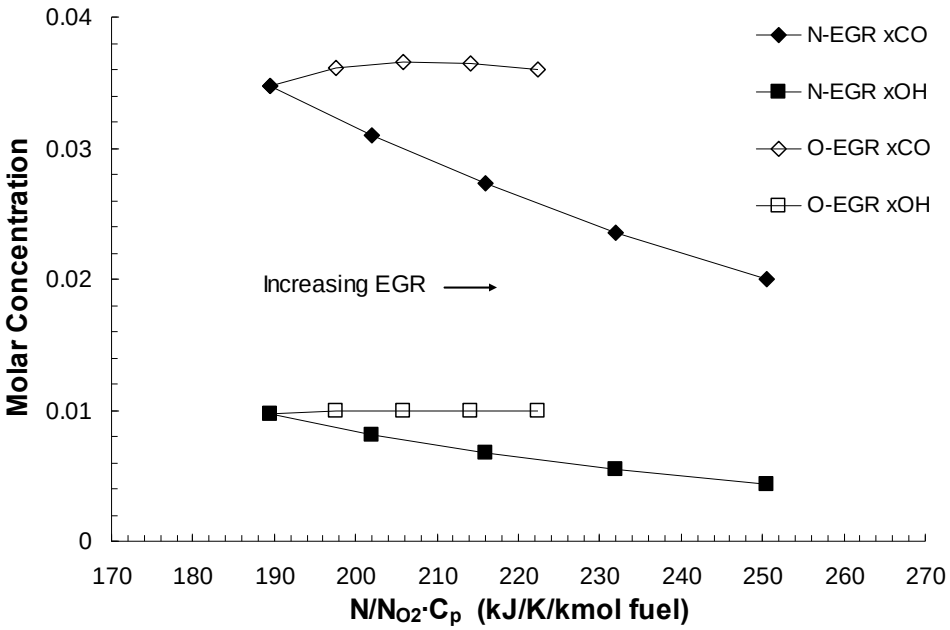

Figure 4.14. Equilibrium concentrations of CO and OH as a function of $N/N_{O2} \cdot C_p$ for two test cases

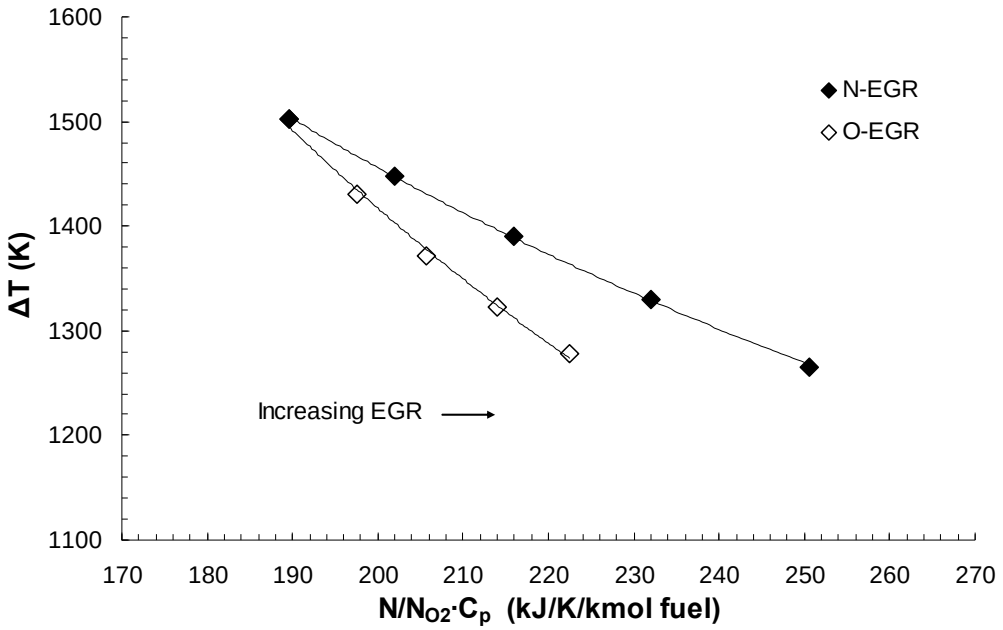

Figure 4.15. Impact of dissociation on temperature rise for two test cases

The question remains as to what role differences in N_2 concentration between N-EGR and O-EGR played in NO_x reduction. In the N-EGR case the N_2 concentration was maintained with increasing EGR whereas in the O-EGR case it decreased significantly. From the global reaction rate equation, Equation (2.2), it can be seen that NO_x formation is impacted linearly by N_2 concentration. Hence, the decreasing N_2 concentration with increasing levels of O-EGR was expected to enhance NO_x reduction above that achieved via temperature reduction, which would explain the divergence in the slopes of $\log(NO_x)$ versus 1/T in Figure 4.9 and Figure 4.10. To validate this hypothesis, a model of the two reaction Zeldovich mechanism was used. An explanation of the model is given in Appendix D. A case of constant N_2 equilibrium concentration representing N-EGR at various temperatures was considered as well as a case in which both N_2 concentration and temperature were varied to represent O-EGR. The temperature range considered (2500-

3000 K) corresponded to typical experimental stoichiometric peak flame temperatures. Theoretical NO_x values predicted by the two-reaction model are plotted in Figure 4.16.

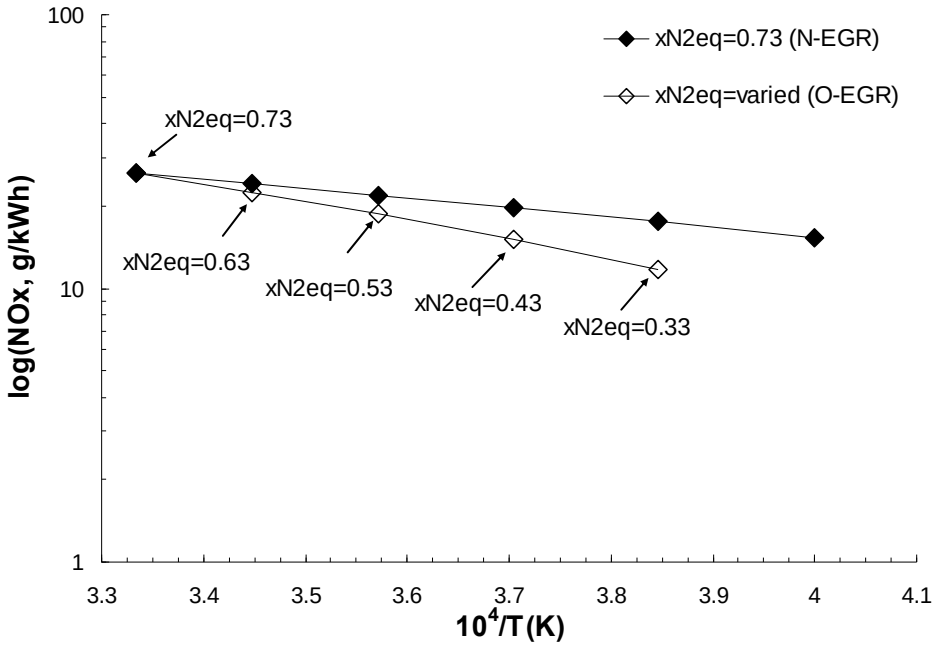

Figure 4.16. Impact of N_2 concentration on NO_x emissions predicted by two reaction mechanism

NO_x emissions predicted by the model differed from experimental values by an order of magnitude, likely due to the model's assumption that NO_x formation occured volumetrically rather than primarily near the flame. When NO_x formation was assumed to occur only in a 2 mm flame surrounding cones of fuel coming from the injectors, predicted NO_x values were on the same order of magnitude as experimental values. Despite the differences in the magnitudes between NO_x values in the model and experimental values, a similar divergence in the slopes for N-EGR versus O-EGR is seen in both the model (Figure 4.16) and the experimental data (Figure 4.9 and Figure 4.10).

The line for O-EGR in both the model and the experimental values produced a larger change in NO_x for a given change in temperature than the lines for N-EGR. The evidence thus suggests that the greater NO_x reduction observed for O-EGR over N-EGR at a given flame temperature in the experimental data at ϕ~0.50 and ϕ~0.65 was due to the decreasing N_2 concentration. It is unclear why there was little divergence in slopes between N-EGR and O-EGR at ϕ~0.33 (see Figure 4.8), though one possibility is that the significant difference in the equivalence ratios (0.32 versus 0.37) made these two slopes less comparable.

4.3 Discussion of O-EGR Effects on Particulate

The NO_x-particulate tradeoff curves in Figure 4.5 to Figure 4.7 show that NO_x reduction with N-EGR occurs only at expense of increased particulate while in the O-EGR cases no increase in particulate was observed. As discussed in Chapter 2, particulate emissions can be reduced by either decreasing the rate of particulate formation or by increasing the rate of particulate oxidation. The rate of particulate oxidation can be approximated by a global Arrhenius rate expression as given in Equation (4.4) below.

$$-\frac{d\mathrm{PM}}{dt} \propto \exp\left(\frac{-E_a}{R_u T}\right) \tag{4.4}$$

Various researchers (Plee, *et al*, 1981.; Iida, 1993) have successfully correlated particulate emissions from a CI engine with flame temperature. Flame temperature affects particulate oxidation rates with increased oxidation at higher flame temperatures. This is the opposite trend observed for NO_x formation and provides an explanation for the difficulty in reducing NO_x and particulate simultaneously. The extent of correlation of

particulate with a representative oxidation temperature will help to understand the relative importance of oxidation and formation in the experimental particulate data. For the purpose of correlating experimental data with flame temperature, the flame temperature when 90% of the fuel was burned (T90) was used. The T90 temperature was found for each set point by calculating the total heat release as a function of crank angle and finding the crank angle at which 90% of the total heat release was reached. The corresponding bulk temperature and pressure were then used in the NASA-Glenn code to find the flame temperature. Figure 4.17 helps to graphically demonstrate how the crank angle of 90% fuel burned was determined.

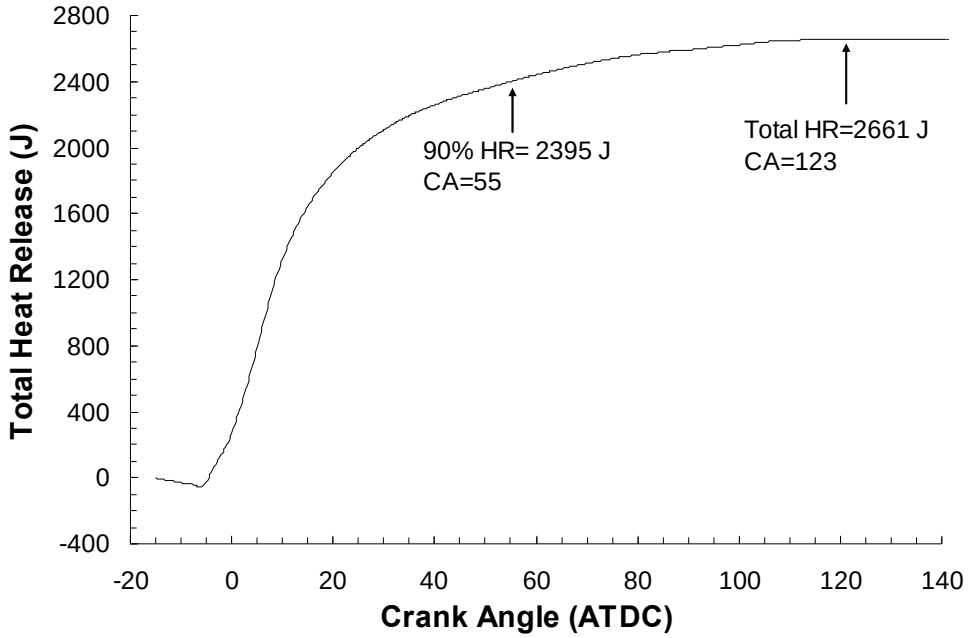

Figure 4.17. Total Heat Release as a function of crank angle, N-EGR (ϕ~0.65, run 3)

Indicated specific particulate is plotted on a log scale versus 1/T90 for each of the N-EGR and O-EGR cases in Figure 4.18 to Figure 4.20. In all of the data for O-EGR, at

the same T90 temperature particulate was lower than for N-EGR. A linear best fit line with the associated R^2 value has been calculated for each equivalence ratio. The correlation of particulate with 1/T90 for N-EGR is very good (R^2=0.99) for ϕ=0.67 with decreasing R^2 for the lower equivalence ratio cases. For O-EGR particulate showed little if any dependence on T90. Points at which low particulate levels were close to or at the low measurement limit of the smoke meter are circled on the plots. For these points the indicated specific particulate was calculated assuming an opacity of 0.5% because opacity values measured as zero yielded indicated particulate values of negative infinity on the log scale, which could not be plotted. Hence, these points could be thought of as an upper limit of particulate values based on measurement uncertainty, with additional error indicated by error bars due to calculating indicated specific particulate.

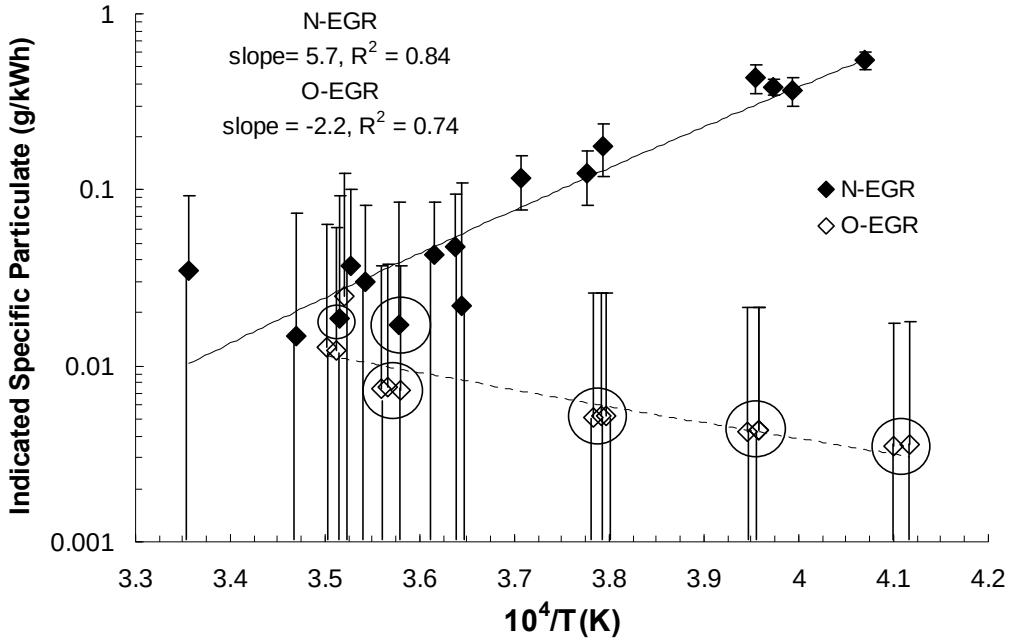

Figure 4.18. Particulate as a function of flame temperature, ϕ~0.33. Circled points are for opacity readings below the measurement uncertainty of the smoke meter, for which the an opacity of 0.5% was assumed when calculating indicated specific particulate.

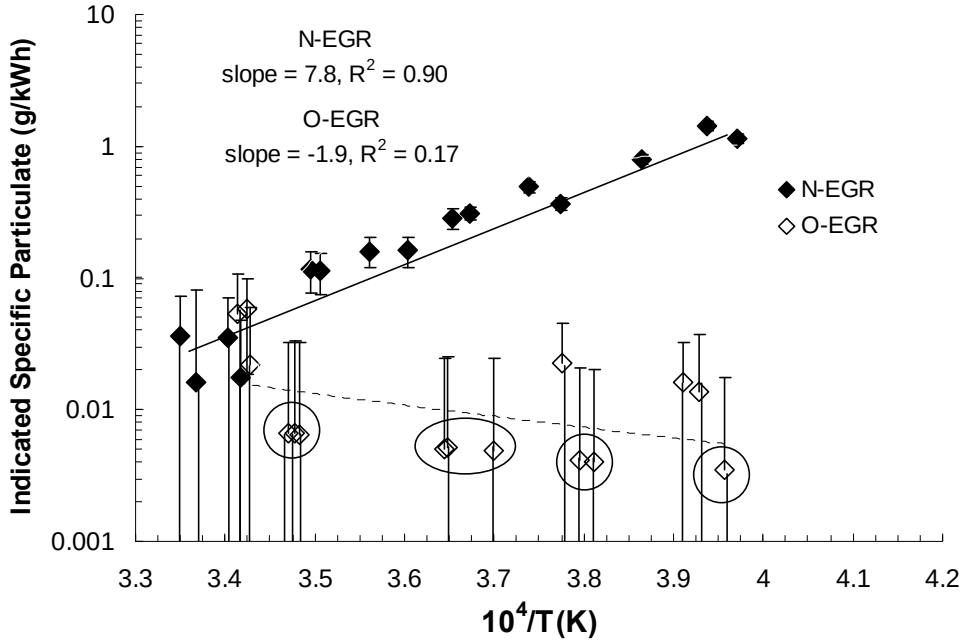

Figure 4.19. Particulate as a function of flame temperature, ϕ~0.50.

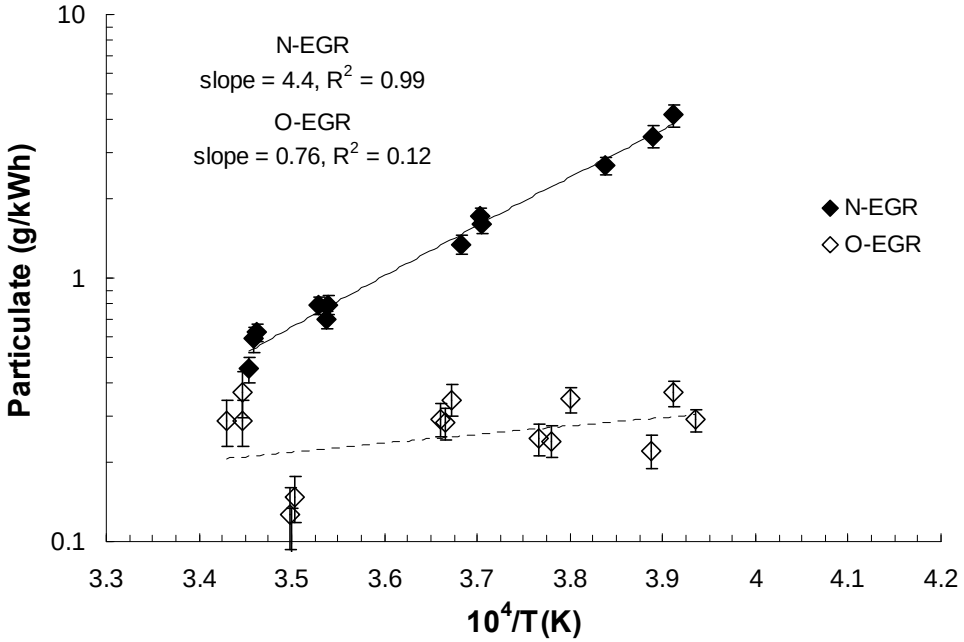

Figure 4.20. Particulate as a function of flame temperature, ϕ~0.65

Siebers and Higgins (2001) show that increasing cylinder density as was done during the N-EGR sweeps to keep the total cylinder O_2 flow constant as the O_2 concentration decreased, produces little change in the mass of oxidizer entrained in a fuel jet. Therefore, as N-EGR was increased the total mass of entrained gas remained constant, yet the decreasing O_2 concentration produced an overall decrease in the amount of entrained O_2. This increased the amount of soot formed while the increased concentration of diluents decreased the flame temperature and hence decreased soot oxidation. The strong correlation of T90 with particulate emissions must be due to the temperature capturing both effects of increased formation and decreased oxidation. In the O-EGR sweeps O_2 concentration was held relatively constant, and therefore the amount of O_2 entrained in the fuel jet was expected to have remained constant. As flame temperature decreased one would have expected the lower oxidation rates and in increase in exhaust particulate, but this was not the case. Therefore, chemical effects from increased CO_2 and H_2O concentrations are thought to have contributed to reducing soot formation and/or increasing soot oxidation. The ability of CO_2 to suppress soot formation in diffusion flames has been well documented in literature as discussed in Chapter 2.

Equilibrium concentrations of dissociated species in a rich flame can give an idea of how varying CO_2 concentration could impact soot formation. Two test cases representing N-EGR and O-EGR were run using the NASA-Glenn code to determine their relative equilibrium concentrations in a rich pre-mixed flame. Intake gas compositions were chosen to mimic those achieved in actual engine tests for N-EGR and O-EGR, and are given in Appendix E. The equivalence ratio of the rich flame was assumed to be 4.0 in both cases, which is a typical for a diesel flame (Dec, 1998). The

initial temperature of the reactants was 800 K and the pressure was 8 MPa, which were representative of values seen at the start of combustion for the experimental runs. Figure 4.21 plots two of the major rich flame equilibrium species, CO and C_{gr}, predicted for the N-EGR and O-EGR test cases as a function of the corresponding peak flame temperatures.

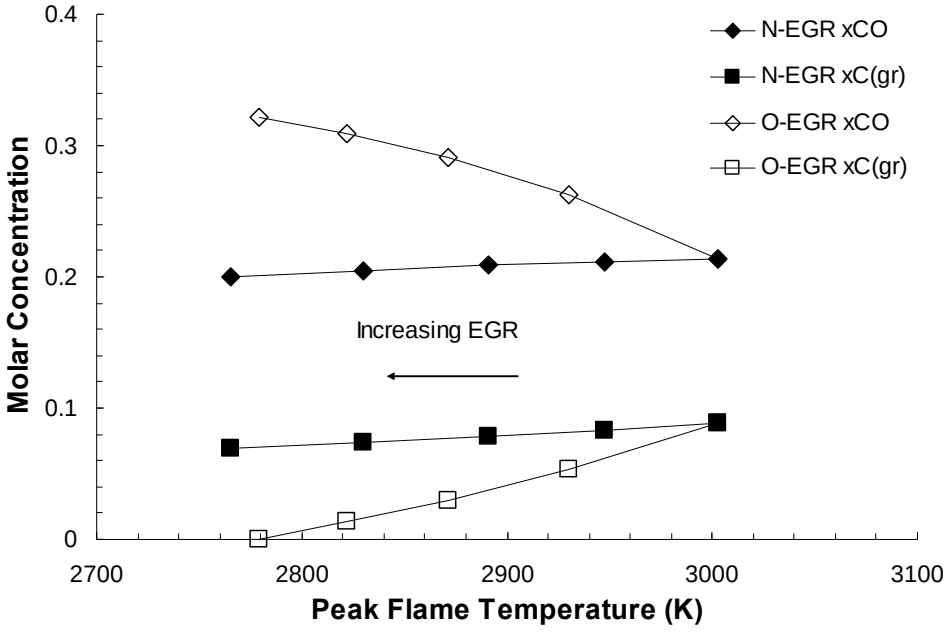

Figure 4.21. Fuel-rich flame equilibrium concentrations for representative N-EGR and O-EGR intake gas compositions

Although the values plotted are equilibrium values and do not represent transient values (which can admittedly be lower or higher than equilibrium), they give some indication of the driving forces behind reaction rates. The concentration of CO remained relatively constant as N-EGR was increased, while it increased significantly with increasing O-EGR. This may indicate the increased significance of the reaction $O_2 + H \rightarrow CO + OH$ due to higher CO_2 concentrations, which according to Guo and

Smallwood (2008) would result in decreased formation of PAH, a component of particulate. The concentration of solid carbon decreased and approached zero with increasing O-EGR but decreased much more gradually with increasing N-EGR. This suggests that intermediate species of soot formation may also be lower in the O-EGR cases. The above reaction suggests that when the CO_2 concentration is higher, OH will increase, which is the primary species responsible for soot oxidation. The equilibrium calculations for both a fuel-rich and stoichiometric flame support the conclusion that CO_2 produces a chemical effect that reduces soot formation and perhaps increase soot oxidation in diesel flames.

4.4 Using O-EGR to Shift the NO_x-Particulate Tradeoff Curve

In the experimental O-EGR cases external O_2 tanks were used to maintain the total intake O_2 concentration relatively constant with increasing EGR. If the amount of O_2 addition had been limited the total O_2 concentration of the cylinder oxidizer could not have been maintained as EGR was increased. Data for this type of operating condition were not collected, yet are of interest in determining the benefit of limited O_2 intake enhancement (for example, if the enhancement were to be provided by an air separation membrane that could increase the O_2 concentration by only 1 – 2 percent). Indicated specific NO_x reduction as a function of the fraction of added O_2 in the total intake gases was calculated as an indicator of how effective a given amount of added O_2 in conjunction with EGR was at reducing NO_x emissions, and results are plotted in Figure 4.22. For ϕ=0.48 and 0.64 data matched quadratic fit lines with R^2 values of 1.0 and 0.99 respectively. A realistic quadratic fit line could not be well matched to the ϕ=0.37 data.

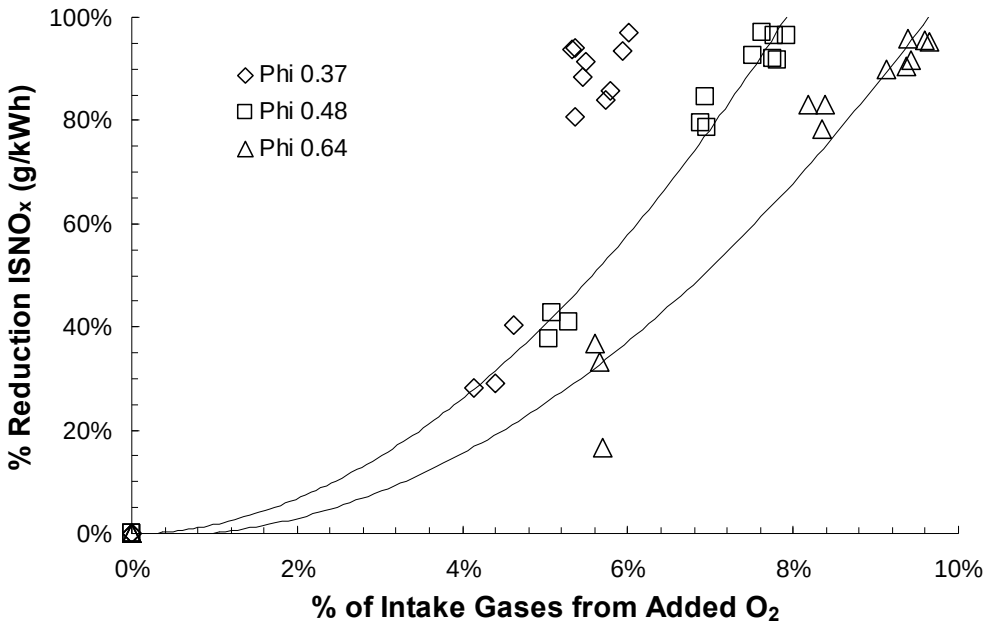

Figure 4.22. Percent reduction in indicated specific NO_x using EGR with increased portion of intake gas coming from added O_2

Shifts in the NO_x-particulate curve when using EGR with limited amounts of O_2 addition can be interpolated by assuming similarity in the shape of the curves. Shifted curves for ϕ=0.48 were interpolated using the quadratic best-fit equation for the ϕ=0.48 data in Figure 4.22 to predict by what percent the curve should shift toward the origin for a given percent of added O_2 in the intake, and are presented in Figure 4.23. Figure 4.24 is a close-up of Figure 4.22 near the origin demonstrating how the U.S. 2010 NO_x and particulate emissions standards could be achieved for the engine used in this research with EGR if 8% of the total intake gases were to come from added O_2. Although this level of oxygen enhancement may not currently be obtainable with air separation membranes, this technology could nonetheless provide part of the solution to achieving increasingly stringent diesel emissions standards.

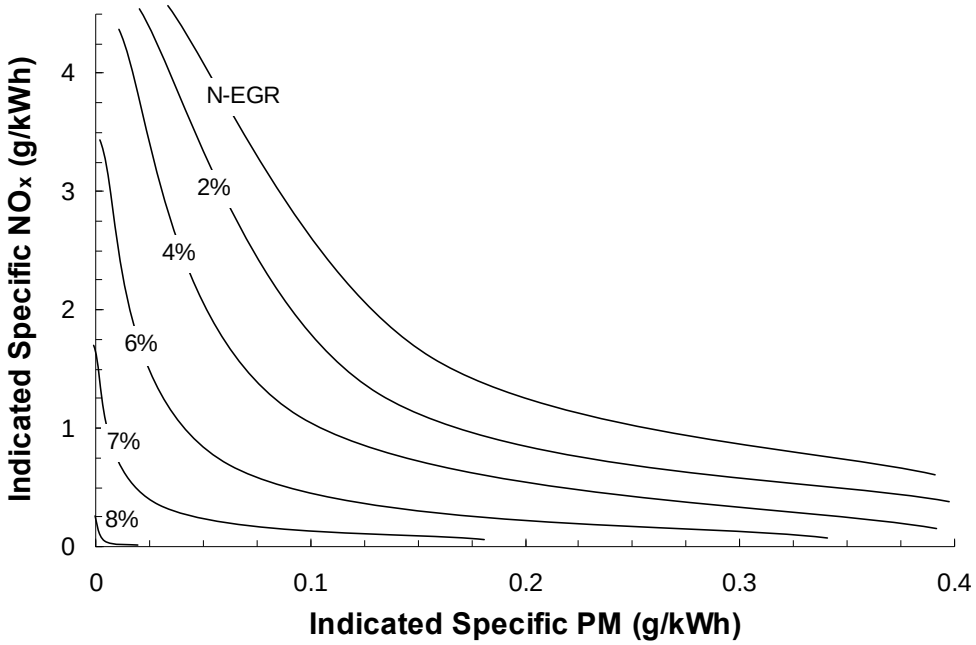

Figure 4.23. Shift in the NO_x-particulate tradeoff curve for EGR with the indicated percent of added O_2 in the intake gas, ϕ=0.48. The highest line is for N-EGR, i.e. EGR with no added O_2.

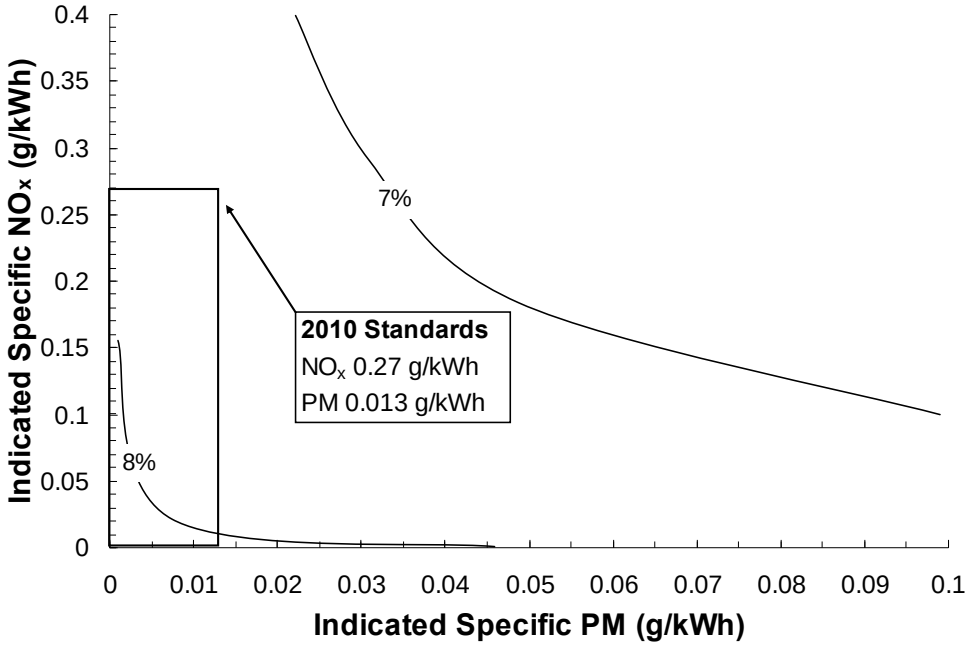

Figure 4.24. Close up of Figure 4.23. Shift in the NO_x-particulate tradeoff for EGR with the indicated percent of added O_2 in the intake gas compared to U.S. 2010 heavy-duty diesel standards, ϕ=0.48.

4.5 Challenges of O-EGR

O-EGR was effective in reducing both NO_x and particulate emissions in the experiments conducted. However, several drawbacks to O-EGR were observed which would need to be addressed if O-EGR is to be successfully implemented in working engines. One of these drawbacks was the lengthening of ignition delay due to a reduced temperature following the compression stroke. This was compensated for by increasing the intake temperature in order to prevent significant loss of engine power or unstable combustion at high levels of EGR. Although engines can easily be designed with higher compression ratios to increase the compression temperature, it would be more difficult to produce a variable compression ratio that accommodates changes in O-EGR rates. Variable valve timing may help in achieving variable compression ratios.

Another drawback of O-EGR is that the high level of H_2O in the intake and exhaust could lead to detrimental effects on the engine over time. High concentrations of water in the intake may lead to corrosion or oil contamination. After several hours of run time with O-EGR, a light grey emulsion was observed in the engine oil. The emulsion returned after oil changes and a change of the head gasket. It was determined that even at normally acceptable levels of blow-by, the high concentration of H_2O in the cylinder prior to compression could produce the observed effect of H_2O in the engine oil. Water concentrations could be reduced by cooling the EGR sufficiently to condense out most of the water.

Finally, there is the obvious issue of the source of pure oxygen required for O-EGR. Storage of compressed oxygen on vehicles is prohibitive due to cost, safety, and weight. An alternative idea is to fit the air intake with an oxygen separation membrane

for which the needed pressure could be supplied by the turbocharger. This could allow the oxygen concentration of the intake to be enhanced without the safety risks and other problems inherent with external oxygen tanks. Air separation membranes have been tested on a diesel engine by Poola *et al.* (2000) for the purpose of increasing intake nitrogen concentration and decreasing NO_x. The current level of O_2 enhancement achievable based on these published data would be on the level of 1-2% of the intake flow being added as O_2.

5 Summary and Conclusions

Experimental tests were conducted to evaluate the benefits of using oxygen enhancement in conjunction with EGR to reduce NO_x and particulate emissions from a CI engine. Tests were conducted at three equivalence ratios using both normal EGR (N-EGR) and oxygen-enhanced EGR (O-EGR) to compare emissions between these two methods of modifying the combustion process. Indicated specific emissions values were determined for NO_x and particulate by normalizing the emissions measurements by gross indicated power output. The peak and 90% burned adiabatic flame temperatures were calculated for each run and correlated with indicated specific NO_x and indicated specific particulate respectively. NO_x formation was modeled using the two-reaction Zeldovich mechanism to investigate the impact of decreasing the intake N_2 concentration in O-EGR. The effect of increased dissociation from higher CO_2 concentrations on flame temperature was also investigated. The role of rich flame equilibrium chemistry for different intake compositions on particulate reduction was considered. The most significant results are given below.

1. NO_x reduction for both EGR and O-EGR correlated well with the peak adiabatic flame temperature of the combustion process.

2. O-EGR produced somewhat lower NO_x emissions for ϕ~0.50 and ϕ~0.65 at equivalent flame temperatures than N-EGR. This reduction agrees well with trends produced in models caused by reduced N_2 intake concentrations.
3. Calculations of total heat absorbing capacity ($N \cdot C_p$) for N-EGR and O-EGR intake gas compositions suggest flame temperature reductions for N-EGR were produced primarily by dilution while flame temperature reductions for O-EGR were produced by a combination of dilution and increased heat capacity of CO_2 and H_2O. It took significantly more (approximately twice as much) EGR to produce a given temperature reduction with O-EGR than it did with N-EGR.
4. Both N-EGR and O-EGR produce dissociated products which lower flame temperature, but the increased concentrations of CO_2 and H_2O contribute more to flame temperature reduction in O-EGR than N-EGR.
5. Indicated specific particulate emissions increased with increasing EGR for the N-EGR cases but remained constant or decreased for the O-EGR cases. Decreasing O_2 concentrations with increasing N-EGR and relatively constant O_2 concentrations with increasing O-EGR likely contributed to these trends.
6. Indicated specific particulate emissions correlated with 90% burned (T90) flame temperatures for the N-EGR cases but not for the O-EGR cases.
7. Increased intake CO_2 concentrations were predicted by the NASA-Glenn code to generate more CO in the fuel-rich flame for O-EGR than for N-EGR. These equilibrium model results, the experimental results, and detailed modeling results of diffusion flames in the literature suggest increased CO_2 concentrations for O-EGR help suppress the formation of soot.

8. Enhancement to the oxygen concentration in a diesel engine using O_2 separation membranes in conjunction with EGR would allow the NO_x-particulate tradeoff to be shifted closer to the origin. Oxy-combustion could thereby supply part of the solution to achieving increasingly stringent emissions standards for diesel engines.

References

Alriksson, M., Rente, T., and Denbratt, I. "Low Soot, Low NO_x in a Heavy Duty Diesel Engine Using High Levels of EGR." SAE Paper 2005-01-3836, 2005.

Angrill, O.G., Streibel, H., Suntz, T., and Bockhornm, H. "Influence of Exhaust Gas Recirculation on Soot Formation in Diffusion Flames." *Proc. of Combustion Inst.*, 28:2643, 2000.

AutoLogic. "Heavy-Duty Diagnostic Center." (User's manual for AutoLogic MOT smoke meter.) 2006.

Bartok, W., and Sarofim, A.F. (eds.). *Fossil Fuel Combustion: A Source Book*. New York: John Wiley & Sons, 1991.

Choi, M.Y., Hamins, A., Muholand, G. W., and Kashiwagi, T. "Simultaneous Optical Measurement of Soot Volume Fraction and Temperature in Premixed Flames." *Combustion and Flame*, 99:174-186, 1994.

Cooley, W. "New Adiabatic Flame Temperature Model for NO_x Formation with Comparision of Diethyl Ether and Diesel Fuel." Ph.D. Dissertation, Brigham Young University, 2000.

Dec, J.E. "A Conceptual Model of DI Combustion Based on Laser-Sheet Imaging." SAE Paper 970873, 1997.

Donahue, R.J., and Foster, D.E. "Effects of Oxygen Enhancement on the Emissions from a DI Diesel via Manipulation of Fuel and Combustion Chamber Gas Composition." SAE Paper 2000-01-0512, 2000.

Dollmeyer, T.A, Vittorio, D.A., Grana, T.A., Katzenmeyer, J.R., Charlton, S.J., Clerc, J., Morphet, R.G., and Schwandt, B.W.. "Meeting the US 2007 Heavy-Duty Diesel Emission Standards-Designing for the Customer." SAE Paper 2007-01-4170, 2007.

Du, D.X., Axelbaum, R.L., and Law, C.K. "The Influence of Carbon Dioxide and Oxygen as Additives on Soot Formation in Diffusion Flames." *Proc. Combustion Inst*. 23:1501, 1990.

Ferguson, C.R., Tree, D.R., DeWitt, D.P., and Wahiduzzman, S.A.H. "Design, Calibration and Error Analysis of Instrumentation for Heat Transfer Measurements in Internal Combustion Engines." *Developments in Experimental Techniques in Heat Transfer and Combustion-HTD*, 71, 1987.

Guo, H., and Smallwood, G.J. "A Numerical Study on the Influence of CO_2 Addition on Soot Formation in an Ethylene/Air Diffusion Flame." *Combustion Science Technology*, 180:1695-1708, 2008.

Haynes, B.S., and Wagner, H.G.G. "Soot Formation." *Progress in Energy and Combustion Science*, 7:229-273, 1981.

Helmantel, A. "Reduction of NO_x Emissions from a Light Duty DI Diesel Engine in Medium Load Conditions with High EGR Rates." SAE Paper 2008-01-0643, 2008.

Heywood, J.B. *Internal Combustion Engine Fundamentals*. Mc-Graw Hill, 1988.

Idicheria, C.A., and Pickett, L.M. "Soot Formation in Diesel Combustion under High-EGR Conditions." SAE Paper 2005-01-3834, 2005.

Iida, N. "Surrounding Gas Effects on Soot Formation and Extinction Observation of Diesel Spray Combustion Using a Rapid Compression Machine." SAE Paper 930603, 1993.

Kee, R. J., Rupley, F. M., and Miller, J. A. "The Chemkin Thermodynamic Data Base." Sandia Report, SAND87-8215B, reprinted March 1991.

Ladommatos, N.S., Abdelhalim, M., Zhao, H., and Hu, Z. "The Effects of Carbon Dioxde in Exhaust Gas Recirculation on Diesel Engine Emissions." *Proc. IMechE*, 212: Part D, 1998.

Liu, F., Guo, H., Smallwood, G.J., and Gülder, Ö. "The Chemical Effects of Carbon Dioxide as an Additive in an Ethylene Diffusion Flame: Implications for Soot and NO_x Formation." *Combustion and Flame*, 125:778-787, 2001.

McBride, B.J., and Gordon, S. "Computer Program for Calculation of Complex Chemical Equilibrium Compositions and Applications II. Users Manual and Program Description." NASA RP-1311, 1996.

McLintock, I.S. "The Effect of Various Diluents on Soot Production in Laminar Ethylene Diffusion Flames." *Combustion and Flame*, 12:217, 1968.

Neeft, J.P., Makkee, A.M., and Moulijn, J.A. "Diesel Particulate Emission Control." *Fuel Processing Technology*, 47:1-69, 1996.

Nikolic, D., and Iida, N. "Effects of Intake CO_2 Concentrations on Fuel Spray Flame Temperatures and Soot Formations." *Proc. IMechE*, 221: Part D, 2007.

Oh, K.C., and Shin, H.D. "The Effect of Oxygen and Carbon Dioxide Concentration on Soot Formation in Non-premixed Flames." *Fuel*, 85:615, 2006.

Plee, S.L., Ahmad, T., Meyers, J.P., and Siegla, D.C. "Effects of Flame Temperature and Air-Fuel Mixing on Emission of Particulate Carbon from a Divided-chamber Diesel Engine." *Particulate Carbon—Formation During Combustion*. Plenum Press, New York, pp. 423-487, 1981.

Poola, R.B., Longman, D.E., Anderson, J.L., Callaghan, K., Nesmer, S., and Bell, R. "Membrane-Based Nitrogen-Enriched Air For NO_x Reduction in Light-Duty Diesel Engines," SAE Paper 2000-01-0228, 2000.

Rakopoulos, C.D., Hountalas, D.T., Zannis, T.C., and Levendis, Y.A. "Operational and Environmental Evaluation of Diesel Engines Burning Oxygen-Enriched Intake Air or Oxygen-Enriched Fuels: A Review." SAE Paper 2004-01-2924, 2004.

Siebers, D., and Higgins, B. "Flame Lift-off on Direct-Injection Diesel Sprays Under Quiescent Conditions." SAE Paper 2001-01-0530, 2001.

Siebers, D.L. "Scaling Liquid-Phase Fuel Penetration in Diesel Sprays Based on Mixing-Limited Vaporization." SAE Paper 1999-01-0528, 1999.

Stanglmaier, R.H., and Roberts, C.E. "Homogeneous Charge Compression Ignition (HCCI): Benefits, Compromises, and Future Engine Applications." SAE Paper 1999-01-3682, 1999.

Tree, D.R., and Svensson, K.I. "Soot Processes in Compression Ignition Engines," *Progress in Energy and Combustion Science Technology*, 33:3, 2007.

Turns, S.R. *An Introduction to Combustion, 2nd Ed.* McGraw-Hill, 2000.

Wark, K. *Advanced Thermodynamics for Engineers*. McGraw-Hill, 1995.

Appendix A. Calculated Values

A.1 Gross Indicated Power (P_{ig})

In-cylinder pressure measurements (P) were used to find the gross indicated work (W_{ig}) per engine cycle by integrating $P \cdot dV$ over the power stroke of the engine, i.e. -180 to 180 CAD.

$$W_{ig} = \oint P \cdot dV \tag{A.1}$$

W_{ig} was converted to gross indicated power, P_{ig} by multiplying W_{ig} by the time to complete one engine cycle as given below, where N is the engine speed.

$$P_{ig} = W_{ig} \cdot \frac{N}{2} \tag{A.2}$$

A.2 Volume

Volume was given by the following expression, where R is the ratio of the connecting rod to the crank radius, and r_c is the compression ratio (Heywood, 1988).

$$V = V_c \left\{ 1 + \frac{1}{2}(r_c - 1) \left[R + 1 - \cos\theta - (R^2 - \sin^2\theta)^{\frac{1}{2}} \right] \right\} \tag{A.3}$$

The derivative of volume was then given by the following expression:

$$dV = \frac{V_c}{2}(r_c - 1)(\sin\theta)\left[1 + \frac{\cos\theta}{\left(R^2 - \sin^2\theta\right)^{\frac{1}{2}}}\right] \cdot d\theta \tag{A.4}$$

A.3 Volumetric Efficiency (η_v)

Volumetric efficiency was found from the following expression, where T_s is the standard ambient temperature, T_{in} is the measured intake temperature, ρ_{in} is the intake gas density, $\dot{m}_{in}$ is the intake mass flow rate, and N is the engine speed (Heywood, 1988):

$$\eta_v = \left(\frac{T_s}{T_{in}}\right)^{\frac{1}{2}} \frac{2\dot{m}_{in}}{\rho_{in} V_d N} \tag{A.5}$$

A.4 In-cylinder Bulk Gas Temperature

The in-cylinder bulk gas temperature as a function of crank-angle was found using pressure data, where P and V are both functions of crank-angle and N_c is the moles of gas trapped in the cylinder.

$$T = \frac{PV}{N_c R_u} \tag{A.6}$$

In calculating the bulk gas temperature, the in-cylinder gas composition was assumed to be constant throughout the combustion process with the exception of fuel addition. Fuel injection was assumed to occur linearly from -15 to 15 CAD (ATDC) as shown in Figure A.1.

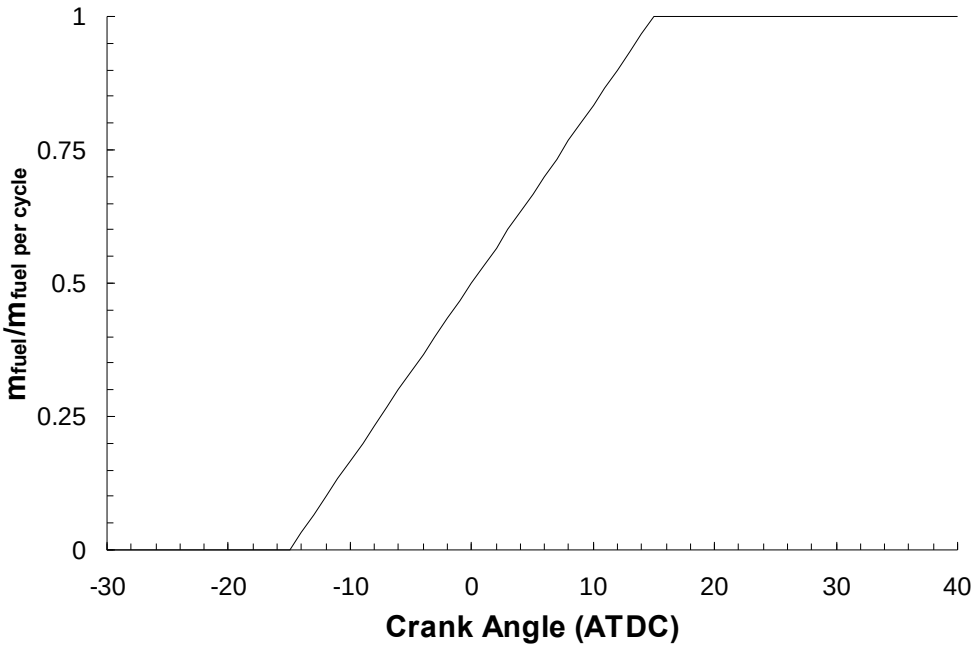

Figure A.1. Model of mass addition to cylinder gas via fuel injection

A.5 Mixture Specific Heat Ratio (γ)

The quantity $\gamma = C_p/C_v$ may be rewritten as

$$\gamma = \frac{C_p}{C_v} = \frac{1}{\left(1 - \left(\frac{C_p}{R_u}\right)^{-1}\right)} \tag{A.7}$$

Once γ_i is found for each species, γ for the mixture is determined by summing over the products of the species mole fraction x_i and their corresponding γ_i.

$$\gamma = \sum_i x_i \cdot \gamma_i \tag{A.8}$$

Equation (A.8) may be solved by first solving for C_p/R_u. C_p/R_u for various gases may in turn be found from coefficients given by Kee *et al* (1991).

A.6 H_2O Saturation Pressure

Steam table data from Wark (1995) was used to generate an H_2O temperature-pressure saturation curve. A sixth order polynomial equation was fit to the steam table data using a Matlab polynomial fit function. The fitted equation is given by Equation (A.9) where the fitted coefficients are given in Table A.1. Pressure is in psi and temperature in Kelvin (experimental measurements were made in psi and Celcius). Figure A.2 shows steam table data along with the 6th order polynomial fit equation.

$$P_{sat} = a_1 + a_2 T + a_3 T^2 + a_4 T^3 + a_5 T^4 + a_6 T^5 + a_7 T^6 \quad \text{(A.9)}$$

Table A.1. Coefficients for H_2O saturation pressure curve

a_1	a_2	a_3	a_4	a_5	a_6	a_7
-1833.87	34.2725	-0.26393	1.06564E-03	-2.34580E-06	2.6558E-09	-1.14226E-12

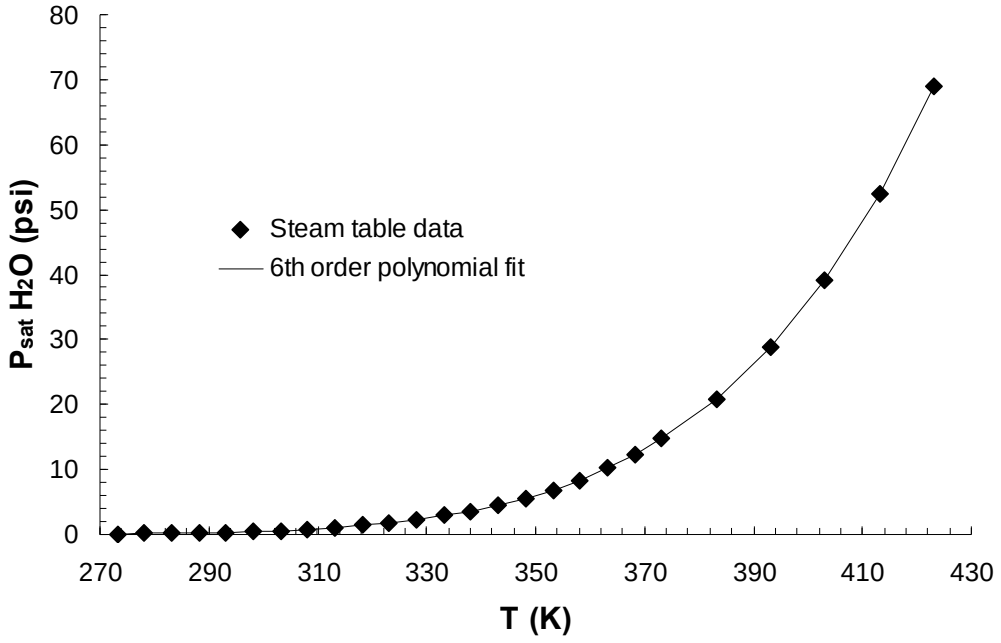

Figure A.2. H_2O temperature-pressure saturation curve

Appendix B. TDC Correction

Properly determining the location of TDC is an important step in using engine cylinder pressure data. If the pressure data does not correspond to the correct crank angle positions, then the pressure-volume trace will be shifted somewhat and error will occur in calculating the indicated power output, bulk temperature, and any other values that rely on pressure data as a function of engine position. Misalignment of the position encoder in the experimental engine can be corrected for using data from motoring the engine. In the motoring case, if the engine position corresponds to the pressure data correctly, then the compression and expansion curves on the log(P)-log(V) diagram should be straight and should align (assuming adiabatic compression and expansion). Another indicator of correct alignment is that the maximum in-cylinder pressure for the motoring case should occur prior to, yet close to TDC.

Pressure data were taken while motoring the engine during the same time period that the N-EGR cases were being run. A log(P)-log(V) plot was generated, and the crank-angles corresponding to the pressure data were adjusted until the compression and expansion traces aligned as nearly as possible. The uncorrected and corrected log(P)-log(V) plots are given in Figure B.1.

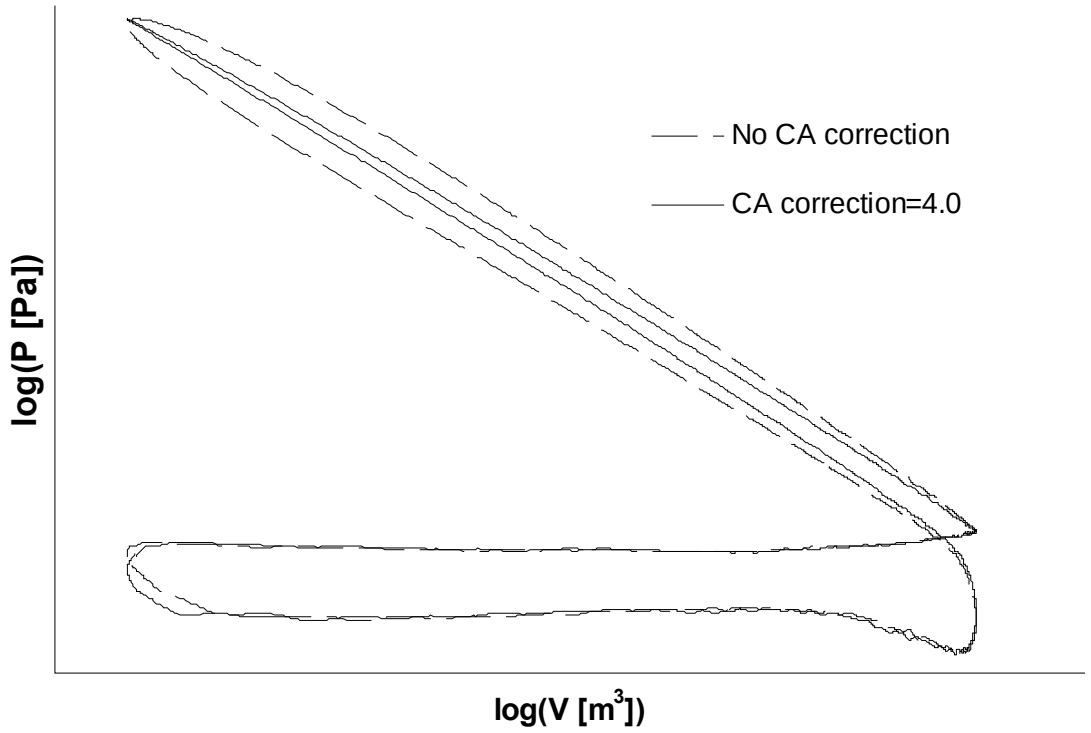

Figure B.1. Crank angle adjustment using motoring data from N-EGR cases.

For no crank angle adjustment to the motored data, the maximum pressure occurred at -4.25 CAD (BDC). The slope of the compression and expansion strokes for the log(P)-log(V) curve most closely aligned for a 4.0 CAD adjustment. The slight difference in the slopes of the compression and expansion curves was likely due to heat transfer.

Between the N-EGR and the O-EGR runs, the experimental engine's head gasket was changed. After this change it was noticed that a shift had occurred in the pressure data. Motoring data was again taken and the same process was repeated as before to find the new adjustment needed to the engine position. The new log(P)-log(V) curve for the corrected and uncorrected motored data is given in Fig. B.2.

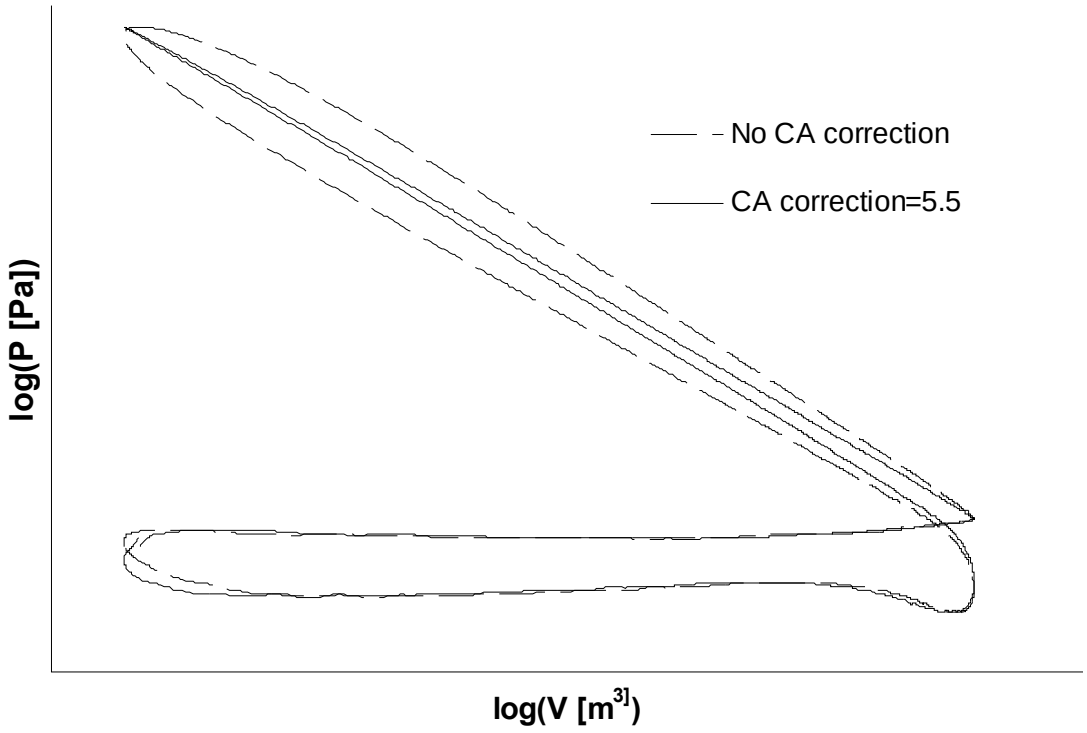

Fig. B.2. Crank angle adjustment using motoring data from O-EGR cases.

For no crank angle adjustment to the data, the maximum in-cylinder pressure occurred at -5.75 CAD (BDC). The slopes of the compression and expansion strokes for log(P)-log(V) were found to most closely align for a 5.5 CAD adjustment to the data. This 5.5 CAD adjustment was applied to all in-cylinder pressure data taken after the head gasket change.

Appendix C. Solving for Flow Rates and Gas Compositions

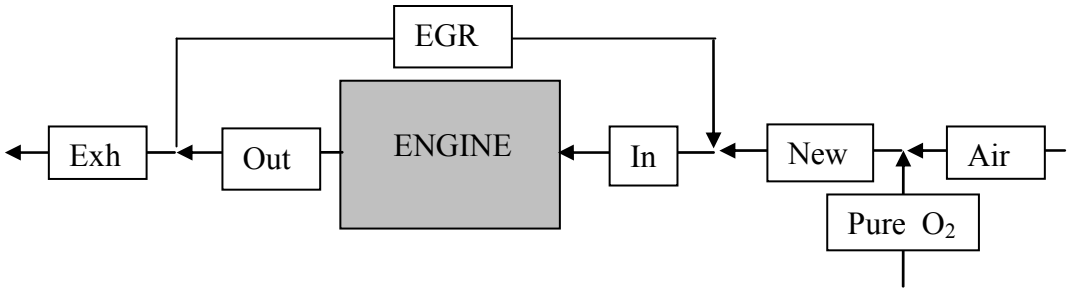

Figure C.1. Visual depiction of flow streams associated with gas composition models

Finding gas compositions for EGR cases:

Goals:

- Estimate intake molar flow rate
- Estimate exhaust molar flow rate
- Estimate intake gas compositions

Assumptions:

- ideal gas
- air is dry
- complete combustion
- steady-state (atom balance on intake and exhaust)
- EGR is dry, all water condensed out (reasonable, since EGR was cooled to temp at which saturation pressure was approximately 1% of intake pressure)
- Air comprised of O_2 and N_2 only, other gases negligible
- Exhaust gases consist of CO_2, O_2, N_2, H_2O
- No addition of pure O_2

Inputs:

- $\dot{V}_{air}$ (measured with Corriolis flow meter):
- $xO_{2,in,measured}$, $xCO_{2,in,dry,measured}$
- $xO_{2,exh,dry,measured}$, $xCO_{2,exh,dry,measured}$
- $xN_{2,amb}$, $xO_{2,amb}$
- Model for H_2O saturation pressure
- fuel properties ($C_{10.8}H_{18.7}$)
- fuel molar flow rate

1. Find molar flow rate of air using the ideal gas law:

$$\dot{N}_{air} = \frac{P_{air}\dot{V}_{air,measured}}{R_u T_{air}} \tag{C.1}$$

2. Find the EGR fraction. An equation for the EGR fraction using measured values is derived below:

$$xO_{2,in} = \frac{\dot{N}_{O_2,in}}{\dot{N}_{in}} = \frac{\left(xO_{2,EGR}\cdot\dot{N}_{EGR} + xO_{2,amb}\cdot\dot{N}_{air}\right)}{\left(\dot{N}_{EGR}+\dot{N}_{air}\right)} \tag{C.2}$$

Solve for $\dot{N}_{EGR}$:

$$\dot{N}_{EGR} = \frac{\left(xO_{2,amb} - xO_{2,in}\right)}{\left(xO_{2,in} - xO_{2,egr}\right)}\dot{N}_{air} \tag{C.3}$$

$$EGR\ fraction = \frac{\dot{N}_{EGR}}{\left(\dot{N}_{EGR}+\dot{N}_{air}\right)}. \tag{C.4}$$

Substitute (C.3) into (C.4):

$$EGR\ Fraction = \frac{\frac{\left(xO_{2,amb} - xO_{2,in}\right)}{\left(xO_{2,in} - xO_{2,egr}\right)}\dot{N}_{air}}{\left(\frac{\left(xO_{2,amb} - xO_{2,in}\right)}{\left(xO_{2,in} - xO_{2,egr}\right)}\dot{N}_{air}+\dot{N}_{air}\right)} = \frac{\left(xO_{2,amb} - xO_{2,in,dry,measured}\right)}{\left(xO_{2,amb} - xO_{2,EGR}\right)} \tag{C.5}$$

3. Estimate exhaust flow rate, EGR flow rate, intake flow rate, intake concentrations

$$\dot{N}_{N_2,exh} = xN_{2,amb} \cdot \dot{N}_{air} \tag{C.6}$$

$$\dot{N}_{H_2O,exh} = \frac{18.7}{2} \cdot \dot{N}_{fuel} \tag{C.7}$$

$$\dot{N}_{O_2,exh} = xO_{2,amb} \cdot \dot{N}_{air} - \left(10.8 + \frac{18.7}{4}\right) \cdot \dot{N}_{fuel} \tag{C.8}$$

$$\dot{N}_{CO_2,exh} = 10.8 \cdot \dot{N}_{fuel} \tag{C.9}$$

$$\dot{N}_{exh} = \dot{N}_{N_2,exh} + \dot{N}_{O_2,exh} + \dot{N}_{H_2O,exh} + N_{CO_2,exh} \tag{C.10}$$

$$\dot{N}_{EGR} = \frac{EGRfrac}{(1 - EGRfrac)} \dot{N}_{air} \tag{C.11}$$

$$\dot{N}_{in} = \dot{N}_{air} + \dot{N}_{EGR} \tag{C.12}$$

$$xO_{2,in} = xO_{2,in,measured} \tag{C.13}$$

$$xCO_{2,in} = xCO_{2,in,measured} \tag{C.14}$$

$$xN_{2,in} = 1 - xO_{2,in,measured} - xCO_{2,in,measured} \tag{C.15}$$

Finding gas compositions and flow rates for O-EGR cases:

A different model for finding species flow rates and compositions was needed for the oxy-combustion case for several reasons. First, the O_2 concentration of the concentration of the combined new gases (air + added O_2) could not always be measured because at high levels of O_2 addition the concentration was >25%, which was the limit of the analyzer's measuring capability. This made it so the previous equation for EGR fraction could not be used Second, the exhaust CO_2 concentration could not always be measured because at high levels of EGR the concentration was greater than 20%, wich was the limit of the analyzer's measuring capability. Third, the flow rate of new gases could not always be measured, because at high levels of EGR this flow rate dropped below the lower limit of the vortex-shedding flow meter's ability to measure it (lower limit was ~6 CFM).

Goals:

- Estimate intake molar flow rate
- Estimate exhaust molar flow rate
- Estimate intake gas composition

Assumptions:

- ideal gases, air is dry
- complete combustion
- steady-state (atom balance on intake and exhaust)
- Air comprised of O_2 and N_2 only, other gases negligible
- Exhaust gases consist of CO_2, O_2, N_2, H_2O
- Volumetric efficiency (η_V) is constant, equal to η_V at the base case with no EGR

Inputs:

- $xO_{2,in,measured}$
- $xCO_{2,in,measured}$
- Model for H_2O saturation pressure
- $\eta_{V,base}$
- fuel properties ($C_{10.8}H_{18.7}$), fuel molar flow rate

Steps:

1. Assume $\eta_V = \eta_{V,base}$. Calculate intake volumetric flow rate, $\dot{V}_{in}$.

$$\dot{V}_{in} = \frac{N}{2 \cdot 60} V_d \cdot \eta_{V,base} \tag{C.16}$$

where N is engine speed in RPM, V_d is the displacement volume, $\eta_{V,base}$ is the volumetric efficiency for the base case with no EGR.

2. Calculate molar flow rate at intake, N_{in}, using ideal gas law.

$$\dot{N}_{in} = \frac{P_{in} \dot{V}_{in}}{R_u T_{in}} \tag{C.17}$$

3. In solving for the gas concentrations and species flow rates, iteration is required because the H_2O concentration in the intake gases is initially unknown.

Iteration "k":

3.1 Initially assume there is no H_2O in the intake gases:

$$\dot{N}_{H_2O_{in}} = 0 \tag{C.18}$$

3.2 Evaluate intake flow rates and compositions. "Dry" refers to gases compositions excluding H_2O.

$$\dot{N}_{in,dry} = \dot{N}_{in} - \dot{N}_{H_2O,in} \tag{C.19}$$

$$xO_{2,in,dry} = xO_{2,in,measured} \tag{C.20}$$

$$xCO_{2,in,dry} = xCO_{2,in,measured} \tag{C.21}$$

$$xN_{2,in,dry} = 1 - xO_{2,in,dry} - xCO_{2,in,dry} \tag{C.22}$$

$$\dot{N}_{O_2,in} = \dot{N}_{in,dry} \cdot xO_{2,in,dry} \tag{C.23}$$

$$\dot{N}_{CO_2,in} = \dot{N}_{in,dry} \cdot xCO_{2,in,dry} \tag{C.24}$$

$$\dot{N}_{N_2,in} = \dot{N}_{in,dry} \cdot xN_{2,in,dry} \tag{C.25}$$

3.3 Evaluate changes in species flow rates due to combustion:

$$\Delta \dot{N}_{CO_2} = 10.8 \cdot \dot{N}_{fuel} \tag{C.26}$$

$$\Delta \dot{N}_{O_2} = \left(10.8 + \frac{18.7}{4}\right) \cdot \dot{N}_{fuel} \tag{C.27}$$

$$\Delta \dot{N}_{H_2O} = \frac{18.7}{2} \cdot \dot{N}_{fuel} \tag{C.28}$$

3.4 Evaluate engine outlet flow rates and compositions:

$$\dot{N}_{O_2,out} = \dot{N}_{O_2,in} + \Delta \dot{N}_{O_2} \tag{C.29}$$

$$\dot{N}_{CO_2,out} = \dot{N}_{CO_2,in} + \Delta \dot{N}_{CO_2} \tag{C.30}$$

$$\dot{N}_{N_2,out} = \dot{N}_{N_2,in} \tag{C.31}$$

$$\dot{N}_{out,dry} = \dot{N}_{O_2,out} + \dot{N}_{CO_2,out} + \dot{N}_{N_2,out} \tag{C.32}$$

$$xO_{2,out,dry} = \frac{\dot{N}_{O_2,out}}{\dot{N}_{out,dry}} \tag{C.33}$$

$$xCO_{2,out,dry} = \frac{\dot{N}_{CO_2,out}}{\dot{N}_{out,dry}} \tag{C.34}$$

$$xN_{2,out,dry} = \frac{\dot{N}_{N_2,out}}{\dot{N}_{out,dry}} \tag{C.35}$$

3.5 Evaluate exhaust (out of system) flow rates:

$$\dot{N}_{CO_2,exh} = \Delta \dot{N}_{CO_2} \tag{C.36}$$

$$\dot{N}_{O_2,exh} = \frac{xO_{2,out,dry}}{xCO_{2,out,dry}} \dot{N}_{CO_2,exh} \tag{C.37}$$

$$\dot{N}_{N_2,exh} = \frac{xN_{2,out,dry}}{xCO_{2,out,dry}} \dot{N}_{CO_2,exh} \tag{C.38}$$

$$\dot{N}_{H_2O,exh} = \Delta \dot{N}_{H_2O} \tag{C.39}$$

$$\dot{N}_{exh,dry} = \dot{N}_{O_2,exh} + \dot{N}_{CO_2,exh} + \dot{N}_{N_2,exh} \tag{C.40}$$

$$\dot{N}_{exh,wet} = \dot{N}_{exh,dry} + \dot{N}_{H_2O,exh} \tag{C.41}$$

3.6 Evaluate EGR flow rates:

$$\dot{N}_{O_2,EGR} = \dot{N}_{O_2,out} + \dot{N}_{O_2,exh} \tag{C.42}$$

$$\dot{N}_{CO_2,EGR} = \dot{N}_{CO_2,out} + \dot{N}_{CO_2,exh} \tag{C.43}$$

$$\dot{N}_{N_2,EGR} = \dot{N}_{N_2,out} + \dot{N}_{N_2,exh} \tag{C.44}$$

$$\dot{N}_{EGR,dry} = \dot{N}_{O_2,EGR} + \dot{N}_{CO_2,EGR} + \dot{N}_{N_2,EGR} \tag{C.45}$$

3.7 Evaluate new gas flow rates:

$$\dot{N}_{O_2,new} = \dot{N}_{O_2,in} - \dot{N}_{O_2,EGR} \tag{C.46}$$

$$\dot{N}_{CO_2,new} = \dot{N}_{CO_2,in} - \dot{N}_{CO_2,EGR} \tag{C.47}$$

$$\dot{N}_{N_2,new} = \dot{N}_{N_2,in} - \dot{N}_{N_2,EGR} \tag{C.48}$$

$$\dot{N}_{new} = \dot{N}_{O_2,new} + \dot{N}_{CO_2,new} + \dot{N}_{N_2,new} \tag{C.49}$$

$$xN_{2,amb} = 1 - xO_{2,amb} \tag{C.50}$$

$$\dot{N}_{O_2,air} = \frac{xO_{2,amb}}{xN_{2,amb}} \dot{N}_{N_2,new} \tag{C.51}$$

$$\dot{N}_{O_2,pure} = \dot{N}_{O_2,new} - \dot{N}_{O_2,air} \tag{C.52}$$

3.8 Estimate saturated concentration of H_2O in EGR using Equation (A.9), based on temperature at EGR heat exchanger outlet. The EGR pressure is essentially same as intake pressure:

$$xH_2O_{sat,EGR} = \frac{P_{sat}}{P_{in}} \tag{C.53}$$

3.9 Estimate H_2O concentration of gases leaving engine:

$$xH_2O_{out} = \frac{\dot{N}_{H_2O,exh}}{\dot{N}_{exh,wet}} \tag{C.54}$$

3.10 Estimate the H_2O concentration in the EGR:

If $xH_2O_{out} < xH_2O_{sat,EGR}$, then $xH_2O_{EGR} = xH_2O_{out}$ (C.55)

Otherwise, $xH_2O_{EGR} = xH_2O_{sat,EGR}$ (C.56)

3.11 Update flow rates, accounting for H_2O:

$$\dot{N}_{H_2O,EGR} = \frac{xH_2O_{EGR}}{(1 - xH_2O_{EGR})} \dot{N}_{EGR,dry} \tag{C.57}$$

$$\dot{N}_{EGR} = \dot{N}_{EGR,dry} + \dot{N}_{H_2O,EGR} \tag{C.58}$$

$$\dot{N}_{H_2O,out} = \dot{N}_{H_2O,EGR} + \Delta\dot{N}_{H_2O} \tag{C.59}$$

$$\dot{N}_{out} = \dot{N}_{out,dry} + \dot{N}_{H_2O,out} \tag{C.60}$$

3.12 Update guess of $\dot{N}_{H_2O,in}$:

$$\dot{N}_{H_2O,in}{}^{k+1} = \dot{N}_{H_2O,EGR} \tag{C.61}$$

4. Iterate on the above equations in Step 3 until the change in intake H_2O flow rate between iterations is less 0.1%, i.e.

$$\left| \frac{\dot{N}_{H_2O,in}{}^{K+1} - \dot{N}_{H_2O,in}{}^{K}}{\dot{N}_{H_2O,in}{}^{K}} \right| < 0.001 \tag{C.62}$$

5. After iterations have converged, evaluate intake wet gas concentrations:

$$xO_{2,in,wet} = \frac{\dot{N}_{O_2,in}}{\dot{N}_{in}}, \quad xCO_{2,in,wet} = \frac{\dot{N}_{CO_2,in}}{\dot{N}_{in}} \tag{C.63}$$

$$xN_{2,in,wet} = \frac{\dot{N}_{N_2,in}}{\dot{N}_{in}}, \quad xH_2O_{,in,wet} = \frac{\dot{N}_{H_2O,in}}{\dot{N}_{in}}$$

Appendix D. NO_x Model

The two reaction Zeldovich mechanism was used in the NO_x formation model as given below:

$$O_2 + N_2 \Leftrightarrow NO + N \tag{N.1}$$

$$N + O_2 \Leftrightarrow NO + O \tag{N.2}$$

Forward and reverse rate coefficients were taken from Turns (2000).

$$\begin{aligned} k_{N.1f} &= 1.8 \cdot 10^{11} \exp[-38{,}270 / T(K)] \quad [=]\text{m}^3/\text{kmol-s} \\ k_{N.1r} &= 3.8 \cdot 10^{10} \exp[-425 / T(K)] \quad [=]\text{m}^3/\text{kmol-s} \\ k_{N.2f} &= 1.8 \cdot 10^{7} T \exp[-4680 / T(K)] \quad [=]\text{m}^3/\text{kmol-s} \\ k_{N.1f} &= 3.8 \cdot 10^{11} T \exp[-20{,}820 / T(K)] \quad [=]\text{m}^3/\text{kmol-s} \end{aligned} \tag{D.1}$$

O, O_2, and N_2 were assumed to be at their equilibrium value, and N was assumed to be in steady state. Using these assumptions, the following rate equation for NO_x can be developed:

$$\frac{d[\text{NO}_x]}{dt} = k_{1f}[\text{O}][\text{N}_2] \cdot \left[1 + \frac{k_{2f}[\text{O}_2] - k_{1r}[\text{NO}]}{k_{1r}[\text{NO}] - k_{2f}[\text{O}_2]}\right] + k_{2r}[\text{NO}][\text{O}] \cdot \left[1 - \frac{k_{2f}[\text{O}_2] - k_{1r}[\text{NO}]}{k_{1r}[\text{NO}] - k_{2f}[\text{O}_2]}\right] \tag{D.2}$$

The same equilibrium values for O, O_2, and N and the same bulk temperature were used fore each intake composition, as given in Table D.1 Using these equilibrium values, Equation(D.2) was numerically integrated over 30 CAD, which was the approximate

duration from start of combustion to peak flame temperature. The rate coefficients were evaluated at the representative peak flame temperatures. Calculated volumetric concentrations [NO_x] (kmol/m^3) were converted to in-cylinder mole fractions using the relationship

$$xNO_x = [NO_x] \cdot \frac{R_u T}{P} \tag{D.3}$$

The temperature used in (D.3) was the in-cylinder bulk temperature at the point of maximum flame temperature and the pressure used was the corresponding in-cylinder pressure. NO_x mole fractions were converted into indicated specific emissions using the same assumed power output for each level of intake N_2 concentration. NO_x emissions predicted by the above model for the hypothetical cases discussed in Section 4.2 are given in Table D.1 below.

Table D.1. NO_x emissions predicted for hypothetical cases by two-reaction Zeldovich mechanism

EGR Level			Tflame (K)	Tbulk (K)	P (kPa)	xN2 eq	xO2 eq	xO eq	xNOx (ppm)	Pig (kW)	NOx (g/kWh)
$xN2_{eq}$=0.73	EGR→	No EGR	3000	1550	8500	0.73	0.01	0.001	5522	18.00	26.51
		Level 1	2900	1550	8500	0.73	0.01	0.001	5039	18.00	24.19
		Level 2	2800	1550	8500	0.73	0.01	0.001	4563	18.00	21.90
		Level 3	2700	1550	8500	0.73	0.01	0.001	4097	18.00	19.67
		Level 4	2600	1550	8500	0.73	0.01	0.001	3645	18.00	17.50
		Level 5	2500	1550	8500	0.73	0.01	0.001	3203	18.00	15.37
$xN2_{eq}$=0.63	EGR→	No EGR	3000	1550	8500	0.73	0.01	0.001	5522	18.00	26.51
		Level 1	2900	1550	8500	0.63	0.01	0.001	4681	18.00	22.47
		Level 2	2800	1550	8500	0.53	0.01	0.001	3888	18.00	18.66
		Level 3	2700	1550	8500	0.43	0.01	0.001	3144	18.00	15.09
		Level 4	2600	1550	8500	0.33	0.01	0.001	2449	18.00	11.76
		Level 5	2500	1550	8500	0.63	0.01	0.001	2975	18.00	14.28

Appendix E. Dissociation Equilibrium Values

Table E.1. Values used to predict xCO and xOH in stoichiometric flame for N-EGR together with predicted equilibrium concentrations

EGR Level	Increasing EGR →				
	No EGR	Level 1	Level 2	Level 3	Level 4
$xN_{2\ intake}$	0.79	0.795	0.8	0.805	0.81
$xCO_{2\ intake}$	0	0.0075	0.015	0.0225	0.03
$xO_{2\ intake}$	0.21	0.1975	0.185	0.1725	0.16
$xH_2O_{\ intake}$	0	0	0	0	0
kmol O_2/kmol fuel	15.48	15.48	15.48	15.48	15.48
kmol CO_2/kmol fuel	0.00	0.59	1.25	2.02	2.90
kmol N_2/kmol fuel	58.22	62.29	66.92	72.22	78.34
kmol H_2O/kmol fuel	0.00	0.00	0.00	0.00	0.00
$P_{\ max}$ (kPa)	8000	8000	8000	8000	8000
$T_{\ bulk}$ (K)	1500	1500	1500	1500	1500
$T_{\ flame}$ (K)	3003	2948	2891	2830	2765
ΔT	1503	1448	1391	1330	1265
$xCO_{\ eq}$	0.035	0.031	0.027	0.024	0.020
$xOH_{\ eq}$	0.010	0.008	0.007	0.006	0.004
$N/N_{O2}{\cdot}C_p$ (kJ/K/kmol fuel)	190	202	216	232	251

Table E.2. Values used to predict xCO and xOH in stoichiometric flame for O-EGR together with predicted equilibrium concentrations

EGR Level	Increasing EGR →				
	No EGR	Level 1	Level 2	Level 3	Level 4
$xN_{2\ intake}$	0.79	0.69	0.59	0.49	0.39
$xCO_{2\ intake}$	0	0.05	0.1	0.15	0.2
$xO_{2\ intake}$	0.21	0.21	0.21	0.21	0.21
$xH_2O_{\ intake}$	0	0.05	0.1	0.15	0.2
kmol O_2/kmol fuel	15.48	15.48	15.48	15.48	15.48
kmol CO_2/kmol fuel	0.00	3.68	7.37	11.05	14.74
kmol N_2/kmol fuel	58.22	50.85	43.48	36.11	28.74
kmol H_2O/kmol fuel	0.00	3.68	7.37	11.05	14.74
P_{max} (kPa)	8000	8000	8000	8000	8000
T_{bulk} (K)	1500	1500	1500	1500	1500
T_{flame} (K)	3003	2930	2872	2822	2779
ΔT	1503	1430	1372	1322	1279
xCO_{eq}	0.035	0.036	0.037	0.037	0.036
xOH_{eq}	0.010	0.010	0.010	0.010	0.010
$N/N_{O2}{\cdot}C_p$ (kJ/K/kmol fuel)	190	198	206	214	222

Table E.3. Values used to predict xCO and xC_{gr} in fuel-rich flame (ϕ=4.0) for N-EGR together with predicted equilibrium concentrations

EGR Level	Increasing EGR →				
	No EGR	Level 1	Level 2	Level 3	Level 4
$xN_{2\ intake}$	0.79	0.80	0.80	0.81	0.81
$xCO_{2\ intake}$	0.00	0.01	0.02	0.02	0.03
$xO_{2\ intake}$	0.21	0.20	0.19	0.17	0.16
$xH_2O_{\ intake}$	0.00	0.00	0.00	0.00	0.00
kmol O_2/kmol fuel	3.87	3.87	3.87	3.87	3.87
kmol CO_2/kmol fuel	0.00	0.15	0.31	0.50	0.73
kmol N_2/kmol fuel	14.55	15.57	16.73	18.05	19.59
kmol H_2O/kmol fuel	0.00	0.00	0.00	0.00	0.00
P_{max} (kPa)	8000	8000	8000	8000	8000
T_{bulk} (K)	800	800	800	800	800
T_{flame} (K) (rich)	1474	1446	1417	1388	1359
ΔT (K)	674	646	617	588	559
xCO_{eq}	0.21	0.21	0.21	0.20	0.20
$xC(gr)_{eq}$	0.089	0.083	0.078	0.074	0.069
T_{flame} (K) (peak)	3003	2948	2891	2830	2765

Table E.4. Values used to predict xCO and xC_{gr} in fuel-rich flame (ϕ=4.0) for O-EGR together with predicted equilibrium concentrations

EGR Level	Increasing EGR →				
	No EGR	Level 1	Level 2	Level 3	Level 4
$xN_{2\ intake}$	0.79	0.69	0.59	0.49	0.39
$xCO_{2\ intake}$	0.00	0.05	0.10	0.15	0.20
$xO_{2\ intake}$	0.21	0.21	0.21	0.21	0.21
$xH_2O_{\ intake}$	0.00	0.05	0.10	0.15	0.20
kmol O_2/kmol fuel	3.87	3.87	3.87	3.87	3.87
kmol CO_2/kmol fuel	0.00	0.92	1.84	2.76	3.68
kmol N_2/kmol fuel	14.55	12.71	10.87	9.03	7.18
kmol H_2O/kmol fuel	0.00	0.92	1.84	2.76	3.68
P_{max} (kPa)	8000	8000	8000	8000	8000
T_{bulk} (K)	800	800	800	800	800
T_{flame} (K) (rich)	1474	1364	1304	1268	1242
ΔT (K)	674	564	504	468	442
xCO_{eq}	0.21	0.26	0.29	0.31	0.32
$xC(gr)_{eq}$	0.089	0.053	0.030	0.013	0.000
T_{flame} (K) (peak)	3003	2930	2872	2822	2779

Appendix F. NO_x Reduction with Increasing Added O_2

Table F.1. Portion of intake gases comprised of added O_2 and corresponding percent reduction in indicated specific NO_x, ϕ=0.37

EGR Level		Increasing EGR →				
		No EGR	**Level 1**	**Level 2**	**Level 3**	**Level 4**
Run 1	% added O_2	0.0%	4.1%	5.7%	5.5%	5.3%
	% NO_x reduction	0%	28%	84%	88%	94%
Run 2	% added O_2	0.0%	4.6%	5.8%	5.9%	6.0%
	% NO_x reduction	0%	40%	86%	93%	97%
Run 3	% added O_2	0.0%	4.4%	5.4%	5.5%	5.4%
	% NO_x reduction	0%	29%	81%	91%	94%
Average	% added O_2	0.0%	4.4%	5.6%	5.6%	5.6%
	% NO_x reduction	0%	33%	84%	91%	95%

Table F.2. Portion of intake gases comprised of added O_2 and corresponding percent reduction in indicated specific NO_x, ϕ=0.48

EGR Level		Increasing EGR →				
		No EGR	**Level 1**	**Level 2**	**Level 3**	**Level 4**
Run 1	% added O_2	0.0%	5.0%	6.9%	7.8%	7.8%
	% NO_x reduction	0%	38%	80%	92%	97%
Run 2	% added O_2	0.0%	5.1%	7.0%	7.8%	7.9%
	% NO_x reduction	0%	40%	86%	93%	97%
Run 3	% added O_2	0.0%	5.3%	6.9%	7.5%	7.6%
	% NO_x reduction	0%	41%	85%	92%	97%
Average	% added O_2	0.0%	5.1%	6.9%	7.7%	7.8%
	% NO_x reduction	0%	40%	83%	93%	97%

Table F.3. Portion of intake gases comprised of added O_2 and corresponding percent reduction in indicated specific NO_x, ϕ=0.64

EGR Level		Increasing EGR →				
		No EGR	**Level 1**	**Level 2**	**Level 3**	**Level 4**
Run 1	% added O_2	0.0%	5.7%	8.4%	9.4%	9.4%
	% NO_x reduction	0%	33%	83%	92%	96%
Run 2	% added O_2	0.0%	5.7%	8.3%	9.1%	9.6%
	% NO_x reduction	0%	40%	86%	93%	97%
Run 3	% added O_2	0.0%	5.6%	8.2%	9.4%	9.6%
	% NO_x reduction	0%	29%	81%	91%	94%
Average	% added O_2	0.0%	5.6%	8.2%	9.4%	9.6%
	% NO_x reduction	0%	34%	83%	92%	96%

Appendix G. Experimental Values

Table G.1. Measured and calculated average values, N-EGR, ϕ=0.32, Run 1

Run		N-EGR, ϕ=0.32, Run 1					
EGR Level		**No EGR**	**10%**	**20%**	**35%**	**46%**	**51%**
Measured Values							
Engine speed	**rpm**	1502	1502	1501	1502	1497	1498
Fuel flow rate	**lbm/min**	0.063	0.063	0.063	0.064	0.063	0.063
Air flow rate	**cfm**	20.8	18.5	16.6	13.6	11.2	10.5
P_{in}	**kPa**	86	93	99	115	132	140
$P_{ambient}$	**kPa**	86	86	86	86	86	86
$P_{air\ flow\ meter}$	**kPa**	97	103	110	126	143	151
$P_{exhaust}$	**kPa**	87	107	114	132	150	158
T_{intake}	**°C**	51	52	52	52	47	36
$T_{ambient}$	**°C**	23	23	23	23	23	23
$T_{sir\ flow\ meter}$	**°C**	14	15	15	16	17	18
$T_{exhaust}$	**°C**	51	52	52	52	47	36
$T_{EGR\ cooler\ outlet}$	**°C**	43	17	17	15	14	14
$T_{smoke\ meter}$	**°C**	32	50	57	60	66	68
$xO_{2,in}$		0.207	0.200	0.192	0.178	0.164	0.158
$xCO2_{in}$		0.000	0.005	0.011	0.031	0.033	0.036
$xO_{2,exh}$		0.143	0.138	0.133	0.123	0.114	0.111
$xCO_{2,exh}$		0.049	0.054	0.058	0.066	0.073	0.075
$xNO_{x,exh}$	**ppm**	621	469	339	162	63	32
Opacity	**%**	0.1	0.1	0.8	6.9	17.6	22.6
Calculated Values							
ϕ		0.32	0.32	0.32	0.33	0.33	0.32
EGR fraction		0.00	0.10	0.20	0.35	0.46	0.51
$\gamma\ (c_p/c_v)_{intake}$ @800 K		1.35	1.35	1.35	1.35	1.35	1.35
C_p @ $T_{flame,\ max}$	**kJ/kmol-K**	37.7	37.8	37.9	38.3	38.2	38.2
$N/N_{O2} \cdot C_p$ @ $T_{flame,\ max}$	**kJ/kmol-K/ kmol O_2/kmol fuel**	182	189	198	216	233	242
P_{ig}	**kW**	9.49	9.58	9.57	9.59	9.73	9.92
Total heat released	**J**	1397	1418	1425	1443	1485	1519
Volumeteric effic.	**%**	0.96	0.95	0.96	0.95	0.93	0.92
$ISNO_x$	**g/kWh**	5.212	3.574	2.383	0.999	0.341	0.165
Uncert. $ISNO_x$	**g/kWh**	0.120	0.082	0.055	0.023	0.008	0.004
ISPM	**g/kWh**	0.002	0.004	0.022	0.179	0.431	0.545
Uncert. ISPM	**g/kWh**	0.074	0.068	0.087	0.061	0.078	0.060
Molar flow rate$_{intake}$	**kmol/s**	7.53E-04	7.70E-04	8.00E-04	8.63E-04	9.29E-04	9.90E-04
Molar flow rate$_{exh}$	**kmol/s**	7.68E-04	7.07E-04	6.54E-04	5.80E-04	5.18E-04	5.02E-04
$T_{bulk\ in\text{-}cylinder,\ max}$	**K**	1336	1319	1297	1242	1182	1131
$T_{flame,\ max}$	**K**	2919	2877	2825	2712	2605	2537
$P_{in\text{-}cylinder,\ max}$	**MPa**	8.21	8.42	8.47	8.72	8.97	9.11
CA Position @ T_{max}	**CAD (ATDC)**	378.25	378.25	378.50	378.75	379.25	379.50
$T_{bulk,\ 90\%\ burned}$	**K**	1235	1207	1186	1139	1079	1023
$T_{flame,\ 90\%\ burned}$	**K**	2845	2795	2745	2637	2529	2458
$P_{in\text{-}cylinder,\ 90\%\ burned}$	**MPa**	4.57	4.39	4.41	4.56	4.54	4.38
CA Position $_{90\%\ burned}$	**CAD (ATDC)**	387.25	388.75	389.00	389.25	390.50	392.00

Table G.2. Measured and calculated average values, N-EGR, ϕ=0.32, Run 2

Run		N-EGR, ϕ=0.32, Run 2				
EGR Level		**No EGR**	**11%**	**24%**	**35%**	**53%**
Measured Values						
Engine speed	**rpm**	1508	1520	1519	1530	1501
Fuel flow rate	**lbm/min**	0.061	0.063	0.063	0.064	0.063
Air flow rate	**cfm**	21.4	19.0	16.3	14.0	10.0
P_{in}	**kPa**	86	93	102	114	145
$P_{ambient}$	**kPa**	87	87	87	87	87
$P_{air\ flow\ meter}$	**kPa**	97	103	108	125	157
$P_{exhaust}$	**kPa**	85	107	110	131	165
T_{intake}	**°C**	53	53	53	52	51
$T_{ambient}$	**°C**	24	24	24	24	24
$T_{sir\ flow\ meter}$	**°C**	18	19	19	20	21
$T_{exhaust}$	**°C**	53	53	53	52	51
$T_{EGR\ cooler\ outlet}$	**°C**	47	19	17	17	18
$T_{smoke\ meter}$	**°C**	-	-	-	-	-
$xO_{2,in}$		0.208	0.200	0.189	0.178	0.155
$xCO2_{in}$		0.001	0.006	0.014	0.023	0.041
$xO_{2,exh}$		0.146	0.141	0.132	0.124	0.108
$xCO_{2,exh}$		0.048	0.053	0.059	0.066	0.078
$xNO_{x,exh}$	**ppm**	631	474	310	165	49
Opacity	**%**	1.4	1.6	2.1	6.1	21.3
Calculated Values						
ϕ		0.30	0.32	0.33	0.32	0.32
EGR fraction		0.00	0.11	0.24	0.35	0.53
$\gamma\ (c_p/c_v)_{intake}$ @800 K		1.35	1.35	1.35	1.35	1.35
C_p @ $T_{flame,\ max}$	**kJ/kmol-K**	37.7	37.8	38.0	38.1	38.4
$N/N_{O2} \cdot C_p$ @ $T_{flame,\ max}$	**kJ/kmol-K/ kmol O_2/kmol fuel**	182	189	201	215	249
P_{ig}	**kW**	10.51	10.76	10.78	10.99	10.96
Total heat released	**J**	1530	1561	1572	1593	1640
Volumeteric effic.	**K**	0.98	0.96	0.94	0.96	0.95
$ISNO_x$	**g/kWh**	4.872	3.267	1.861	0.906	0.220
Uncert. $ISNO_x$	**g/kWh**	0.112	0.075	0.043	0.021	0.005
ISPM	**g/kWh**	0.034	0.037	0.043	0.118	0.386
Uncert. ISPM	**g/kWh**	0.059	0.063	0.043	0.040	0.042
Molar flow rate$_{intake}$	**kmol/s**	7.67E-04	7.86E-04	8.10E-04	8.87E-04	1.00E-03
Molar flow rate$_{exh}$	**kmol/s**	7.82E-04	7.18E-04	6.30E-04	5.89E-04	4.86E-04
$T_{bulk\ in\text{-}cylinder,\ max}$	**K**	1387	1367	1334	1304	1215
$T_{flame,\ max}$	**K**	2942	2899	2828	2752	2564
$P_{in\text{-}cylinder,\ max}$	**MPa**	8.02	8.21	8.40	8.78	9.39
CA Position @ T_{max}	**CAD (ATDC)**	379.75	379.75	379.75	379.75	380.00
$T_{bulk,\ 90\%\ burned}$	**K**	1303	1282	1253	1233	1155
$T_{flame,\ 90\%\ burned}$	**K**	2980	2836	2767	2698	2517
$P_{in\text{-}cylinder,\ 90\%\ burned}$	**MPa**	4.90	4.91	4.98	5.34	5.80
CA Position $_{90\%\ burned}$	**CAD (ADC)**	386.63	387.25	387.50	386.88	386.88

Table G.3. Measured and calculated average values, N-EGR, ϕ=0.32, Run 3

Run		N-EGR, ϕ=0.32, Run 3				
EGR Level		**No EGR**	**11%**	**24%**	**39%**	**51%**
Measured Values						
Engine speed	**rpm**	1503	1510	1506	1502	1503
Fuel flow rate	**lbm/min**	0.061	0.062	0.063	0.063	0.062
Air flow rate	**cfm**	21.3	18.9	16.4	13.3	10.9
P_{in}	**kPa**	86	94	103	119	140
$P_{ambient}$	**kPa**	86	86	86	86	86
$P_{air\ flow\ meter}$	**kPa**	97	104	113	137	151
$P_{exhaust}$	**kPa**	86	108	118	137	165
T_{intake}	**°C**	50	52	52	51	48
$T_{ambient}$	**°C**	23	23	23	23	23
$T_{sir\ flow\ meter}$	**°C**	15	15	15	17	19
$T_{exhaust}$	**°C**	50	52	52	51	48
$T_{EGR\ cooler\ outlet}$	**°C**	41	18	15	15	16
$T_{smoke\ meter}$	**°C**	-	-	-	-	-
$xO_{2,in}$		0.208	0.200	0.189	0.174	0.157
$xCO2_{in}$		0.000	0.006	0.013	0.025	0.039
$xO_{2,exh}$		0.143	0.137	0.131	0.122	0.107
$xCO_{2,exh}$		0.049	0.053	0.058	0.066	0.077
$xNO_{x,exh}$	**ppm**	664	495	318	141	46
Opacity	**%**	0.6	1.3	2.2	6.2	18.5
Calculated Values						
ϕ		0.31	0.31	0.31	0.30	0.31
EGR fraction		0.00	0.11	0.24	0.39	0.51
$\gamma\ (c_p/c_v)_{intake}$ @800 K		1.35	1.35	1.35	1.35	1.35
C_p @ $T_{flame,\ max}$	**kJ/kmol-K**	37.7	37.8	37.9	38.1	38.3
$N/N_{O2} \cdot C_p$ @ $T_{flame,\ max}$	**kJ/kmol-K/ kmol O_2/kmol fuel**	182	190	201	219	246
P_{ig}	**kW**	10.05	10.24	10.28	10.30	10.30
Total heat released	**J**	1455	1489	1511	1526	1544
Volumeteric effic.	**0.0000**	0.98	0.98	0.99	1.02	0.99
$ISNO_x$	**g/kWh**	5.373	3.617	2.096	0.833	0.236
Uncert. $ISNO_x$	**g/kWh**	0.124	0.083	0.048	0.019	0.005
ISPM	**g/kWh**	0.015	0.030	0.048	0.123	0.367
Uncert. ISPM	**g/kWh**	0.059	0.051	0.048	0.042	0.066
Molar flow rate$_{intake}$	**kmol/s**	7.68E-04	7.98E-04	8.43E-04	9.44E-04	1.02E-03
Molar flow rate$_{exh}$	**kmol/s**	7.83E-04	7.83E-04	7.83E-04	7.83E-04	7.83E-04
$T_{bulk\ in\text{-}cylinder,\ max}$	**K**	1379	1354	1319	1270	1192
$T_{flame,\ max}$	**K**	2941	2891	2822	2715	2563
$P_{in\text{-}cylinder,\ max}$	**MPa**	8.48	8.47	8.58	8.97	9.30
CA Position @ T_{max}	**CAD (ATDC)**	378.25	378.75	379.00	379.00	379.25
$T_{bulk,\ 90\%\ burned}$	**K**	1300	1262	1219	1179	1114
$T_{flame,\ 90\%\ burned}$	**K**	2882	2823	2749	2648	2504
$P_{in\text{-}cylinder,\ 90\%\ burned}$	**MPa**	5.29	4.94	4.73	5.02	5.29
CA Position $_{90\%\ burned}$	**CAD (ATDC)**	384.75	386.63	388.13	387.88	388.00

Table G.4. Measured and calculated average values, N-EGR, ϕ=0.53, Run 1

Run		N-EGR, ϕ=0.53, Run 1			
EGR Level		**No EGR**	**17%**	**32%**	**42%**
Measured Values					
Engine speed	**rpm**	1502	1508	1497	1496
Fuel flow rate	**lbm/min**	0.105	0.105	0.103	0.104
Air flow rate	**cfm**	20.6	17.2	14.4	12.1
P_{in}	**kPa**	86	105	128	151
$P_{ambient}$	**kPa**	86	86	86	86
$P_{air\ flow\ meter}$	**kPa**	97	110	138	163
$P_{exhaust}$	**kPa**	90	121	145	171
T_{intake}	**°C**	51	52	51	50
$T_{ambient}$	**°C**	21	21	21	21
$T_{sir\ flow\ meter}$	**°C**	14	15	16	17
$T_{exhaust}$	**°C**	51	52	51	50
$T_{EGR\ cooler\ outlet}$	**°C**	45	14	14	15
$T_{smoke\ meter}$	**°C**	41	67	77	85
$xO_{2,in}$		0.207	0.186	0.166	0.150
$xCO2_{in}$		0.000	0.015	0.031	0.043
$xO_{2,exh}$		0.097	0.087	0.080	0.072
$xCO_{2,exh}$		0.086	0.094	0.099	0.105
$xNO_{x,exh}$	**ppm**	1091	482	170	53
Opacity	**%**	0.0	8.5	24.0	56.6
Calculated Values					
ϕ		0.54	0.56	0.53	0.54
EGR fraction		0.00	0.17	0.32	0.42
$\gamma\ (c_p/c_v)_{intake}$ **@800 K**		1.35	1.35	1.35	1.35
C_p **@** $T_{flame,\ max}$	**kJ/kmol-K**	37.8	38.1	38.3	38.4
$N/N_{O2} \cdot C_p$ **@** $T_{flame,\ max}$	**kJ/kmol-K/ kmol O_2/kmol fuel**	183	205	231	257
P_{ig}	**kW**	15.44	15.96	15.92	15.89
Total heat released	**J**	2292	2393	2416	2441
Volumeteric effic.	**%**	0.96	0.93	0.97	0.96
$ISNO_x$	**g/kWh**	5.492	2.070	0.700	0.206
Uncert. $ISNO_x$	**g/kWh**	0.126	0.048	0.016	0.005
ISPM	**g/kWh**	0.000	0.160	0.491	1.442
Uncert. ISPM	**g/kWh**	0.046	0.042	0.054	0.115
Molar flow rate$_{intake}$	**kmol/s**	7.45E-04	8.00E-04	9.34E-04	1.02E-03
Molar flow rate$_{exh}$	**kmol/s**	7.71E-04	6.87E-04	6.59E-04	6.18E-04
$T_{bulk\ in\text{-}cylinder,\ max}$	**K**	1623	1553	1461	1371
$T_{flame,\ max}$	**K**	3061	2925	2777	2633
$P_{in\text{-}cylinder,\ max}$	**MPa**	8.81	9.04	9.43	9.64
CA Position @ T_{max}	**CAD (ATDC)**	381.50	382.25	382.50	383.00
$T_{bulk,\ 90\%\ burned}$	**K**	1471	1395	1326	1248
$T_{flame,\ 90\%\ burned}$	**K**	2947	2808	2675	2539
$P_{in\text{-}cylinder,\ 90\%\ burned}$	**MPa**	3.77	3.68	4.11	4.23
CA Position $_{90\%\ burned}$	**CAD (ATDC)**	397.75	399.88	398.50	399.00

Table G.5. Measured and calculated average values, N-EGR, ϕ=0.53, Run 2

Run		N-EGR, ϕ=0.53, Run 2					
EGR Level		**No EGR**	**7%**	**18%**	**28%**	**33%**	**43%**
Measured Values							
Engine speed	**rpm**	1497	1492	1495	1501	1498	1495
Fuel flow rate	**lbm/min**	0.102	0.102	0.102	0.101	0.102	0.101
Air flow rate	**cfm**	20.7	19.2	17.1	15.4	14.2	12.3
P_{in}	**kPa**	87	94	107	121	127	152
$P_{ambient}$	**kPa**	85	85	85	85	85	85
$P_{air\ flow\ meter}$	**kPa**	97	103	117	132	138	164
$P_{exhaust}$	**kPa**	87	108	123	139	146	171
T_{intake}	**°C**	56	57	56	55	55	55
$T_{ambient}$	**°C**	25	25	25	25	25	25
$T_{sir\ flow\ meter}$	**°C**	18	19	19	20	20	20
$T_{exhaust}$	**°C**	56	57	56	55	55	55
$T_{EGR\ cooler\ outlet}$	**°C**	43	20	17	16	16	22
$T_{smoke\ meter}$	**°C**	1	2	7	1	19	40
$xO_{2,in}$		0.208	0.200	0.187	0.174	0.167	0.152
$xCO2_{in}$		0.000	0.005	0.015	0.025	0.031	0.042
$xO_{2,exh}$		0.099	0.095	0.090	0.087	0.080	0.076
$xCO_{2,exh}$		0.084	0.087	0.091	0.094	0.099	0.103
$xNO_{x\ ,exh}$	**ppm**	1199	945	540	281	171	72
Opacity	**%**	2.2	2.2	7.4	10.7	19.4	41.5
Calculated Values							
ϕ		0.53	0.53	0.52	0.51	0.53	0.51
EGR fraction		0.00	0.07	0.18	0.28	0.33	0.43
$\gamma\ (c_p/c_v)_{intake}$ **@800 K**		1.35	1.35	1.35	1.35	1.35	1.35
C_p **@** $T_{flame,\ max}$	**kJ/kmol-K**	37.9	37.9	38.1	38.3	38.3	38.5
$N/N_{O2} \cdot C_p$ **@** $T_{flame,\ max}$	**kJ/kmol-K/ kmol O_2/kmol fuel**	182	190	204	221	231	255
P_{ig}	**kW**	15.84	15.89	16.14	16.24	16.30	16.40
Total heat released	**J**	2332	2356	2392	2408	2432	2483
Volumeteric effic.	**K**	0.96	0.96	0.96	0.98	0.96	0.98
$ISNO_x$	**g/kWh**	5.824	4.375	2.342	1.167	0.670	0.268
Uncert. $ISNO_x$	**g/kWh**	0.134	0.101	0.054	0.027	0.015	0.006
ISPM	**g/kWh**	0.037	0.035	0.117	0.161	0.308	0.790
Uncert. ISPM	**g/kWh**	0.037	0.035	0.040	0.042	0.034	0.063
Molar flow rate$_{intake}$	**kmol/s**	7.38E-04	7.61E-04	8.22E-04	9.06E-04	9.14E-04	1.03E-03
Molar flow rate$_{exh}$	**kmol/s**	7.63E-04	7.32E-04	6.98E-04	6.73E-04	6.41E-04	6.18E-04
$T_{bulk\ in\text{-}cylinder,\ max}$	**K**	1683	1654	1597	1539	1504	1415
$T_{flame,\ max}$	**K**	3083	3036	2950	2856	2800	2667
$P_{in\text{-}cylinder,\ max}$	**MPa**	8.81	8.89	9.13	9.26	9.27	9.63
CA Position @ T_{max}	**CAD (ATDC)**	382.00	382.25	382.50	383.00	383.25	383.50
$T_{bulk,\ 90\%\ burned}$	**K**	1554	1524	1480	1430	1401	1312
$T_{flame,\ 90\%\ burned}$	**K**	2985	2939	2862	2775	2722	2588
$P_{in\text{-}cylinder,\ 90\%\ burned}$	**MPa**	4.37	4.37	4.64	4.90	4.87	4.84
CA Position $_{90\%\ burned}$	**CAD (ATDC)**	394.50	394.88	394.38	393.88	394.50	396.00

Table G.6. Measured and calculated average values, N-EGR, ϕ=0.53, Run 3

Run		N-EGR, ϕ=0.53, Run 3					
EGR Level		**No EGR**	**7%**	**18%**	**30%**	**40%**	**43%**
Measured Values							
Engine speed	**rpm**	1504	1496	1502	1501	1500	1502
Fuel flow rate	**lbm/min**	0.102	0.104	0.103	0.104	0.102	0.102
Air flow rate	**cfm**	20.7	19.3	17.1	14.7	13.8	12.0
P_{in}	**kPa**	87	94	107	124	133	156
$P_{ambient}$	**kPa**	86	86	86	86	86	86
$P_{air\ flow\ meter}$	**kPa**	97	90	118	137	145	168
$P_{exhaust}$	**kPa**	85	109	123	143	152	177
T_{intake}	**°C**	56	57	57	56	54	36
$T_{ambient}$	**°C**	23	23	23	23	23	23
$T_{sir\ flow\ meter}$	**°C**	16	17	17	17	18	18
$T_{exhaust}$	**°C**	56	57	57	56	54	36
$T_{EGR\ cooler\ outlet}$	**°C**	45	18	17	16	16	16
$T_{smoke\ meter}$	**°C**	-	-	-	-	-	-
$xO_{2,in}$		0.209	0.201	0.188	0.172	0.158	0.151
$xCO2_{in}$		0.000	0.005	0.014	0.027	0.033	0.043
$xO_{2,exh}$		0.099	0.096	0.091	0.082	0.080	0.073
$xCO_{2,exh}$		0.084	0.086	0.090	0.098	0.100	0.103
$xNO_{x,exh}$	**ppm**	1201	1008	578	238	154	42
Opacity	**CAD (ADC)**	1.0	1.2	7.3	18.9	24.3	58.8
Calculated Values							
ϕ		0.52	0.57	0.52	0.53	0.50	0.51
EGR fraction		0.00	0.07	0.18	0.30	0.40	0.43
$\gamma\ (c_p/c_v)_{intake}$ **@800 K**		1.35	1.35	1.35	1.35	1.35	1.35
C_p **@** $T_{flame,\ max}$	**kJ/kmol-K**	37.9	37.9	38.1	38.3	38.3	38.4
$N/N_{O2} \cdot C_p$ **@** $T_{flame,\ max}$	**kJ/kmol-K/ kmol O_2/kmol fuel**	181	189	203	224	243	256
P_{ig}	**kW**	15.68	15.84	16.08	16.28	16.31	16.31
Total heat released	**J**	2316	2356	2386	2442	2451	2488
Volumeteric effic.	**0.0000**	0.96	0.90	0.97	0.97	1.05	0.92
$ISNO_x$	**g/kWh**	5.936	4.392	2.547	0.969	0.607	0.159
Uncert. $ISNO_x$	**g/kWh**	0.137	0.101	0.059	0.022	0.014	0.004
ISPM	**g/kWh**	0.016	0.018	0.114	0.286	0.369	1.137
Uncert. ISPM	**g/kWh**	0.065	0.030	0.039	0.052	0.041	0.091
Molar flow rate$_{intake}$	**kmol/s**	7.43E-04	7.16E-04	8.32E-04	9.09E-04	1.03E-03	1.05E-03
Molar flow rate$_{exh}$	**kmol/s**	7.68E-04	6.90E-04	7.07E-04	6.66E-04	6.45E-04	6.20E-04
$T_{bulk\ in\text{-}cylinder,\ max}$	**K**	1666	1643	1595	1519	1476	1315
$T_{flame,\ max}$	**K**	3077	3036	2954	2836	2743	2603
$P_{in\text{-}cylinder,\ max}$	**MPa**	8.74	9.05	9.22	9.48	9.58	9.74
CA Position @ T_{max}	**CAD (ATDC)**	382.00	381.75	382.25	382.50	382.75	383.25
$T_{bulk,\ 90\%\ burned}$	**K**	1522	1498	1460	1388	1352	1205
$T_{flame,\ 90\%\ burned}$	**K**	2970	2927	2853	2737	2650	2518
$P_{in\text{-}cylinder,\ 90\%\ burned}$	**MPa**	4.01	4.07	4.31	4.33	4.46	4.45
CA Position $_{90\%\ burned}$	**CAD (ATDC)**	396.50	396.75	396.13	397.25	396.88	398.13

Table G.7. Measured and calculated average values, N-EGR, ϕ=0.67, Run 1

Run		N-EGR, ϕ=0.67, Run 1			
EGR Level		**No EGR**	**10%**	**21%**	**32%**
Measured Values					
Engine speed	**rpm**	1498	1501	1496	1501
Fuel flow rate	**lbm/min**	0.130	0.131	0.129	0.129
Air flow rate	**cfm**	20.3	18.6	16.2	14.2
P_{in}	**kPa**	87	98	117	140
$P_{ambient}$	**kPa**	87	87	87	87
$P_{air\ flow\ meter}$	**kPa**	97	108	128	151
$P_{exhaust}$	**kPa**	90	113	135	159
T_{intake}	**°C**	54	55	55	53
$T_{ambient}$	**°C**	25	25	25	25
$T_{sir\ flow\ meter}$	**°C**	15	16	16	17
$T_{exhaust}$	**°C**	54	55	55	53
$T_{EGR\ cooler\ outlet}$	**°C**	45	17	15	15
$T_{smoke\ meter}$	**°C**	47	63	85	98
$xO_{2,in}$		0.209	0.195	0.178	0.159
$xCO2_{in}$		0.000	0.009	0.023	0.031
$xO_{2,exh}$		0.068	0.064	0.059	0.055
$xCO_{2,exh}$		0.110	0.114	0.118	0.120
$xNO_{x,exh}$	**ppm**	1135.4	679	314	128
Opacity	**%**	22.9	33.0	53.8	78.8
Calculated Values					
ϕ		0.67	0.67	0.67	0.66
EGR fraction		0.00	0.10	0.21	0.32
$\gamma\ (c_p/c_v)_{intake}$ @800 K		1.35	1.35	1.35	1.35
C_p @ $T_{flame,\ max}$	**kJ/kmol-K**	37.9	38.0	38.2	38.3
$N/N_{O2} \cdot C_p$ @ $T_{flame,\ max}$	**kJ/kmol-K/ kmol O_2/kmol fuel**	181	195	215	241
P_{ig}	**kW**	17.46	17.67	17.98	18.32
Total heat released	**J**	2714	2750	2825	2873
Volumeteric effic.	**%**	0.94	0.96	0.95	0.95
ISNO$_x$	**g/kWh**	4.955	2.824	1.227	0.474
Uncert. ISNO$_x$	**g/kWh**	0.023	0.023	0.023	0.023
ISPM	**g/kWh**	0.451	0.696	1.343	2.661
Uncert. ISPM	**g/kWh**	0.050	0.056	0.107	0.213
Molar flow rate$_{intake}$	**kmol/s**	7.38E-04	7.90E-04	8.65E-04	9.76E-04
Molar flow rate$_{exh}$	**kmol/s**	7.69E-04	7.45E-04	7.14E-04	6.92E-04
$T_{bulk\ in\text{-}cylinder,\ max}$	**K**	1710	1669	1587	1500
$T_{flame,\ max}$	**K**	3096	3019	2900	2765
$P_{in\text{-}cylinder,\ max}$	**MPa**	8.59	8.85	9.12	9.55
CA Position @ T_{max}	**CAD (ATDC)**	383.50	383.50	384.00	384.25
$T_{bulk,\ 90\%\ burned}$	**K**	1424	1397	1327	1281
$T_{flame,\ 90\%\ burned}$	**K**	2895	2827	2715	2606
$P_{in\text{-}cylinder,\ 90\%\ burned}$	**MPa**	2.22	2.34	2.44	2.86
CA Position $_{90\%\ burned}$	**CAD (ATDC)**	415.38	414.75	415.00	411.75

Table G.8. Measured and calculated average values, N-EGR, ϕ=0.67, Run 2

Run		N-EGR, ϕ=0.67, Run 2			
EGR Level		**No EGR**	**8%**	**20%**	**35%**
Measured Values					
Engine speed	**rpm**	1500	1503	1497	1499
Fuel flow rate	**lbm/min**	0.130	0.129	0.129	0.129
Air flow rate	**cfm**	20.3	18.8	16.2	13.5
P_{in}	**kPa**	87	96	115	147
$P_{ambient}$	**kPa**	88	88	88	88
$P_{air\ flow\ meter}$	**kPa**	97	106	125	158
$P_{exhaust}$	**kPa**	87	98	132	0
T_{intake}	**°C**	57	56	55	53
$T_{ambient}$	**°C**	25	25	25	25
$T_{sir\ flow\ meter}$	**°C**	16	16	16	17
$T_{exhaust}$	**°C**	57	56	55	53
$T_{EGR\ cooler\ outlet}$	**°C**	44	17	16	15
$T_{smoke\ meter}$	**°C**	46	65	79	96
$xO_{2,in}$		0.208	0.197	0.178	0.154
$xCO2_{in}$		0.000	0.008	0.023	0.031
$xO_{2,exh}$		0.067	0.065	0.057	0.054
$xCO_{2,exh}$		0.112	0.114	0.120	0.122
$xNO_{x,exh}$	**ppm**	1025.2	747	312	99.6
Opacity	**%**	30.3	36.4	63.1	87.1
Calculated Values					
ϕ		0.67	0.67	0.68	0.67
EGR fraction		0.00	0.08	0.20	0.35
$\gamma\ (c_p/c_v)_{intake}$ @800 K		1.35	1.35	1.35	1.35
C_p @ $T_{flame,\ max}$	**kJ/kmol-K**	37.9	38.0	38.2	38.2
$N/N_{O2} \cdot C_p$ @ $T_{flame,\ max}$	**kJ/kmol-K/ kmol O_2/kmol fuel**	182	193	216	249
P_{ig}	**kW**	17.28	17.60	17.66	18.17
Total heat released	**J**	2687	2736	2792	2862
Volumeteric effic.	**K**	0.95	0.94	0.94	0.95
$ISNO_x$	**g/kWh**	4.500	3.130	1.229	0.366
Uncert. $ISNO_x$	**g/kWh**	0.023	0.023	0.023	0.023
ISPM	**g/kWh**	0.620	0.789	1.712	3.443
Uncert. ISPM	**g/kWh**	0.050	0.063	0.137	0.344
Molar flow $rate_{intake}$	**kmol/s**	7.34E-04	7.76E-04	8.48E-04	9.99E-04
Molar flow $rate_{exh}$	**kmol/s**	7.66E-04	7.46E-04	7.07E-04	6.81E-04
$T_{bulk\ in\text{-}cylinder,\ max}$	**K**	1712	1677	1574	1468
$T_{flame,\ max}$	**K**	3093	3030	2892	2720
$P_{in\text{-}cylinder,\ max}$	**MPa**	8.63	8.92	9.14	9.45
CA Position @ T_{max}	**CAD (ATDC)**	383.25	383.25	383.50	384.75
$T_{bulk,\ 90\%\ burned}$	**K**	1420	1398	1305	1265
$T_{flame,\ 90\%\ burned}$	**K**	2888	2834	2700	2571
$P_{in\text{-}cylinder,\ 90\%\ burned}$	**MPa**	2.16	2.30	2.26	2.97
CA Position $_{90\%\ burned}$	**CAD (ATDC)**	416.25	415.25	417.13	411.00

Table G.9. Measured and calculated average values, N-EGR, ϕ=0.67, Run 3

Run		N-EGR, ϕ=0.67, Run 3			
EGR Level		**No EGR**	**9%**	**22%**	**34%**
Measured Values					
Engine speed	**rpm**	1499	1495	1503	1505
Fuel flow rate	**lbm/min**	0.129	0.130	0.131	0.130
Air flow rate	**cfm**	20.3	18.6	16.1	13.8
P_{in}	**kPa**	87	98	119	144
$P_{ambient}$	**kPa**	88	88	88	88
$P_{air\ flow\ meter}$	**kPa**	97	108	130	154
$P_{exhaust}$	**kPa**	93	114	137	164
T_{intake}	**°C**	54	56	55	42
$T_{ambient}$	**°C**	25	25	25	25
$T_{sir\ flow\ meter}$	**°C**	16	17	17	18
$T_{exhaust}$	**°C**	54	56	55	42
$T_{EGR\ cooler\ outlet}$	**°C**	46	18	15	15
$T_{smoke\ meter}$	**°C**	50	68	85	98
$xO_{2,in}$		0.209	0.196	0.176	0.156
$xCO2_{in}$		0.000	0.008	0.024	0.031
$xO_{2,exh}$		0.068	0.064	0.059	0.052
$xCO_{2,exh}$		0.107	0.110	0.115	0.117
$xNO_{x,exh}$	**ppm**	1021.2	701.8	290	71.6
Opacity	**%**	28.4	35.9	60.1	91.2
Calculated Values					
ϕ		0.67	0.67	0.67	0.67
EGR fraction		0.00	0.09	0.22	0.34
$\gamma\ (c_p/c_v)_{intake}$ @800 K		1.35	1.35	1.35	1.35
C_p @ $T_{flame,\ max}$	**kJ/kmol-K**	37.9	38.0	38.2	38.2
$N/N_{O2} \cdot C_p$ @ $T_{flame,\ max}$	**kJ/kmol-K/ kmol O_2/kmol fuel**	181	194	218	245
P_{ig}	**kW**	17.15	17.48	17.79	17.99
Total heat released	**J**	2661	2737	2790	2831
Volumeteric effic.	**0.0000**	0.94	0.95	0.95	0.90
$ISNO_x$	**g/kWh**	4.522	2.965	1.150	0.266
Uncert. $ISNO_x$	**g/kWh**	0.023	0.023	0.023	0.023
ISPM	**g/kWh**	0.587	0.790	1.613	4.149
Uncert. ISPM	**g/kWh**	0.065	0.063	0.129	0.415
Molar flow rate$_{intake}$	**kmol/s**	7.35E-04	7.84E-04	8.82E-04	9.79E-04
Molar flow rate$_{exh}$	**kmol/s**	7.67E-04	7.48E-04	7.17E-04	6.82E-04
$T_{bulk\ in\text{-}cylinder,\ max}$	**K**	1697	1660	1568	1415
$T_{flame,\ max}$	**K**	3090	3022	2881	2701
$P_{in\text{-}cylinder,\ max}$	**MPa**	8.71	9.02	9.30	9.22
CA Position @ T_{max}	**CAD (ATDC)**	383.00	383.00	383.50	385.00
$T_{bulk,\ 90\%\ burned}$	**K**	1415	1382	1313	1221
$T_{flame,\ 90\%\ burned}$	**K**	2891	2825	2699	2557
$P_{in\text{-}cylinder,\ 90\%\ burned}$	**MPa**	2.25	2.27	2.46	2.89
CA Position $_{90\%\ burned}$	**CAD (ATDC)**	414.63	415.75	414.63	411.38

Table G.10. Measured and calculated average values, O-EGR, ϕ=0.37, Run 1

Run		O-EGR, ϕ=0.37, Run 1				
EGR Level		**No EGR**	**47%**	**66%**	**75%**	**81%**
Measured Values						
Engine speed	**rpm**	1502	1498	1504	1492	1475
Fuel flow rate	**lbm/min**	0.074	0.074	0.074	0.075	0.075
P_{in}	**kPa**	87	93	105	120	136
$P_{ambient}$	**kPa**	86	86	86	86	86
$P_{exhaust}$	**kPa**	90	110	125	141	157
T_{intake}	**°C**	34	46	58	68	78
$T_{ambient}$	**°C**	26	26	26	26	26
$T_{exhaust}$	**°C**	328	344	346	343	346
$T_{EGR\ cooler\ outlet}$	**°C**	47	17	87	83	100
$T_{smoke\ meter}$	**°C**	33	47	54	59	59
$xO_{2,in\ (dry)}$		0.207	0.209	0.210	0.211	0.211
$xCO2_{in(dry)}$		0.000	0.047	0.101	0.150	0.200
$xO_{2,exh\ (dry)}$		0.132	0.141	0.135	0.146	0.148
$xCO_{2,exh\ (dry)}$		0.058	0.105	0.165	Over	Over
$xNO_{x\ ,exh\ (dry)}$	**ppm**	706	934	323	299	201
Opacity	**%**	0.0	0.0	0.0	0.0	0.0
Calculated Values						
ϕ		0.36	0.36	0.37	0.37	0.37
EGR fraction		0.01	0.47	0.66	0.75	0.81
$\gamma\ (c_p/c_v)_{intake}$ @ 800 K		1.35	1.35	1.34	1.34	1.34
C_p @ $T_{flame,\ max}$	**kJ/kmol-K**	37.7	38.9	41.1	43.0	45.0
$N/N_{O2}{\cdot}C_p$ @ $T_{flame,\ max}$	**kJ/kmol-K/ kmol O_2/kmol fuel**	182	187	209	227	250
P_{ig}	**kW**	12.03	11.58	11.55	11.42	11.53
Total Heat Released	**J**	1780	1757	1851	1899	1980
Volumeteric effic.	**%**	0.96	-	-	-	-
$ISNO_x$	**g/kWh**	4.844	3.485	0.778	0.561	0.299
Uncert. $ISNO_x$	**g/kWh**	0.354	0.254	0.057	0.041	0.022
ISPM	**g/kWh**	0.000	0.000	0.000	0.000	0.000
Uncert. ISPM	**g/kWh**	0.051	0.030	0.021	0.017	0.014
Molar flow $rate_{intake}$	**kmol/s**	7.93E-04	7.87E-04	8.16E-04	8.46E-04	8.78E-04
Molar flow $rate_{exh}$	**kmol/s**	8.01E-04	4.37E-04	2.94E-04	2.35E-04	1.96E-04
$xO_{2,in}$		0.207	0.208	0.198	0.191	0.183
$xCO_{2,in}$		0.000	0.047	0.095	0.136	0.174
xH_2O_{in}		0.000	0.005	0.063	0.106	0.153
$xO_{2,exh}$		0.126	0.130	0.121	0.126	0.124
$xCO_{2,exh}$		0.051	0.093	0.140	0.179	0.217
xH_2O_{exh}		0.046	0.083	0.124	0.157	0.188
xH_2O_{egr}		0.031	0.011	0.095	0.141	0.188
$T_{bulk,\ max}$	**K**	1399	1383	1322	1286	1262
$T_{flame,\ max}$	**K**	2951	2897	2760	2668	2578
$P_{in\text{-}cylinder,\ max}$	**MPa**	8.80	8.66	8.30	8.36	8.53
CA Position @ T_{max}	**CAD (ATDC)**	379.00	379.00	379.75	380.00	380.25
$T_{bulk,\ 90\%\ burned}$	**K**	1269	1257	1147	1100	1069
$T_{flame,\ 90\%\ burned}$	**K**	2855	2804	2634	2534	2439
$P_{in\text{-}cylinder,\ 90\%\ burned}$	**MPa**	4.1	4.06	2.80	2.53	2.36
CA Position $_{90\%\ burned}$	**CAD (ATDC)**	390.63	390.63	400.25	403.75	406.88

Table G.11. Measured and calculated average values, O-EGR, ϕ=0.37, Run 2

Run		O-EGR, ϕ=0.37, Run 2				
EGR Level		**No EGR**	**47%**	**66%**	**74%**	**81%**
Measured Values						
Engine speed	**rpm**	1499	1502	1503	1495	1459
Fuel flow rate	**lbm/min**	0.078	0.077	0.076	0.076	0.074
P_{in}	**kPa**	87	92	107	120	136
$P_{ambient}$	**kPa**	86	86	86	86	86
$P_{exhaust}$	**kPa**	93	110	126	142	154
T_{intake}	**°C**	35	46	57	68	77
$T_{ambient}$	**°C**	24	24	24	24	24
$T_{exhaust}$	**°C**	327	342	344	346	340
$T_{EGR\ cooler\ outlet}$	**°C**	27	14	109	90	99
$T_{smoke\ meter}$	**°C**	37	52	58	65	65
$xO_{2,in\ (dry)}$		0.207	0.210	0.209	0.208	0.210
$xCO2_{in(dry)}$		0.000	0.050	0.102	0.148	0.201
$xO_{2,exh\ (dry)}$		0.132	0.134	0.133	0.135	0.138
$xCO_{2,exh\ (dry)}$		0.058	0.112	0.167	Over	Over
$xNO_{x\ ,exh\ (dry)}$	**ppm**	702	795	284	169	91
Opacity	**%**	1.0	0.0	0.0	0.0	0.0
Calculated Values						
ϕ		0.38	0.37	0.37	0.38	0.37
EGR fraction		0.01	0.47	0.66	0.74	0.81
$\gamma\ (c_p/c_v)_{intake}$ @ 800 K		1.35	1.34	1.34	1.34	1.34
C_p @ $T_{flame,\ max}$	**kJ/kmol-K**	37.7	39.0	41.1	42.9	44.9
$N/N_{O2}{\cdot}C_p$ @ $T_{flame,\ max}$	**kJ/kmol-K/ kmol O_2/kmol fuel**	182	187	210	230	251
P_{ig}	**kW**	12.18	12.00	11.80	11.53	11.26
Total Heat Released	**J**	1819	1831	1884	1919	1962
Volumeteric effic.	**%**	0.96	-	-	-	-
$ISNO_x$	**g/kWh**	4.763	2.838	0.673	0.317	0.135
Uncert. $ISNO_x$	**g/kWh**	0.348	0.207	0.049	0.023	0.010
ISPM	**g/kWh**	0.025	0.000	0.000	0.000	0.000
Uncert. ISPM	**g/kWh**	0.100	0.029	0.021	0.017	0.014
Molar flow $rate_{intake}$	**kmol/s**	7.90E-04	7.90E-04	8.27E-04	8.49E-04	8.70E-04
Molar flow $rate_{exh}$	**kmol/s**	8.03E-04	4.35E-04	2.96E-04	2.37E-04	1.91E-04
$xO_{2,in}$		0.207	0.209	0.197	0.188	0.182
$xCO_{2,in}$		0.000	0.049	0.096	0.134	0.174
xH_2O_{in}		0.000	0.004	0.060	0.105	0.152
$xO_{2,exh}$		0.126	0.123	0.118	0.117	0.116
$xCO_{2,exh}$		0.053	0.097	0.142	0.179	0.219
xH_2O_{exh}		0.048	0.087	0.126	0.157	0.190
xH_2O_{egr}		0.021	0.009	0.091	0.141	0.189
$T_{bulk,\ max}$	**K**	1387	1381	1315	1278	1246
$T_{flame,\ max}$	**K**	2944	2896	2754	2653	2564
$P_{in\text{-}cylinder,\ max}$	**MPa**	8.56	8.50	8.31	8.01	8.20
CA Position @ T_{max}	**CAD (ATDC)**	379.50	379.50	380.00	381.00	381.00
$T_{bulk,\ 90\%\ burned}$	**K**	1249	1243	1157	1103	1057
$T_{flame,\ 90\%\ burned}$	**K**	2841	2793	2638	2526	2429
$P_{in\text{-}cylinder,\ 90\%\ burned}$	**MPa**	3.7	3.63	2.96	2.51	2.31
CA Position $_{90\%\ burned}$	**CAD (ATDC)**	393.25	393.63	399.13	404.25	407.38

Table G.12. Measured and calculated average values, O-EGR, ϕ=0.37, Run 3

Run		O-EGR, ϕ=0.37, Run 3				
EGR Level		**No EGR**	**47%**	**67%**	**75%**	**81%**
Measured Values						
Engine speed	**rpm**	1503	1497	1495	1483	1437
Fuel flow rate	**lbm/min**	0.074	0.075	0.074	0.076	0.073
P_{in}	**kPa**	86	93	107	120	136
$P_{ambient}$	**kPa**	86	86	86	86	86
$P_{exhaust}$	**kPa**	97	110	126	141	157
T_{intake}	**°C**	35	47	55	69	78
$T_{ambient}$	**°C**	21	21	21	21	21
$T_{exhaust}$	**°C**	327	343	343	349	340
$T_{EGR\ cooler\ outlet}$	**°C**	41	16	67	103	112
$T_{smoke\ meter}$	**°C**	33	44	54	64	68
$xO_{2,in\ (dry)}$		0.207	0.210	0.209	0.209	0.211
$xCO2_{in(dry)}$		0.001	0.048	0.100	0.152	0.203
$xO_{2,exh\ (dry)}$		0.132	0.138	0.141	0.142	0.147
$xCO_{2,exh\ (dry)}$		0.059	0.108	0.161	Over	Over
$xNO_{x\ ,exh\ (dry)}$	**ppm**	728	928	388	224	186
Opacity	**%**	0.0	0.0	0.0	0.0	0.1
Calculated Values						
ϕ		0.36	0.36	0.35	0.38	0.37
EGR fraction		0.01	0.47	0.67	0.75	0.81
$\gamma\ (c_p/c_v)_{intake}$ @ 800 K		1.35	1.34	1.34	1.34	1.34
C_p @ $T_{flame,\ max}$	**kJ/kmol-K**	37.7	38.9	41.0	43.1	45.0
$N/N_{O2}{\cdot}C_p$ @ $T_{flame,\ max}$	**kJ/kmol-K/ kmol O_2/kmol fuel**	182	186	207	231	252
P_{ig}	**kW**	12.37	11.74	11.71	11.42	10.82
Total Heat Released	**J**	1833	1781	1871	1914	1906
Volumeteric effic.	**%**	0.96	-	-	-	-
$ISNO_x$	**g/kWh**	4.854	3.438	0.933	0.419	0.283
Uncert. $ISNO_x$	**g/kWh**	0.354	0.251	0.068	0.031	0.021
ISPM	**g/kWh**	0.000	0.000	0.000	0.000	0.000
Uncert. ISPM	**g/kWh**	0.049	0.029	0.021	0.017	0.002
Molar flow $rate_{intake}$	**kmol/s**	7.95E-04	7.93E-04	8.32E-04	8.45E-04	8.59E-04
Molar flow $rate_{exh}$	**kmol/s**	8.00E-04	4.40E-04	2.97E-04	2.36E-04	1.88E-04
$xO_{2,in}$		0.207	0.209	0.198	0.188	0.183
$xCO_{2,in}$		0.001	0.047	0.095	0.137	0.176
xH_2O_{in}		0.000	0.005	0.055	0.108	0.154
$xO_{2,exh}$		0.127	0.127	0.126	0.122	0.124
$xCO_{2,exh}$		0.051	0.094	0.138	0.181	0.219
xH_2O_{exh}		0.046	0.084	0.122	0.159	0.190
xH_2O_{egr}		0.032	0.010	0.082	0.144	0.190
$T_{bulk,\ max}$	**K**	1406	1384	1322	1287	1248
$T_{flame,\ max}$	**K**	2954	2901	2768	2655	2566
$P_{in\text{-}cylinder,\ max}$	**MPa**	8.83	8.62	8.48	8.29	8.52
CA Position @ T_{max}	**CAD (ATDC)**	379.00	379.25	379.75	380.25	380.00
$T_{bulk,\ 90\%\ burned}$	**K**	1262	1260	1148	1111	1064
$T_{flame,\ 90\%\ burned}$	**K**	2847	2809	2644	2527	2434
$P_{in\text{-}cylinder,\ 90\%\ burned}$	**MPa**	3.8	4.06	2.98	2.60	2.50
CA Position $_{90\%\ burned}$	**CAD (ATDC)**	393.00	391.00	398.88	403.25	404.63

Table G.13. Measured and calculated average values, O-EGR, ϕ=0.48, Run 1

Run		O-EGR, ϕ=0.48, Run 1				
EGR Level		**No EGR**	**40%**	**59%**	**69%**	**76%**
Measured Values						
Engine speed	**rpm**	1501	1497	1498	1493	1494
Fuel flow rate	**lbm/min**	0.105	0.105	0.106	0.106	0.105
P_{in}	**kPa**	86	103	120	137	155
$P_{ambient}$	**kPa**	86	86	86	86	86
$P_{exhaust}$	**kPa**	90	121	142	160	181
T_{intake}	**°C**	36	47	55	65	73
$T_{ambient}$	**°C**	29	29	29	29	29
$T_{exhaust}$	**°C**	444	438	431	429	415
$T_{EGR\ cooler\ outlet}$	**°C**	37	15	66	73	84
$T_{smoke\ meter}$	**°C**	46	58	71	80	78
$xO_{2,in\ (dry)}$		0.207	0.209	0.211	0.210	0.210
$xCO2_{in(dry)}$		0.000	0.048	0.100	0.151	0.201
$xO_{2,exh\ (dry)}$		0.102	0.110	0.113	0.112	0.115
$xCO_{2,exh\ (dry)}$		0.0826	0.130	0.185	Over	Over
$xNO_{x\ ,exh\ (dry)}$	**ppm**	855	841	387	196	104
Opacity	**%**	1.1	0.0	0.0	0.0	1.9
Calculated Values						
ϕ		0.52	0.49	0.48	0.47	0.46
EGR fraction		0.01	0.40	0.59	0.69	0.76
$\gamma\ (c_p/c_v)_{intake}$ @ 800 K		1.35	1.34	1.34	1.33	1.33
C_p @ $T_{flame,\ max}$	**kJ/kmol-K**	37.8	39.0	40.9	42.6	44.2
$N/N_{O2}{\cdot}C_p$ @ $T_{flame,\ max}$	**kJ/kmol-K/ kmol O_2/kmol fuel**	182	187	203	219	236
P_{ig}	**kW**	16.17	16.04	16.03	15.97	15.79
Total Heat Released	**J**	2429	2445	2542	2642	2678
Volumeteric effic.	**%**	0.94	-	-	-	-
$ISNO_x$	**g/kWh**	4.260	2.652	0.866	0.338	0.148
Uncert. $ISNO_x$	**g/kWh**	0.311	0.194	0.063	0.025	0.011
ISPM	**g/kWh**	0.038	0.027	0.020	0.017	0.023
Uncert. ISPM	**g/kWh**	0.038	0.027	0.020	0.017	0.023
Molar flow rate$_{intake}$	**kmol/s**	7.77E-04	8.20E-04	8.73E-04	9.15E-04	9.67E-04
Molar flow rate$_{exh}$	**kmol/s**	7.98E-04	5.20E-04	3.84E-04	3.07E-04	2.60E-04
$xO_{2,in}$		0.207	0.208	0.202	0.195	0.189
$xCO_{2,in}$		0.000	0.048	0.095	0.140	0.181
xH_2O_{in}		0.000	0.004	0.044	0.078	0.110
$xO_{2,exh}$		0.096	0.100	0.100	0.095	0.096
$xCO_{2,exh}$		0.072	0.112	0.154	0.194	0.230
xH_2O_{exh}		0.065	0.100	0.136	0.170	0.199
xH_2O_{egr}		0.034	0.009	0.075	0.112	0.145
$T_{bulk,\ max}$	**K**	1592	1553	1466	1411	1354
$T_{flame,\ max}$	**K**	3039	2977	2856	2759	2667
$P_{in\text{-}cylinder,\ max}$	**MPa**	8.90	9.26	9.03	8.96	8.90
CA Position @ T_{max}	**CAD (ATDC)**	382.00	381.75	382.50	383.00	383.50
$T_{bulk,\ 90\%\ burned}$	**K**	1430	1420	1313	1246	1192
$T_{flame,\ 90\%\ burned}$	**K**	2918	2876	2741	2635	2546
$P_{in\text{-}cylinder,\ 90\%\ burned}$	**MPa**	3.58	4.18	3.45	3.00	2.85
CA Position $_{90\%\ burned}$	**CAD (ATDC)**	398.38	395.25	400.63	405.38	407.75

Table G.14. Measured and calculated average values, O-EGR, ϕ=0. 48, Run 2

Run		O-EGR, ϕ=0.48, Run 2				
EGR Level		**No EGR**	**42%**	**59%**	**70%**	**76%**
Measured Values						
Engine speed	**rpm**	1502	1500	1500	1500	1496
Fuel flow rate	**lbm/min**	0.105	0.104	0.104	0.103	0.103
P_{in}	**kPa**	86	103	120	133	154
$P_{ambient}$	**kPa**	86	86	86	86	86
$P_{exhaust}$	**kPa**	90	122	141	163	179
T_{intake}	**°C**	38	46	55	65	73
$T_{ambient}$	**°C**	27	27	27	27	27
$T_{exhaust}$	**°C**	443	434	432	430	421
$T_{EGR\ cooler\ outlet}$	**°C**	39	14	67	72	99
$T_{smoke\ meter}$	**°C**	39	58	63	73	76
$xO_{2,in\ (dry)}$		0.207	0.209	0.208	0.209	0.207
$xCO2_{in(dry)}$		0.000	0.052	0.100	0.152	0.200
$xO_{2,exh\ (dry)}$		0.102	0.110	0.109	0.114	0.114
$xCO_{2,exh\ (dry)}$		0.0815	0.131	0.186	Over	Over
$xNO_{x\ ,exh\ (dry)}$	**ppm**	885	846	307	196	89
Opacity	**%**	3.0	0.0	0.0	0.0	0.0
Calculated Values						
ϕ		0.52	0.48	0.47	0.47	0.45
EGR fraction		0.00	0.42	0.59	0.70	0.76
$\gamma\ (c_p/c_v)_{intake}$ @ 800 K		1.35	1.34	1.34	1.33	1.33
C_p @ $T_{flame,\ max}$	**kJ/kmol-K**	37.8	39.1	40.9	42.7	44.2
$N/N_{O2}{\cdot}C_p$ @ $T_{flame,\ max}$	**kJ/kmol-K/ kmol O_2/kmol fuel**	182	188	206	222	240
P_{ig}	**kW**	16.31	16.10	16.19	15.97	15.75
Total Heat Released	**J**	2452	2448	2621	2642	2683
Volumeteric effic.	**%**	0.95	-	-	-	-
$ISNO_x$	**g/kWh**	4.375	2.579	0.669	0.330	0.125
Uncert. $ISNO_x$	**g/kWh**	0.319	0.188	0.049	0.024	0.009
ISPM	**g/kWh**	0.040	0.026	0.019	0.016	0.014
Uncert. ISPM	**g/kWh**	0.040	0.026	0.019	0.016	0.014
Molar flow rate$_{intake}$	**kmol/s**	7.87E-04	8.30E-04	8.72E-04	9.21E-04	9.74E-04
Molar flow rate$_{exh}$	**kmol/s**	7.98E-04	5.06E-04	3.78E-04	2.99E-04	2.56E-04
$xO_{2,in}$		0.207	0.208	0.199	0.194	0.186
$xCO_{2,in}$		0.000	0.052	0.095	0.141	0.180
xH_2O_{in}		0.000	0.004	0.046	0.081	0.111
$xO_{2,exh}$		0.096	0.100	0.096	0.097	0.095
$xCO_{2,exh}$		0.072	0.114	0.153	0.194	0.229
xH_2O_{exh}		0.065	0.101	0.135	0.170	0.198
xH_2O_{egr}		0.037	0.009	0.078	0.116	0.147
$T_{bulk,\ max}$	**K**	1598	1544	1453	1419	1349
$T_{flame,\ max}$	**K**	3041	2969	2839	2754	2652
$P_{in\text{-}cylinder,\ max}$	**MPa**	8.70	9.06	8.85	8.75	8.72
CA Position @ T_{max}	**CAD (ATDC)**	382.50	382.25	382.75	383.25	383.75
$T_{bulk,\ 90\%\ burned}$	**K**	1437	1417	1272	1243	1182
$T_{flame,\ 90\%\ burned}$	**K**	2920	2872	2703	2623	2527
$P_{in\text{-}cylinder,\ 90\%\ burned}$	**MPa**	3.50	4.18	2.77	2.74	2.65
CA Position $_{90\%\ burned}$	**CAD (ATDC)**	399.13	395.25	407.25	408.00	410.00

Table G.15. Measured and calculated average values, O-EGR, ϕ=0. 48, Run 3

Run		O-EGR, ϕ=0.48, Run 3				
EGR Level		**No EGR**	**41%**	**59%**	**69%**	**76%**
Measured Values						
Engine speed	**rpm**	1501	1502	1502	1498	1502
Fuel flow rate	**lbm/min**	0.102	0.107	0.106	0.106	0.105
P_{in}	**kPa**	86	103	119	137	154
$P_{ambient}$	**kPa**	86	86	86	86	86
$P_{exhaust}$	**kPa**	90	122	140	165	178
T_{intake}	**°C**	34	46	58	65	73
$T_{ambient}$	**°C**	27	27	27	27	27
$T_{exhaust}$	**°C**	427	439	435	426	423
$T_{EGR\ cooler\ outlet}$	**°C**	44	15	68	86	78
$T_{smoke\ meter}$	**°C**	39	55	67	83	75
$xO_{2,in\ (dry)}$		0.207	0.209	0.211	0.211	0.210
$xCO2_{in(dry)}$		0.000	0.051	0.101	0.152	0.203
$xO_{2,exh\ (dry)}$		0.105	0.113	0.112	0.112	0.114
$xCO_{2,exh\ (dry)}$		0.07856	0.132	0.190	Over	Over
$xNO_{x\ ,exh\ (dry)}$	**ppm**	854	805	428	209	116
Opacity	**%**	2.7	0.0	0.0	2.6	2.3
Calculated Values						
ϕ		0.49	0.49	0.48	0.47	0.45
EGR fraction		0.00	0.41	0.59	0.69	0.76
$\gamma\ (c_p/c_v)_{intake}$ @ 800 K		1.35	1.34	1.34	1.33	1.33
C_p @ $T_{flame,\ max}$	**kJ/kmol-K**	37.8	39.1	41.0	42.6	44.3
$N/N_{O2}{\cdot}C_p$ @ $T_{flame,\ max}$	**kJ/kmol-K/ kmol O_2/kmol fuel**	182	187	205	219	236
P_{ig}	**kW**	15.83	16.11	16.13	15.97	16.11
Total Heat Released	**J**	2352	2441	2554	2616	2695
Volumeteric effic.	**%**	0.95	-	-	-	-
$ISNO_x$	**g/kWh**	4.405	2.528	0.940	0.360	0.160
Uncert. $ISNO_x$	**g/kWh**	0.322	0.185	0.069	0.026	0.012
ISPM	**g/kWh**	0.053	0.026	0.020	0.022	0.016
Uncert. ISPM	**g/kWh**	0.053	0.026	0.020	0.022	0.016
Molar flow rate$_{intake}$	**kmol/s**	7.76E-04	8.28E-04	8.77E-04	9.05E-04	9.67E-04
Molar flow rate$_{exh}$	**kmol/s**	8.06E-04	5.21E-04	3.80E-04	3.07E-04	2.58E-04
$xO_{2,in}$		0.207	0.209	0.201	0.196	0.189
$xCO_{2,in}$		0.000	0.050	0.096	0.141	0.183
xH_2O_{in}		0.000	0.004	0.052	0.078	0.110
$xO_{2,exh}$		0.099	0.102	0.099	0.095	0.095
$xCO_{2,exh}$		0.069	0.114	0.155	0.195	0.232
xH_2O_{exh}		0.062	0.101	0.137	0.170	0.201
xH_2O_{egr}		0.031	0.009	0.087	0.113	0.145
$T_{bulk,\ max}$	**K**	1585	1561	1488	1421	1375
$T_{flame,\ max}$	**K**	3037	2980	2859	2764	2677
$P_{in\text{-}cylinder,\ max}$	**MPa**	8.98	9.33	8.97	8.90	8.89
CA Position @ T_{max}	**CAD (ATDC)**	381.75	381.75	382.75	383.25	383.75
$T_{bulk,\ 90\%\ burned}$	**K**	1441	1431	1334	1266	1212
$T_{flame,\ 90\%\ burned}$	**K**	2929	2882	2744	2649	2557
$P_{in\text{-}cylinder,\ 90\%\ burned}$	**MPa**	4.03	4.36	3.49	3.24	2.98
CA Position $_{90\%\ burned}$	**CAD (ATDC)**	395.13	394.13	400.38	403.13	406.38

Table G.16. Measured and calculated average values, O-EGR, ϕ=0.64, Run 1

Run		O-EGR, ϕ=0.64, Run 1				
EGR Level		**No EGR**	**34%**	**52%**	**62%**	**70%**
Measured Values						
Engine speed	**rpm**	1500	1500	1495	1497	1497
Fuel flow rate	**lbm/min**	0.129	0.129	0.129	0.129	0.129
P_{in}	**kPa**	86	93	108	121	135
$P_{ambient}$	**kPa**	86	86	86	86	86
$P_{exhaust}$	**kPa**	90	111	127	144	158
T_{intake}	**°C**	35	47	57	69	80
$T_{ambient}$	**°C**	24	24	24	24	24
$T_{exhaust}$	**°C**	538	557	554	549	539
$T_{EGR\ cooler\ outlet}$	**°C**	24	17	83	112	124
$T_{smoke\ meter}$	**°C**	56	59	66	72	61
$xO_{2,in\ (dry)}$		0.207	0.209	0.210	0.211	0.209
$xCO2_{in(dry)}$		0.000	0.049	0.100	0.149	0.200
$xO_{2,exh\ (dry)}$		0.075	0.077	0.071	0.073	0.076
$xCO_{2,exh\ (dry)}$		0.1037	0.162	Over	Over	Over
$xNO_{x\ ,exh\ (dry)}$	**ppm**	946	962	327	200	118
Opacity	**%**	18.6	9.8	24.9	25.3	34.2
Calculated Values						
ϕ		0.64	0.63	0.63	0.63	0.65
EGR fraction		0.00	0.34	0.52	0.62	0.70
$\gamma\ (c_p/c_v)_{intake}$ @ 800 K		1.35	1.34	1.34	1.33	1.34
C_p @ $T_{flame,\ max}$	**kJ/kmol-K**	37.8	39.1	41.0	42.8	45.1
$N/N_{O2}{\cdot}C_p$ @ $T_{flame,\ max}$	**kJ/kmol-K/ kmol O_2/kmol fuel**	183	188	205	223	252
P_{ig}	**kW**	18.23	18.13	17.65	17.70	17.49
Total Heat Released	**J**	2804	2843	2909	2995	2994
Volumeteric effic.	**%**	0.94	-	-	-	-
$ISNO_x$	**g/kWh**	4.139	2.758	0.700	0.340	0.167
Uncert. $ISNO_x$	**g/kWh**	0.302	0.201	0.051	0.025	0.012
ISPM	**g/kWh**	0.368	0.127	0.281	0.241	0.289
Uncert. ISPM	**g/kWh**	0.074	0.034	0.039	0.034	0.029
Molar flow rate$_{intake}$	**kmol/s**	7.75E-04	7.78E-04	8.12E-04	8.38E-04	8.69E-04
Molar flow rate$_{exh}$	**kmol/s**	8.01E-04	5.45E-04	4.14E-04	3.42E-04	2.92E-04
$xO_{2,in}$		0.207	0.208	0.200	0.193	0.182
$xCO_{2,in}$		0.000	0.049	0.096	0.137	0.174
xH_2O_{in}		0.000	0.004	0.047	0.090	0.149
$xO_{2,exh}$		0.069	0.069	0.062	0.062	0.062
$xCO_{2,exh}$		0.088	0.131	0.175	0.214	0.253
xH_2O_{exh}		0.079	0.117	0.154	0.186	0.217
xH_2O_{egr}		0.017	0.011	0.090	0.145	0.212
$T_{bulk,\ max}$	**K**	1674	1667	1565	1530	1488
$T_{flame,\ max}$	**K**	3075	3021	2889	2801	2690
$P_{in\text{-}cylinder,\ max}$	**MPa**	8.82	8.72	8.32	8.23	8.13
CA Position @ T_{max}	**CAD (ATDC)**	383.50	383.75	384.50	385.00	385.50
$T_{bulk,\ 90\%\ burned}$	**K**	1431	1441	1349	1324	1291
$T_{flame,\ 90\%\ burned}$	**K**	2901	2858	2729	2646	2541
$P_{in\text{-}cylinder,\ 90\%\ burned}$	**MPa**	2.62	2.68	2.25	2.11	2.08
CA Position $_{90\%\ burned}$	**CAD (ATDC)**	409.50	409.00	415.13	418.38	419.75

Table G.17. Measured and calculated average values, O-EGR, ϕ=0. 64, Run 2

Run		O-EGR, ϕ=0.64, Run 2				
EGR Level		**No EGR**	**33%**	**51%**	**62%**	**70%**
Measured Values						
Engine speed	**rpm**	1506	1497	1498	1501	1500
Fuel flow rate	**lbm/min**	0.126	0.129	0.128	0.129	0.129
P_{in}	**kPa**	86	93	102	115	127
$P_{ambient}$	**kPa**	87	87	87	87	87
$P_{exhaust}$	**kPa**	94	112	123	138	127
T_{intake}	**°C**	34	45	61	73	81
$T_{ambient}$	**°C**	22	22	22	22	22
$T_{exhaust}$	**°C**	538	558	569	562	552
$T_{EGR\ cooler\ outlet}$	**°C**	22	15	79	147	190
$T_{smoke\ meter}$	**°C**	40	57	66	76	76
$xO_{2,in\ (dry)}$		0.207	0.210	0.211	0.210	0.210
$xCO2_{in(dry)}$		0.000	0.048	0.098	0.149	0.204
$xO_{2,exh\ (dry)}$		0.075	0.078	0.069	0.071	0.071
$xCO_{2,exh\ (dry)}$		0.10304	0.161	Over	Over	Over
$xNO_{x\ ,exh\ (dry)}$	**ppm**	736	920	325	189	107
Opacity	**%**	15.7	7.8	30.0	34.2	40.3
Calculated Values						
ϕ		0.62	0.63	0.66	0.67	0.68
EGR fraction		0.00	0.33	0.51	0.62	0.70
$\gamma\ (c_p/c_v)_{intake}$ @ **800 K**		1.35	1.35	1.34	1.34	1.34
C_p @ $T_{flame,\ max}$	**kJ/kmol-K**	37.8	39.1	41.1	43.2	45.3
$N/N_{O2}{\cdot}C_p$ @ $T_{flame,\ max}$	**kJ/kmol-K/ kmol O_2/kmol fuel**	183	187	207	230	254
P_{ig}	**kW**	18.44	18.10	17.52	17.41	17.35
Total Heat Released	**J**	2829	2849	2924	2947	2946
Volumeteric effic.	**%**	0.94	-	-	-	-
$ISNO_x$	**g/kWh**	3.190	2.660	0.690	0.320	0.148
Uncert. $ISNO_x$	**g/kWh**	0.233	0.194	0.050	0.023	0.011
ISPM	**g/kWh**	0.286	0.099	0.345	0.347	0.366
Uncert. ISPM	**g/kWh**	0.057	0.035	0.048	0.038	0.040
Molar flow rate$_{intake}$	**kmol/s**	7.80E-04	7.77E-04	7.79E-04	8.07E-04	8.32E-04
Molar flow rate$_{exh}$	**kmol/s**	8.02E-04	5.48E-04	4.07E-04	3.36E-04	2.87E-04
$xO_{2,in}$		0.207	0.209	0.199	0.189	0.182
$xCO_{2,in}$		0.000	0.048	0.093	0.134	0.176
xH_2O_{in}		0.000	0.003	0.058	0.109	0.155
$xO_{2,exh}$		0.070	0.070	0.060	0.060	0.058
$xCO_{2,exh}$		0.086	0.130	0.177	0.217	0.260
xH_2O_{exh}		0.077	0.116	0.155	0.188	0.222
xH_2O_{egr}		0.015	0.010	0.113	0.175	0.222
$T_{bulk,\ max}$	**K**	1677	1658	1585	1545	1516
$T_{flame,\ max}$	**K**	3077	3022	2890	2784	2700
$P_{in\text{-}cylinder,\ max}$	**MPa**	8.98	8.72	7.95	7.70	7.95
CA Position @ T_{max}	**CAD (ATDC)**	383.25	383.75	385.00	386.00	385.50
$T_{bulk,\ 90\%\ burned}$	**K**	1433	1429	1363	1342	1329
$T_{flame,\ 90\%\ burned}$	**K**	2901	2857	2723	2631	2557
$P_{in\text{-}cylinder,\ 90\%\ burned}$	**MPa**	2.62	2.62	1.97	2.01	2.12
CA Position $_{90\%\ burned}$	**CAD (ATDC)**	409.75	409.75	419.63	419.75	418.13

Table G.18. Measured and calculated average values, O-EGR, ϕ=0. 64, Run 3

Run		O-EGR, ϕ=0.64, Run 3				
EGR Level		**No EGR**	**34%**	**52%**	**63%**	**70%**
Measured Values						
Engine speed	**rpm**	1504	1509	1500	1496	1502
Fuel flow rate	**lbm/min**	0.128	0.129	0.128	0.127	0.128
P_{in}	**kPa**	86	93	105	119	136
$P_{ambient}$	**kPa**	86	86	86	86	86
$P_{exhaust}$	**kPa**	98	111	127	142	160
T_{intake}	**°C**	34	48	57	67	76
$T_{ambient}$	**°C**	26	26	26	26	26
$T_{exhaust}$	**°C**	544	560	554	555	534
$T_{EGR\ cooler\ outlet}$	**°C**	30	15	73	154	86
$T_{smoke\ meter}$	**°C**	41	48	66	71	75
$xO_{2,in\ (dry)}$		0.207	0.207	0.208	0.210	0.209
$xCO2_{in(dry)}$		0.000	0.051	0.100	0.151	0.203
$xO_{2,exh\ (dry)}$		0.074	0.076	0.071	0.075	0.078
$xCO_{2,exh\ (dry)}$		0.10246	0.160	Over	Over	Over
$xNO_{x\ ,exh\ (dry)}$	**ppm**	844	811	288	203	117
Opacity	**%**	16.0	12.0	26.2	26.4	27.0
Calculated Values						
ϕ		0.63	0.65	0.64	0.63	0.63
EGR fraction		0.00	0.34	0.52	0.63	0.70
$\gamma\ (c_p/c_v)_{intake}$ @ 800 K		1.35	1.34	1.34	1.33	1.33
C_p @ $T_{flame,\ max}$	**kJ/kmol-K**	37.8	39.1	41.0	42.8	44.7
$N/N_{O2}{\cdot}C_p$ @ $T_{flame,\ max}$	**kJ/kmol-K/ kmol O_2/kmol fuel**	182	189	207	222	245
P_{ig}	**kW**	18.63	18.32	17.78	17.74	17.71
Total Heat Released	**J**	2855	2863	2926	3002	3012
Volumeteric effic.	**%**	0.93	-	-	-	-
$ISNO_x$	**g/kWh**	3.574	2.263	0.603	0.337	0.161
Uncert. $ISNO_x$	**g/kWh**	0.261	0.165	0.044	0.025	0.012
ISPM	**g/kWh**	0.288	0.148	0.292	0.246	0.221
Uncert. ISPM	**g/kWh**	0.058	0.030	0.041	0.034	0.031
Molar flow $rate_{intake}$	**kmol/s**	7.69E-04	7.71E-04	7.94E-04	8.22E-04	8.71E-04
Molar flow $rate_{exh}$	**kmol/s**	7.93E-04	5.37E-04	4.08E-04	3.35E-04	2.89E-04
$xO_{2,in}$		0.207	0.206	0.198	0.194	0.185
$xCO_{2,in}$		0.000	0.051	0.096	0.139	0.180
xH_2O_{in}		0.000	0.003	0.048	0.085	0.129
$xO_{2,exh}$		0.069	0.068	0.062	0.063	0.064
$xCO_{2,exh}$		0.088	0.134	0.175	0.215	0.254
xH_2O_{exh}		0.079	0.119	0.154	0.187	0.217
xH_2O_{egr}		0.024	0.009	0.091	0.136	0.183
$T_{bulk,\ max}$	**K**	1679	1663	1580	1531	1481
$T_{flame,\ max}$	**K**	3077	3011	2888	2802	2704
$P_{in\text{-}cylinder,\ max}$	**MPa**	8.81	8.54	8.16	7.97	7.90
CA Position @ T_{max}	**CAD (ATDC)**	383.75	384.25	385.00	385.75	386.50
$T_{bulk,\ 90\%\ burned}$	**K**	1460	1449	1371	1339	1308
$T_{flame,\ 90\%\ burned}$	**K**	2916	2855	2732	2656	2572
$P_{in\text{-}cylinder,\ 90\%\ burned}$	**MPa**	2.76	2.68	2.28	2.20	2.35
CA Position $_{90\%\ burned}$	**CAD (ATDC)**	408.38	409.25	415.00	416.88	415.50